AFWAL-TR-83-3082, VOLUME II

EVALUATION OF THE CRACK GROWTH GAGE CONCEPT AS AN INDIVIDUAL AIRCRAFT TRACKING DEVICE

VOLUME II

School of Aeronautics & Astronautics
Purdue University
W. Lafayette, IN 47907

September 1983

Final Report for Period 14 November 1980 - 9 May 1983

AIR FORCE FLIGHT DYNAMICS LABORATORY
AIR FORCE WRIGHT AERONAUTICAL LABORATORIES
AIR FORCE SYSTEMS COMMAND
WRIGHT-PATTERSON AIR FORCE BASE, OHIO 45433

NOTICE

When Government drawings, specifications, or other data are used for any purpose other than in connection with a definitely related Government procurement operation, the United States Government thereby incurs no responsibility nor any obligation whatsoever; and the fact that the government may have formulated, furnished, or in any way supplied the said drawings, specifications, or other data, is not to be regarded by implication or otherwise as in any manner licensing the holder or any other person or corporation, or conveying any rights or permission to manufacture use, or sell any patented invention that may in any way be related thereto.

This report has been reviewed by the Office of Public Affairs (ASD/PA) and is releasable to the National Technical Information Service (NTIS). At NTIS, it will be available to the general public, including foreign nations.

This technical report has been reviewed and is approved for publication.

Rodney L. Wilkinson

LT. RODNEY L. WILKINSON
Project Engineer

Davey L. Smith

DAVEY L. SMITH, Chief
Structural Integrity Branch

FOR THE COMMANDER

Ralph L. Kuster Jr.

RALPH L. KUSTER, JR., Colonel, USAF
Chief, Structures & Dynamics Division

"If your address has changed, if you wish to be removed from our mailing list, or if the addressee is no longer employed by your organization please notify AFWAL/FIBE, W-PAFB, OH 45433 to help us maintain a current mailing list."

Copies of this report should not be returned unless return is required by security considerations, contractural obligations, or notice on a specific document.

SECURITY CLASSIFICATION OF THIS PAGE (When Data Entered)

REPORT DOCUMENTATION PAGE

READ INSTRUCTIONS BEFORE COMPLETING FORM

1. REPORT NUMBER: AFWAL-TR-83-3082, Vol. II	2. GOVT ACCESSION NO.: AD-A136933
3. RECIPIENT'S CATALOG NUMBER:	
4. TITLE (and Subtitle): EVALUATION OF THE CRACK GROWTH GAGE CONCEPT AS AN ~~ADVANCED~~ INDIVIDUAL AIRCRAFT TRACKING DEVICE, VOLUME II	5. TYPE OF REPORT & PERIOD COVERED: Final Report 14 November 1980 to 9 May 1983
	6. PERFORMING ORG. REPORT NUMBER:
7. AUTHOR(s): A.F. Grandt, Jr. and A. Dumanis-Modan	8. CONTRACT OR GRANT NUMBER(s): F33615-80-C-3234
9. PERFORMING ORGANIZATION NAME AND ADDRESS: School of Aeronautics and Astronautics, Purdue University, W. Lafayette, IN 47907	10. PROGRAM ELEMENT, PROJECT, TASK AREA & WORK UNIT NUMBERS: PE 62201F, 24010149
11. CONTROLLING OFFICE NAME AND ADDRESS: AFWAL/FIBEC, Wright-Patterson AFB, Ohio 45433	12. REPORT DATE: September 1983
	13. NUMBER OF PAGES: 129
14. MONITORING AGENCY NAME & ADDRESS (if different from Controlling Office)	15. SECURITY CLASS. (of this report): Unclassified
	15a. DECLASSIFICATION/DOWNGRADING SCHEDULE

16. DISTRIBUTION STATEMENT (of this Report)

Approved for public release; distribution unlimited

17. DISTRIBUTION STATEMENT (of the abstract entered in Block 20, if different from Report)

18. SUPPLEMENTARY NOTES

The work reported herein was conducted by Purdue University under subcontract to the University of Dayton Research Institute. The University of Dayton Research Institute served as prime contractor for the research program.

19. KEY WORDS (Continue on reverse side if necessary and identify by block number)

Crack Growth Gage, Individual Aircraft Tracking, Force Management, Fatigue Crack Growth, Fracture Mechanics

20. ABSTRACT (Continue on reverse side if necessary and identify by block number)

This report summarizes research conducted to develop the crack growth gage technique for individual aircraft tracking. The crack growth gage concept consists of mounting precracked coupons on a structural component so that service loads cause measureable crack extension in the coupon (or gage). Fracture mechanics techniques are then used to relate the gage crack growth with extension of an assumed structural flaw. Thus, the precracked coupon serves as a sensor which records service loads and →

DD FORM 1 JAN 73 1473 EDITION OF 1 NOV 65 IS OBSOLETE

UNCLASSIFIED

SECURITY CLASSIFICATION OF THIS PAGE (When Data Entered)

responds with an output which may be related to the service life of the parent structural member.

The effort described here involved two primary goals: development of a thin crack gage coupon which simulates thick section flaw growth, and development of an improved analysis method for relating gage and assumed structural crack growth. The approach employed for the first task was to design a crack gage which contained side-grooves along the crack plane. The side-grooves forced plane strain conditions in the thin coupon, and provided fatigue crack retardation behavior which more nearly matched that seen in the thicker structural member. A series of experiments conducted with the side-grooved gage geometry compared favorably with numerical predictions for the gage response. The second task developed an algorithm which assumes two crack gages are located at the control point. The information from the second crack gage allowed an extra degree of freedom in the analysis, and provided the means to employ more general fatigue crack growth models in the numerical scheme. Calculations were evaluated through comparison with experimental results available in the literature, and showed improvement over the original analysis method.

FOREWORD

This report has been prepared by the School of Aeronautics and Astronautics, Purdue University, W. Lafayette, Indiana under subcontract to the University of Dayton Research Institute, who served as prime contractor for the total effort conducted under Contract F33615-80-C-3234, entitled "Evaluation of the Crack Growth Gage Concept as an Advanced Individual Aircraft Tracking Device".

The work reported herein was performed during the period 14 November 1980 to 9 May 1983, under the direction of Professor A.F. Grandt, Jr. He was assisted by Graduate Research Assistant A. Dumanis-Modan. Mr. F.J. Giessler was the University of Dayton Research Institute Project Monitor, while Lt. R.L. Wilkinson was the Air Force Project Engineer.

This report is a companion volume to a report issued by the University of Dayton Research Institute, which describes their effort as prime contractor. The report was released by the authors in May 1983.

Portions of this research were conducted by Dr. A. Dumanis-Modan in partial fulfillment of requirements for the degree of Doctor of Philosophy, Purdue University. A thesis describing additional details of that research is given in Reference 7, and may be obtained from University Microfilms International, Dissertation Copies, P.O. Box 1764, Ann Arbor, Michigan 48106. University Microfilms International has assigned the thesis the control number UM 83-10820.

TABLE OF CONTENTS

Table of Contents (con't)

Table of Contents (con't)

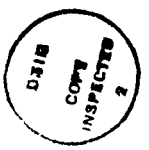

LIST OF ILLUSTRATIONS

Table of Illustrations (con't)

Table of Illustrations (con't)

Section 1

INTRODUCTION

This report summarizes research sponsored under USAF Contract No. F33615-80-C-3234, entitled "Evaluation of a Crack Growth Gage as an Individual Aircraft Tracking Concept." The specific work described here was conducted by Purdue University, through a subcontract with the University of Dayton Research Institute, who served as prime contractor for the effort.

Experience has shown that the actual usage of both civil and military airplanes may vary significantly from the usage assumed during design, and that individual aircraft within a fleet may experience a widely different pattern of usage severity as compared to the average aircraft. To ensure safety and to allow for repair and modifications on a timely and economical basis, continual adjustments to initially determined safe crack growth intervals are required. The USAF Individual Aircraft Tracking (IAT) Program, specified by USAF Structural Integrity Program requirements [1], is intended to provide the information needed to schedule individual aircraft maintenance and/or repair.

The objective of the IAT program is to predict potential flaw growth in critical airframe locations based on individual aircraft usage data. A tracking analysis method is developed to determine and adjust inspection and repair intervals for each critical structural location of the airframe. This analysis provides the capability to predict crack growth rates, time to reach crack size limits, and crack length as a function of cumulative flight time and usage data.

At present, fatigue tracking techniques require sophisticated management programs for recording and interpreting loads experienced at control points [2,3]. Techniques such as counting accelerometers, flight load recorders, pilot logs, and mechanical or electronic strain recorders often require significant effort and expense. Moreover, many assumptions and analyses may be required to reduce the collected data into stress histories which are then used to predict crack growth in different critical locations.

It is possible that significant simplification and cost saving may be achieved by employing the crack growth gage for fleet tracking. The crack growth gage approach consists of mounting a precracked coupon onto a load bearing structural member as shown schematically in Figure 1. The coupon receives a scaled load which is applied to the structural member, and responds with measurable crack growth. This gage crack growth is then related to "cumulative damage" in the structural member to evaluate the severity of the service load applied to the structure. By use of fracture mechanics principles, "transfer functions" can be developed to relate the crack growth in the gage to the crack growth in the structure as shown schematically in Figure 2. In this sense the crack gage (coupon) acts as an analog computer which receives the load history, determines its effect on crack growth and responds with a measurable crack growth. A brief review of prior research with the crack growth gage approach is described in the next section, and provides the background for goals of the current program.

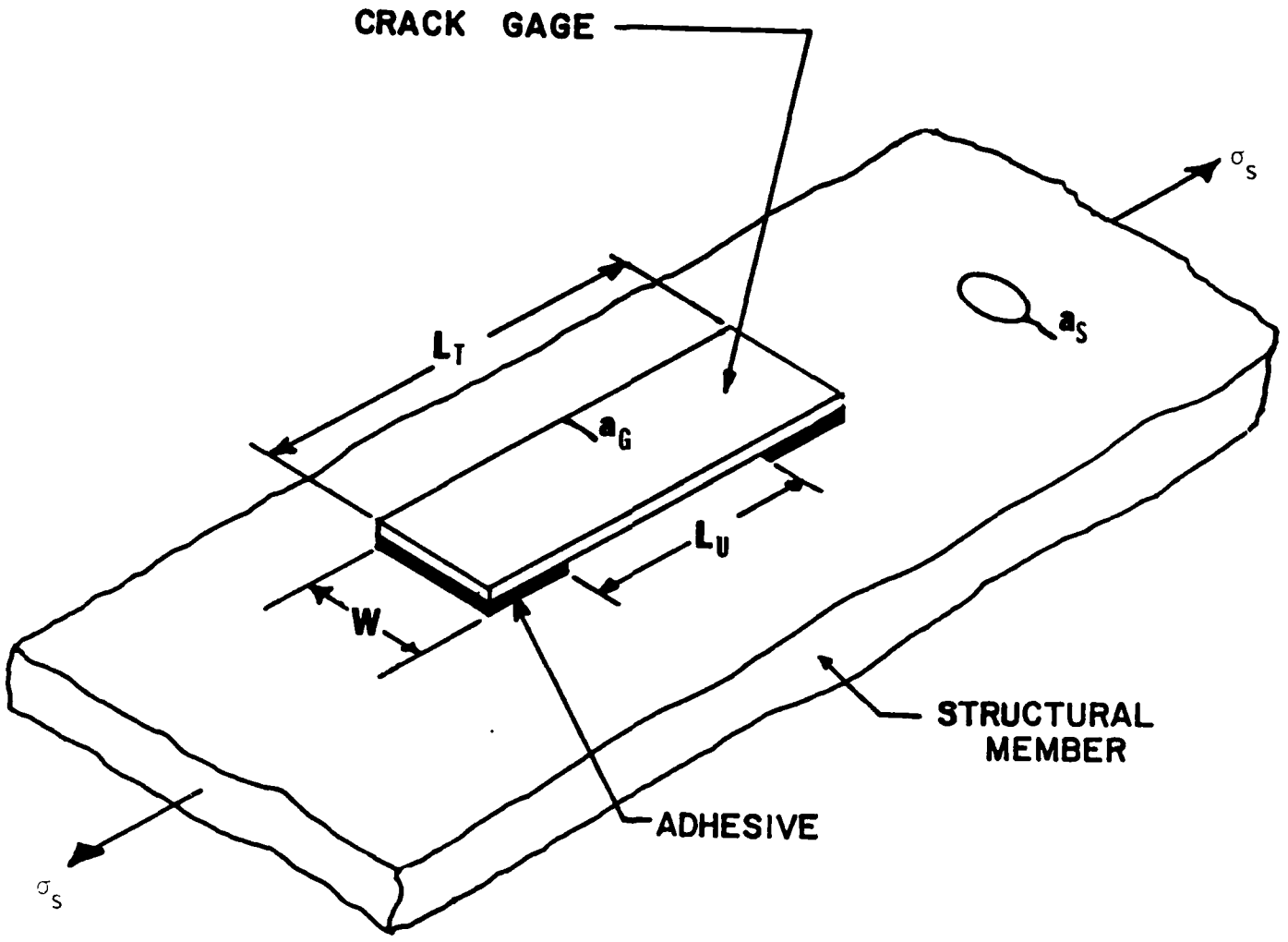

Figure 1. Schematic view of an edge crack gage attached to a structural member

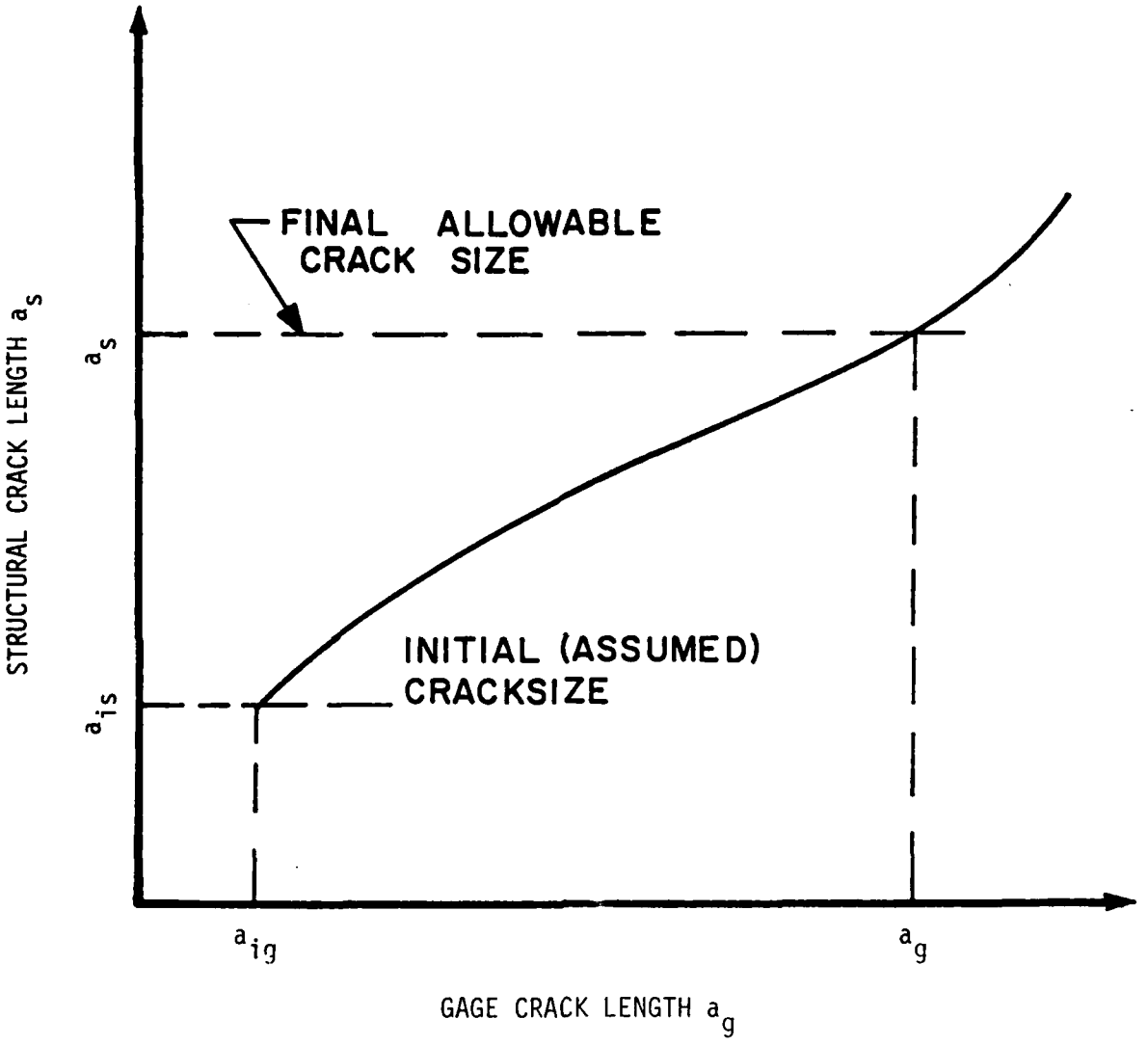

Figure 2 Schematic transfer function relating structural flaw length a_s with corresponding gage crack size a_g.

Section 2

BACKGROUND

1. REVIEW OF PRIOR WORK

The crack length a_g in the coupon shown in Figure 1, can be related to the growth of the assumed structural flaw a_s, by use of a mathematical model. The initial structural flaw size and shape are based on appropriate assumptions (such as the criteria given in Reference 1), while the coupon geometry may be designed for a desired response. It is assumed that the edges of the coupon are attached to the structural member (e.g. adhesively bonded, riveted, bolted, welded, etc.) so that when the structure is exposed to remotely applied stress σ_s, an effective stress σ_g is transferred to the coupon. The relationship between structural and gage loads can be expressed in the form

$$\sigma_g = f\,\sigma_s \tag{1}$$

Here the load-transfer function f may depend on geometry and material properties, but not on stress level. Determining an expression for f is essentially a stress analysis problem which can be readily approached by several analytical and/or experimental techniques [4-7].

Now, assume that crack growth in the gage and structural materials can be described by a model of the form

$$\frac{da}{dN} = F(K) \tag{2}$$

Here da/dN is the fatigue crack growth rate and F(K) is an appropriate function relating the stress intensity factor K, material properties, and other significant load variables. Solving Equation 2 for cyclic life N,

and observing that at any instant of time the gage and structural defects receive the same number of load cycles, leads to

$$N = \int_{a_{is}}^{a_s} \frac{da}{F_s(K)} = \int_{a_{ig}}^{a_g} \frac{da}{F_g(K)} \tag{3}$$

Here a_i and a are the initial and final crack lengths, while the subscripts s and g refer, respectively, to structural and gage quantities.

An interesting special case occurs when crack growth in the structural and gage materials can be described by a simple power law [8].

$$\frac{da}{dN} = C\bar{K}^m = F(K) \tag{4}$$

Here $\bar{K}$ is the range in cyclic stress intensity factor and C and m are empirical constants. Now, expressing $\bar{K}$ in the common form

$$\bar{K} = \bar{\sigma}\sqrt{\pi a}\ \beta \tag{5}$$

where $\bar{\sigma}$ is the cyclic stress, a is the crack length, and β is the usual flaw geometry dependent stress intensity factor coefficient, and combining Equations 1, 3, 4, and 5 leads to

$$N = \int_{a_{is}}^{a_s} \frac{da}{C_s(\bar{\sigma}_s\sqrt{\pi a}\beta_s)^{m_s}} = \int_{a_{ig}}^{a_g} \frac{da}{C_g(f\bar{\sigma}_s\sqrt{\pi a}\beta_g)^{m_g}} \tag{6}$$

Note that a is the dummy variable of integration in Equation 6 and that, while f and β depend on geometric and possibly material properties, neither function depends on the load level $\bar{\sigma}_s$.

Further assuming that the gage and structural materials have the same crack growth exponent $m_s = m_g = m$ (a reasonable assumption if gage and structure are made from the same material) leads to

$$\int_{a_{is}}^{a_s} \frac{da}{C_s(\sqrt{\pi a}\beta_s)^m} = \int_{a_{ig}}^{a_g} \frac{da}{C_g(f\sqrt{\pi a}\beta_g)^m} \qquad (7)$$

Note that all stress level terms effectively cancel in Equation 7. Although this expression no longer specifies the cyclic life N, it still represents a valid relationship between gage and structural quantities. Since the material properties C_s, C_g, and m can be determined from conventional baseline testing, the stress intensity factor coefficients, β, are readily available from handbooks or are obtainable by standard analysis methods, and the initial gage and structural crack lengths a_{ig} and a_{is} are specified, Equation 7 can be integrated numerically to obtain the structural crack size a_s as a function of gage crack size a_g. Thus, measuring the gage crack length also effectively determines the growth of the initially assumed structural defect during service. Of special significance is the fact that when crack growth can be described by a simple Paris law (Equation 4), the a_s versus a_g relationship is <u>independent of loading</u>.

References 5 and 6 present results of several comparisons which indicate good agreement between experiments and predictions based on Equation 7. In those cases, crack growth could be described by Equation 4, and the resulting structural crack versus gage crack relation was independent of load level as described above. Although this apparent load independence is one feature of the crack gage approach which seems especially attractive for Individual Aircraft Tracking, it may not occur for situations when Equation 4 is no longer valid. The following two subsections review two such potential problems and provide the background for the two major program objectives considered here: developing a "thin"

crack gage which exhibits the same crack growth behavior found in "thick" structural members, and extending the structural crack versus gage flaw relation to account for more general crack growth models.

2. THICKNESS DEPENDENT RETARDATION

Practical considerations (e.g. weight, access, gage cost, etc.) usually dictate that the crack gage coupon be small in physical size. Moreover, it is desirable to have a thin coupon relative to the structural thickness to minimize bending caused by local reinforcement, and to reduce load transfer requirements from the parent member. Since the load needed to achieve a given stress level is less in a thin gage, the attachment problem (e.g. adhesive bonding) is simpler. Thus, longer, more reliable, gage lives are possible. Typical crack gage thicknesses studied in the literature [4-6, 9-11] vary from 0.02 in. to 0.10 in.

These motivations for thin crack gages, however, are offset by the influence specimen thickness can have on fatigue crack growth in many structural materials. Although constant amplitude crack growth data are often insensitive to thickness variation, variable amplitude testing can yield significantly longer crack growth lives in thin sections than in thick specimens [11-16]. These thickness effects are attributed to the difference in plastic zone sizes associated with plane stress and plane strain conditions, and to the effect of plastic zone size on fatigue crack retardation (delay in crack growth rate caused by peak overloads). Under plane strain conditions (found in thick specimens), for example, plastic zone sizes are smaller, and retardation effects are minimized (peak loads have less of an influence in reducing subsequent crack growth rates). Under plane stress conditions (found in thin specimens such as

crack gages), plastic zone sizes are larger, and peak overloads can cause more retardation than in thicker sections.

Since crack growth rates in thin crack gage coupons could be slower, under variable amplitude loading, then that experienced in thicker structural components, crack growth measurements in thin crack gages could give an erroneous measure of damage accumulation in the structure. In particular, crack gage measures of damage for fighter missions (which often see higher peak loads) could give an unconservative indication of damage in the structure. (The peak loads cause more retardation in the crack gage than actually occurs in the structure). In order to eliminate this possibility, research was directed to developing a crack gage geometry which maintains the advantages of a "thin" cross section, without introducing complications related to the thickness effect. As discussed in Chapter 3, the approach followed here involved use of deep side-grooves to simulate plane strain behavior in the crack growth gage. First, however, the following subsection briefly reviews the objective and approach followed for the second program goal.

3. A LOAD DEPENDENT CRACK GAGE MODEL

The purpose of this section is to briefly describe a mathematical model to analyze crack gage data for load histories which cannot be correlated by the simple power law of Equation 4. The main objective here is to present an analysis scheme which incorporates stress level effects in the computational procedure.

Returning to Equation 3, recall that the key assumption which led to the load independent result of Equation 7 was the choice of the simple Paris model (Equation 4) for describing fatigue crack growth.

This assumption allows one to eliminate stress explicitly in subsequent development of Equation 7. The choice of more complex crack growth laws precludes cancellation of load terms in this manner, however, and requires some measure of stress level to complete the relationship between gage and structural crack sizes. Since the desired tracking device is to be as simple as possible, the requirement for another load monitoring system (i.e., strain recorders) to reduce the crack gage data could be a severe limitation of the crack gage method for IAT. Thus, the following scheme was developed for determining the effective stress level for use with crack gage data reduction.

The major change in the proposed approach is to employ two independent crack gages at each tracking location, as shown schematically in Figure 3. Now, returning to Equation 3, an analogous relationship can be written for the cyclic life of the two crack gages, giving

$$N = \int_{a_{i1}}^{a_1} \frac{da}{F_1(K)} = \int_{a_{i2}}^{a_2} \frac{da}{F_2(K)} \qquad (8)$$

where the subscripts 1 and 2 now refer to gages 1 and 2. The functions $F_1(K)$ and $F_2(K)$, relating stress intensity level with fatigue crack growth rate, are now the appropriate expressions for the gage material. Since the crack lengths in the gages will be recorded during service, the upper limits (a_1 and a_2) on the integrals will be known, as well as the initial crack sizes a_{i1} and a_{i2}. Thus, it is possible to introduce an effective stress level as an unknown in the expressions for F(K) in Equation 8. After solving Equation 8 for this stress term, one (or both) of the gages would again be matched with the assumed structural flaw as in Equation 3, and solved for the structural crack size a_s. Development of an algorithm based on this double gage concept, including comparison with experimental results is described in Section 4.

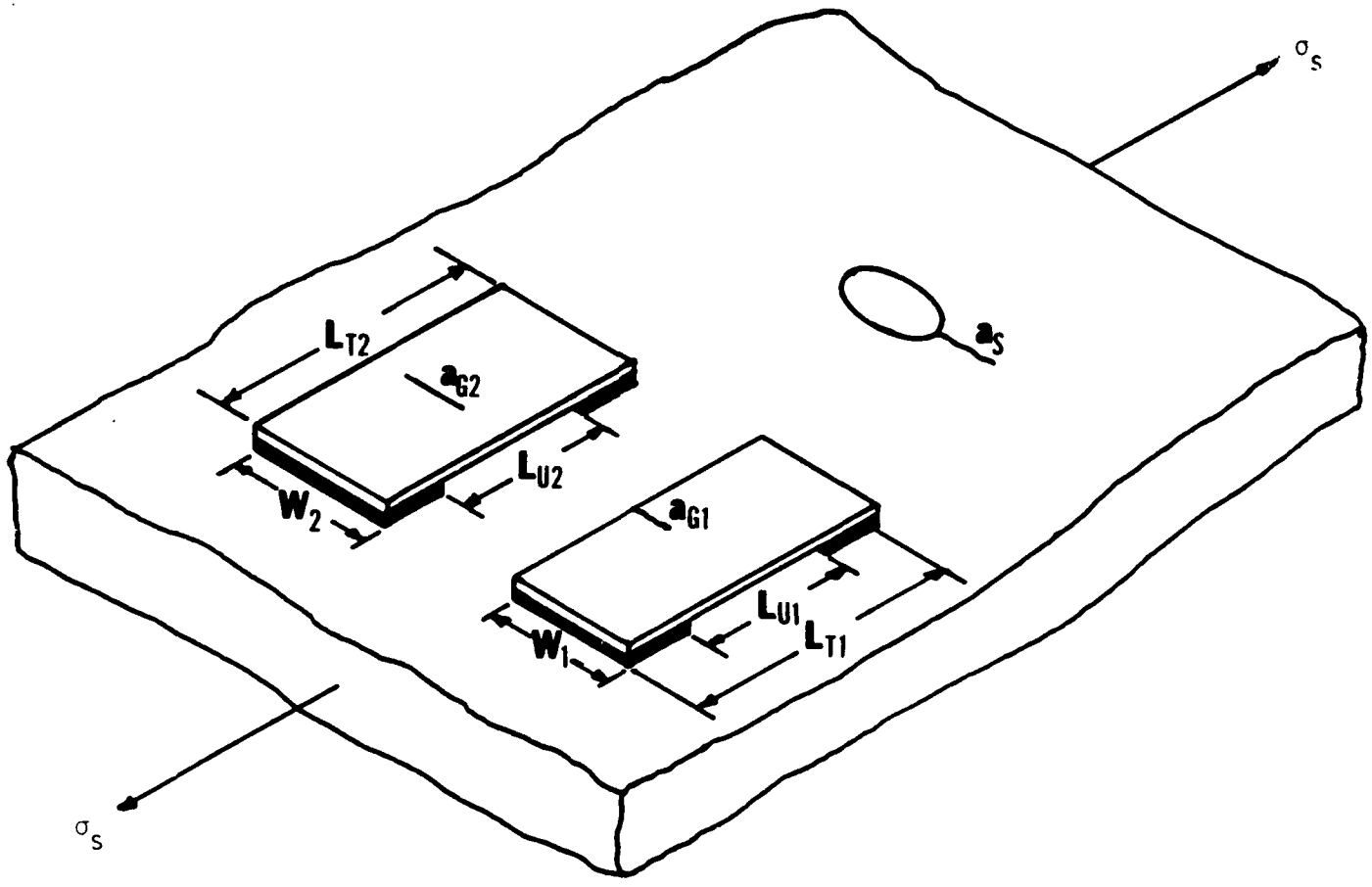

Figure 3. Schematic view of two crack growth gages attached to a structural member

4. RESEARCH OBJECTIVES

The objectives and approaches for the current research tasks are briefly summarized below.

a. Side-Grooved Crack Gage

The objective of this task was to determine the feasibility of designing a thin section crack growth gage which simulates thick section (plane strain) crack growth behavior. The approach employed deep side-grooves along the crack plane to introduce a three dimensional stress state which forces plane strain conditions in the thin crack growth gage, and minimizes thickness effects on fatigue crack growth.

b. Double Gage Model

The objective of this task was to develop a load dependent transfer function for relating flaw growth in crack gages with extension of the assumed structural crack. The approach employed two independent crack gages at a given control point. The additional information gained from the second crack gage allows computation of an effective system stress and provides the means to employ more general fatigue crack growth laws than were possible in the original "load independent" transfer function given by Equation 7.

Section 3

SIDE-GROOVED CRACK GROWTH GAGE

1. BACKGROUND

As discussed in the previous section, the goal of this task was to design a "thin" crack growth gage which would give "thick" section fatigue crack growth response. The particular objective was to minimize thickness dependent fatigue crack retardation effects which could be associated with thicker structural components. The approach considered was to force plane strain conditions in the thin crack gage by employing deep side-grooves as shown schematically in Figure 4. Here a crack of length a_g grows along the plane formed by the side-grooves. The gross thickness of the crack gage is B, while the net thickness remaining between the side-grooves is B_N. (Thickness B_N was desired to be on the order of 0.03 in. to minimize load transfer through the adhesive). The side-groove angle is θ, the root radius of the groove is ρ, the gage width is W, and its unbonded length is L_u.

Prior investigations [17-20] have indicated that side-grooves can promote plane strain <u>fracture</u> in thin sections which usually exhibit ductile behavior. Other studies show that side-grooves may also affect <u>fatigue</u> crack growth by lowering closure loads [21] and slightly decreasing thick specimen retardation [22]. These latter two studies did not, however, examine fatigue crack retardation behavior in the thin test sections of interest here. Thus, as described in the following subsection, preliminary experiments and analyses were required to incorporate side-grooves with crack growth gages.

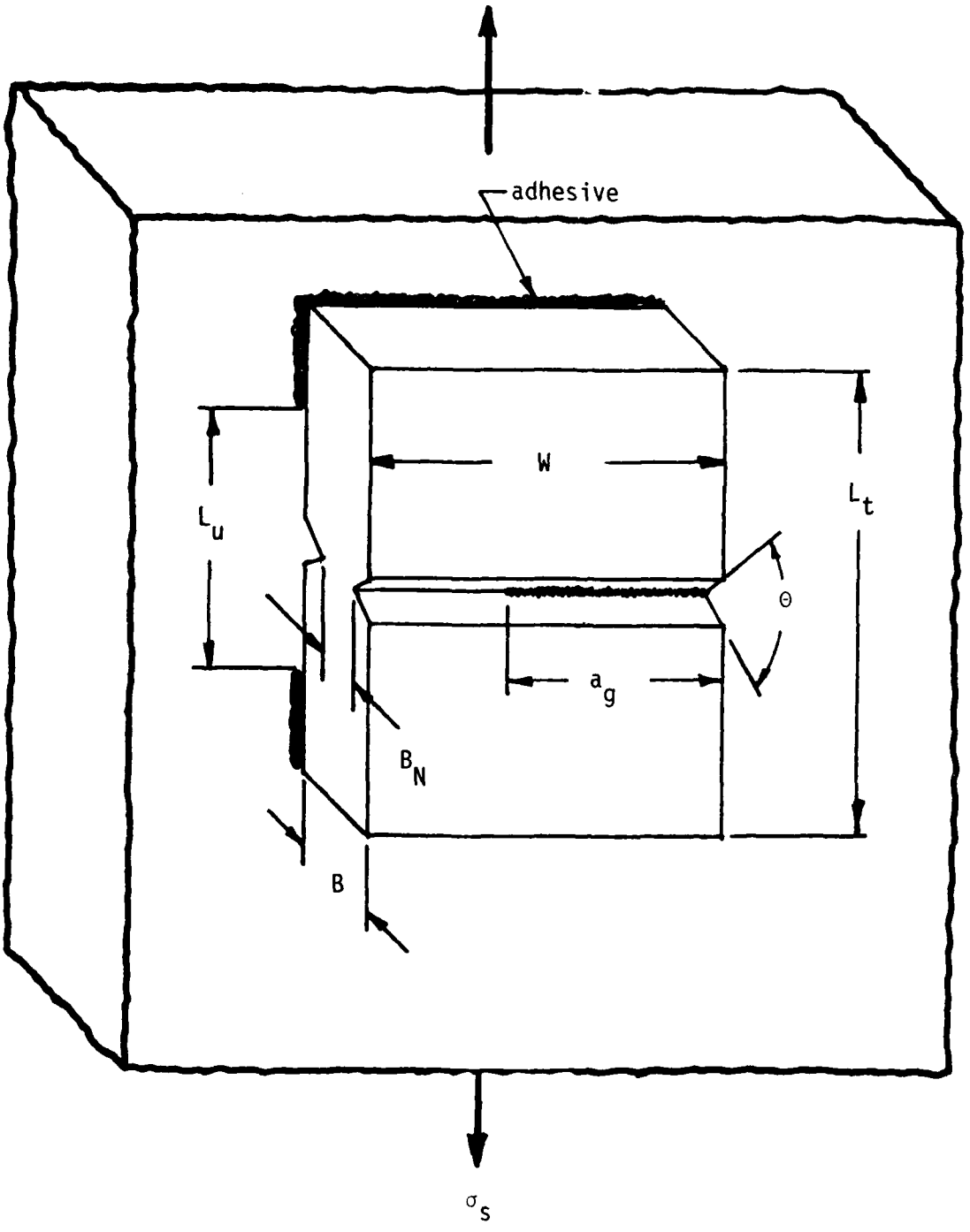

Figure 4 Schematic view of side-grooved crack growth gage bonded to structural component

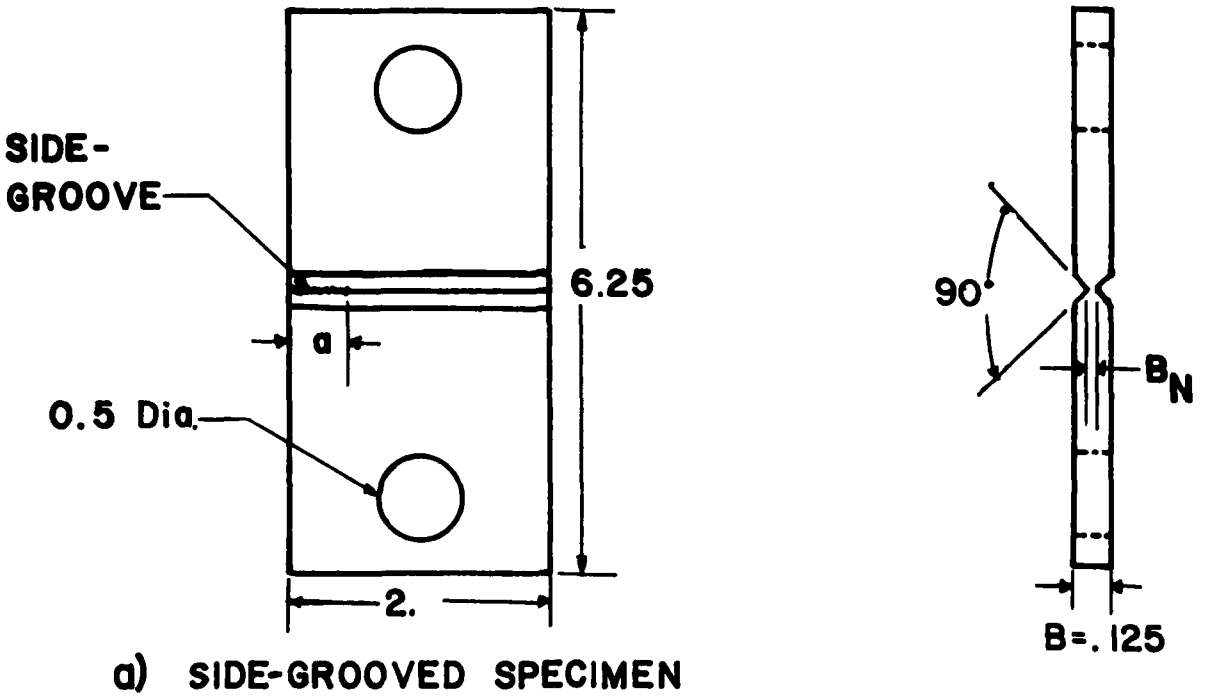

a) SIDE-GROOVED SPECIMEN

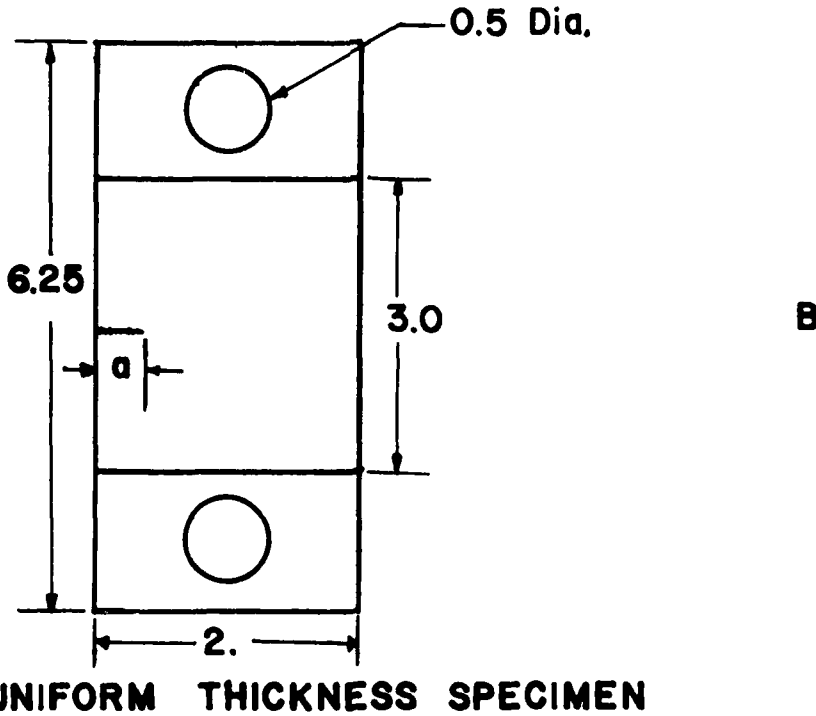

b) UNIFORM THICKNESS SPECIMEN

Figure 5 Side-grooved and uniform thickness test specimens employed for fatigue crack retardation experiments (all dimensions in inches)

2. PRELIMINARY SIDE-GROOVE RESEARCH

Several experiments and analyses were conducted to verify that side-grooves would provide the desired "thick section" fatigue crack growth behavior, and to characterize various side-groove parameters needed to design an appropriate crack growth gage. Those preliminary considerations are briefly summarized below.

a. Retardation Experiments

The main purpose of the side-grooves is to provide plane strain conditions in thin coupons which give crack tip plastic zone sizes and fatigue crack retardation behavior similar to that seen in the thicker structural component. To verify this concept, a series of peak overload experiments were conducted with side-groove and uniform thickness specimens of various thicknesses.

All specimens were machined from a single sheet of 0.125 in. thick 7075-T6 aluminum to the dimensions shown in Figure 5. At least one side-groove and one reduced thickness specimen were tested in thicknesses of 0.025, 0.030, and 0.050 in. Baseline fatigue crack growth tests were also conducted in the original 0.125 in. thickness with a 3.0 by 12.0 in. specimen. With one exception (a center crack geometry), all specimens were tested in a single edge-crack tension configuration. The 90° side-grooves and reduced specimen thicknesses were obtained by standard machining methods, with light cuts taken to minimize residual stresses. Starter notches were cut with a 10/0 jeweler's blade in a manner which oriented all cracks perpendicular to the sheet rolling direction. All specimens were lightly sanded to remove surface scratches and polished with alumina micropolish to facilitate crack length measurement. The specimens were pinned at each end and loaded in cyclic tension on a

10,000 pound capacity MTS electrohydraulic fatigue machine. The cyclic frequency was either 10 or 15 H_z and the load ratio (R = minimum/maximum load) was fixed at 0.05. The retardation experiments were conducted under constant cyclic stress intensity factory (ΔK) conditions by load shedding techniques. Reducing load at predetermined crack lengths allowed ΔK to be maintained within five percent of a specified value for all crack lengths. A nominal K_{max} of 15 ksi-in$^{1/2}$ was selected for the baseline cycling since it yielded a convenient fatigue crack growth rate on the order of 2×10^{-5} in./cycle.

After a uniform crack growth rate was established under the constant ΔK loading, single peak overloads with an overload ratio of 2.0 (K_{peak} = 30 ksi-in$^{1/2}$) were applied. By conducting the tests under constant ΔK conditions, the delay period caused by the overload was readily determined from the linear fatigue crack growth curves. The constant ΔK loading also permitted repetition of overload tests on a single specimen by avoiding K-gradient difficulties which would be encountered with different crack lengths in specimens loaded under remote load (increasing ΔK) conditions.

Figure 6 shows a typical fatigue crack growth curve for a set of 0.03 in. thick side-grooved and uniform thickness specimens. Note both the linear crack growth curves achieved by the constant ΔK loading and the significant delay periods caused by the peak overload. Similar results for other specimen thicknesses are given in Reference 23. The delay period N_D is summarized in Figure 7 as a function of specimen thickness for the various side-grooved and uniform thickness specimens.

Two points are readily apparent from Figures 6 and 7. First, as expected, the uniform thickness specimens showed a significant increase

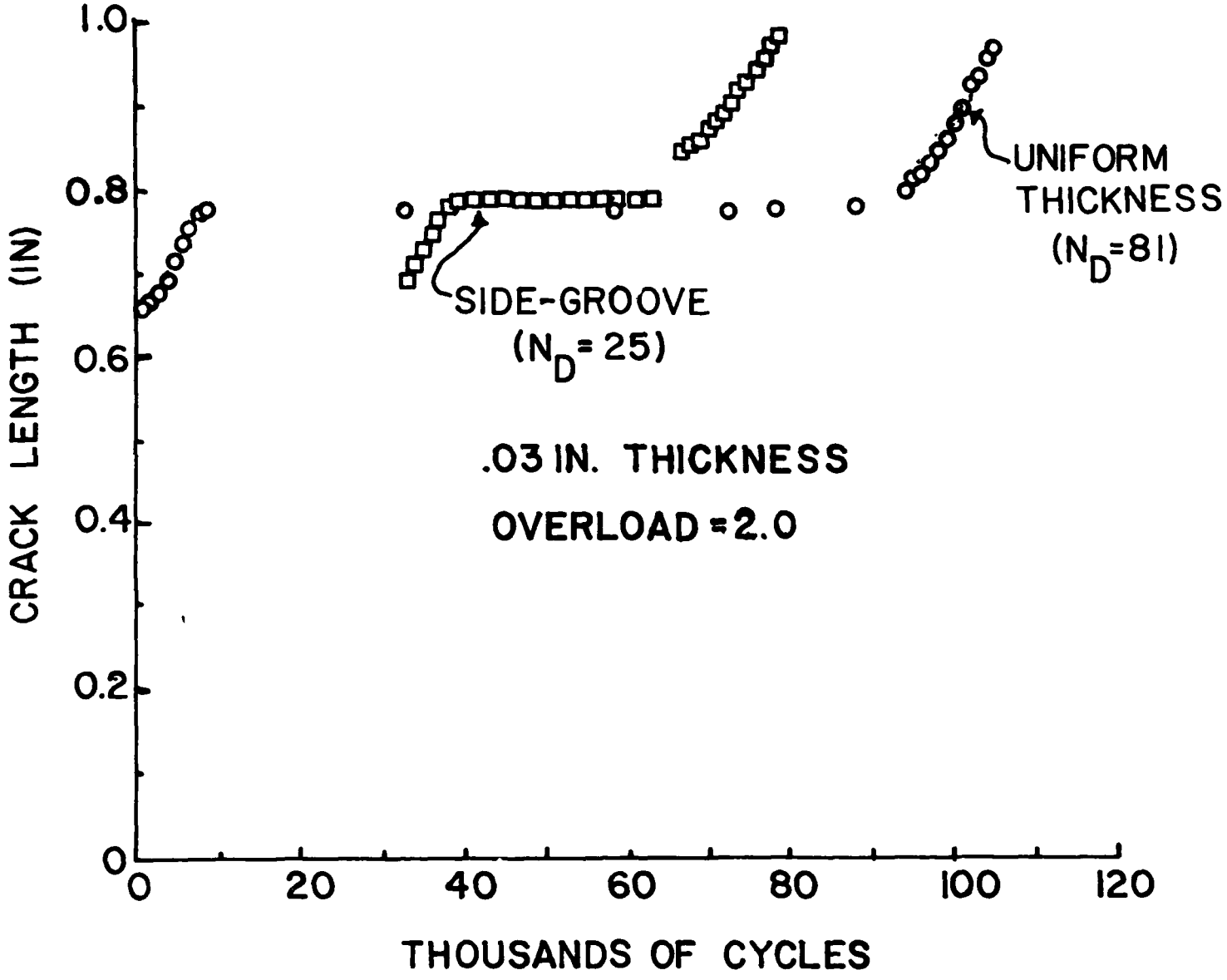

Figure 6 Comparison of fatigue crack retardation for side-grooved and uniform thickness specimen (thickness = 0.03 inch)

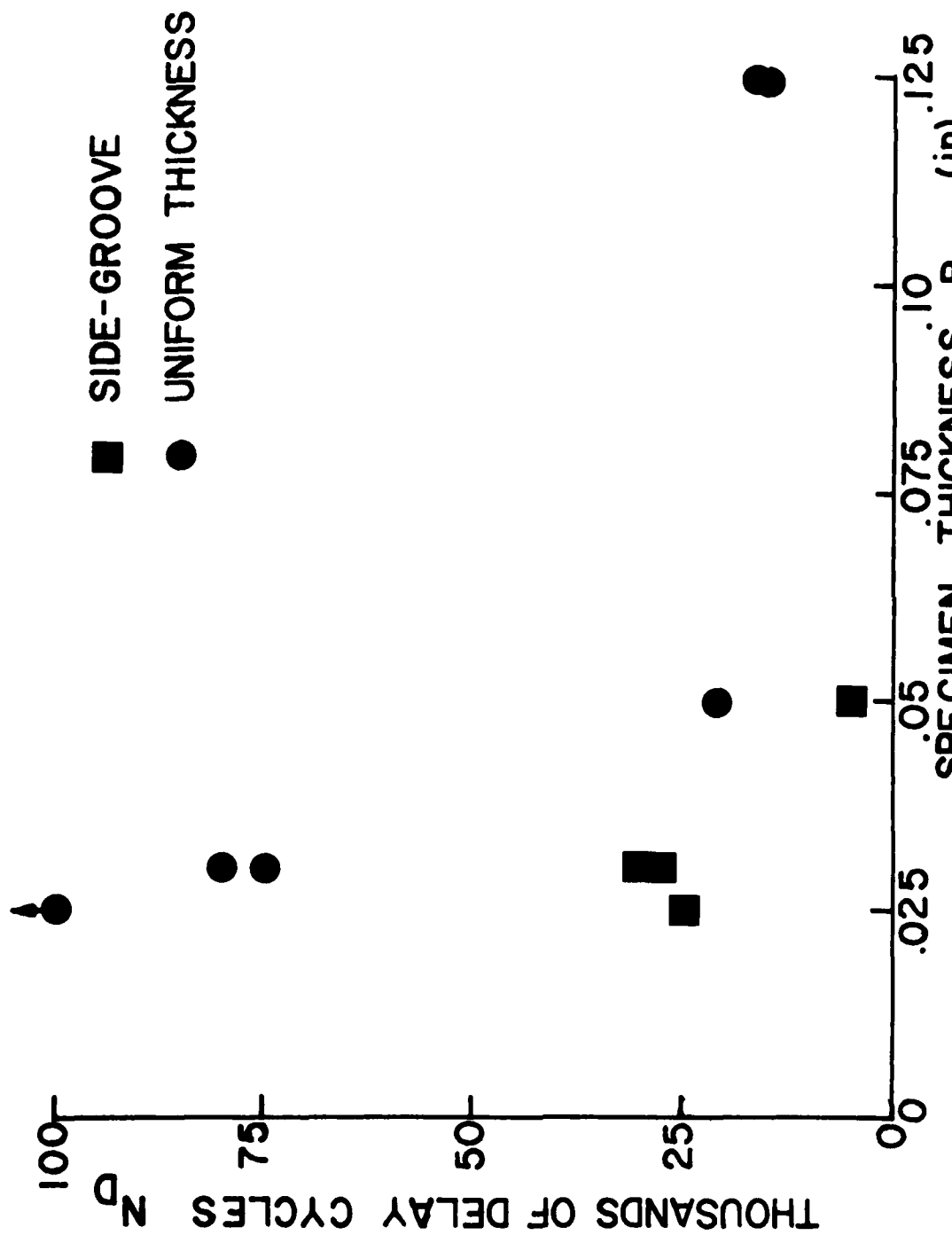

Figure 7 Summary of retardation tests (overload ratio = 2) showing reduction in delay caused by side-grooves as function of specimen thickness

in delay cycles as the specimen thickness decreased. (Recall that the baseline K_{max} was fixed at 15 ksi-in$^{1/2}$ and that the overload ratio was 2.0 for all cases). Second, the side-grooved specimens demonstrated much less retardation than the comparable uniform thickness specimen. The effectiveness of the side-grooves in reducing fatigue crack retardation is especially dramatic for the 0.025 in. thick specimens. The side-groove member gave 25,000 delay cycles, while the companion uniform thickness specimen gave at least 190,000 delay cycles. (A malfunction in the testing machine forced termination of that test, with no observed crack growth following the overload). Thus, these tests clearly demonstrate that side-grooves provide an effective means for providing thick section fatigue crack retardation behavior in thin test sections. (Additional results and details are discussed in References 7 and 23.)

b. Crack Length Measurement

All crack length measurements were made with the aid of a low power microscope. It was observed that crack tips were more difficult to locate in the side-grooved than in the uniform thickness specimens. Since ease of crack length measurement is a factor in crack gage applications, several crack detection methods were examined, including: cellulose acetate replicas, stereo microscope examination, Fractomat electrical resistance metal foil Krack-Gages, and dye penetrants. During preliminary side-groove gage testing, a conventional red dye penetrant (Magnaflux spotcheck) was found to provide a simple and effective means for highlighting the fatigue crack tip at the bottom of the side groove. All remaining experiments with the side-groove crack gages used the dye penetrant, along with a low power traveling microscope, to detect and measure crack lengths in the side grooves.

c. Finite Element Analysis

Finite element analyses were conducted to confirm that the side-grooves simulate plane strain conditions in thin test sections, and to study the effect of various side-groove parameters. Although only the uncracked configuration was considered, the results support the experimental observations regarding fatigue crack retardation in side-grooved specimens.

The two-dimensional analyses were conducted with the SAP IV computer program [24]. A typical finite element mesh is shown in Figure 8. Since both the x and y axes are lines of symmetry, only one quarter of the side-groove specimen was modeled in this case. The z-direction strain was assumed to be zero for purposes of the two-dimensional analysis. The goal here was to compare the x-direction strain distribution for the side-grooved and uniform thickness specimen. Although only strain distributions are given here, stresses were also examined. Stress concentration factors computed at the root of the side-groove agreed well with handbook values [25, 26] and served to verify the accuracy of the finite element model [7].

Several combinations of side-groove depth (B/B_N), notch radius (ρ/B_N) and flank angle θ were examined (See Figure 8). Typical strain distributions are given in Figures 9 and 10. Here the x-direction strains along the y = 0 plane are presented as a function of $2x/B_N$. The strains are presented in terms of the ratio $\varepsilon_{XSG}/\varepsilon_{XUT}$, where ε_{XSG} is the x-component of strain for a side-grooved specimen and ε_{XUT} is the strain resulting for a member of uniform thickness B.

The results in Figure 9 are for the $\theta = 90°$ flank angle used for the retardation experiments and for a dimensionless notch radius

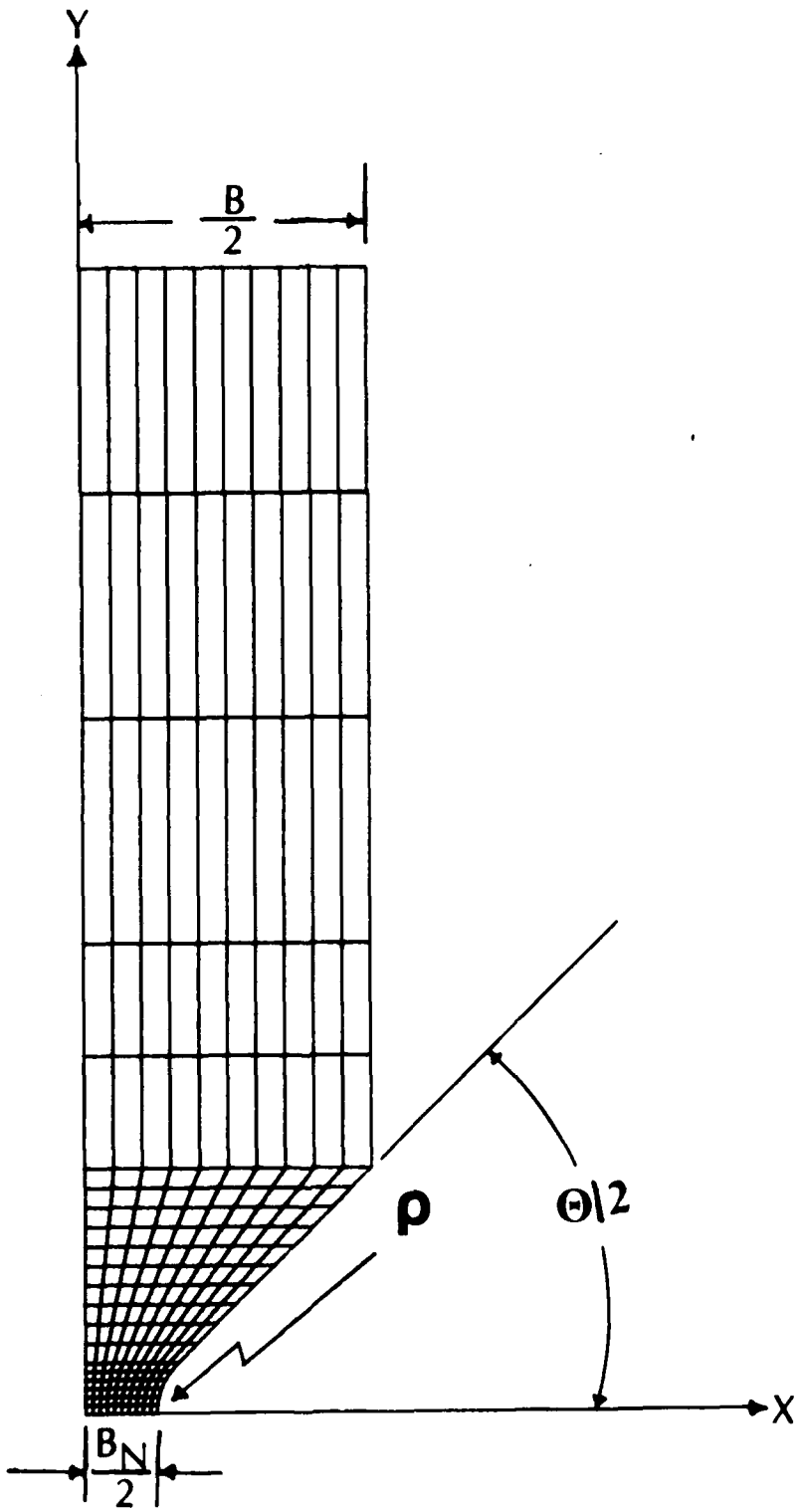

Figure 8 Typical finite element model for one quarter of uncracked symmetric side-groove configuration ($B/B_N = 4$, $\rho/B_N = 0.5$)

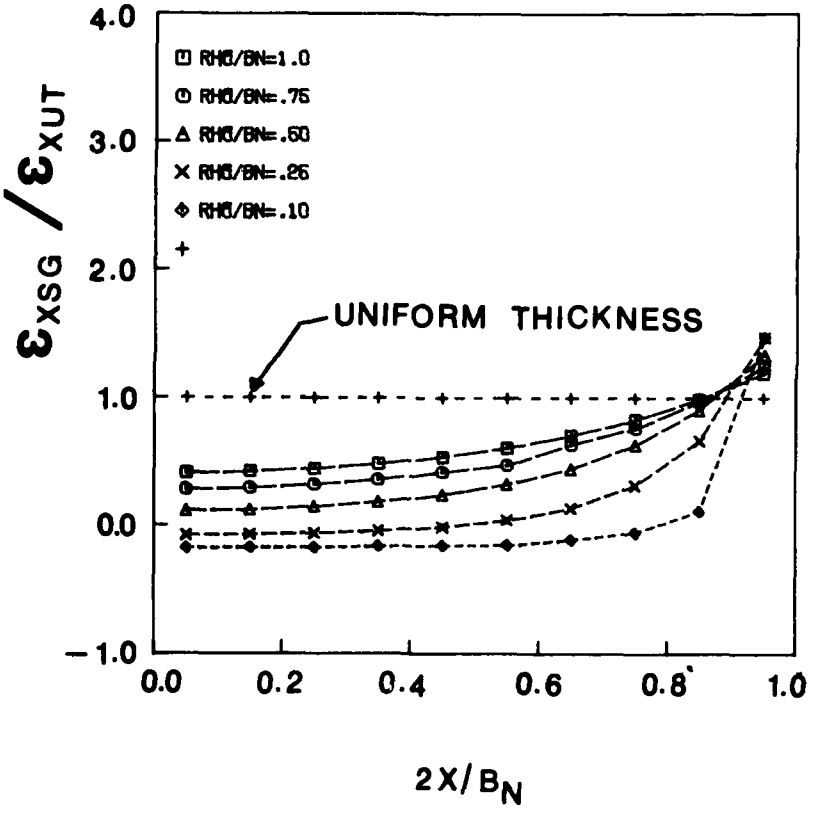

Figure 9 Effect of side-groove depth on X-direction dimensionless strain distribution (ρ/B_N = 0.5) showing reduction in strain due to side-grooves

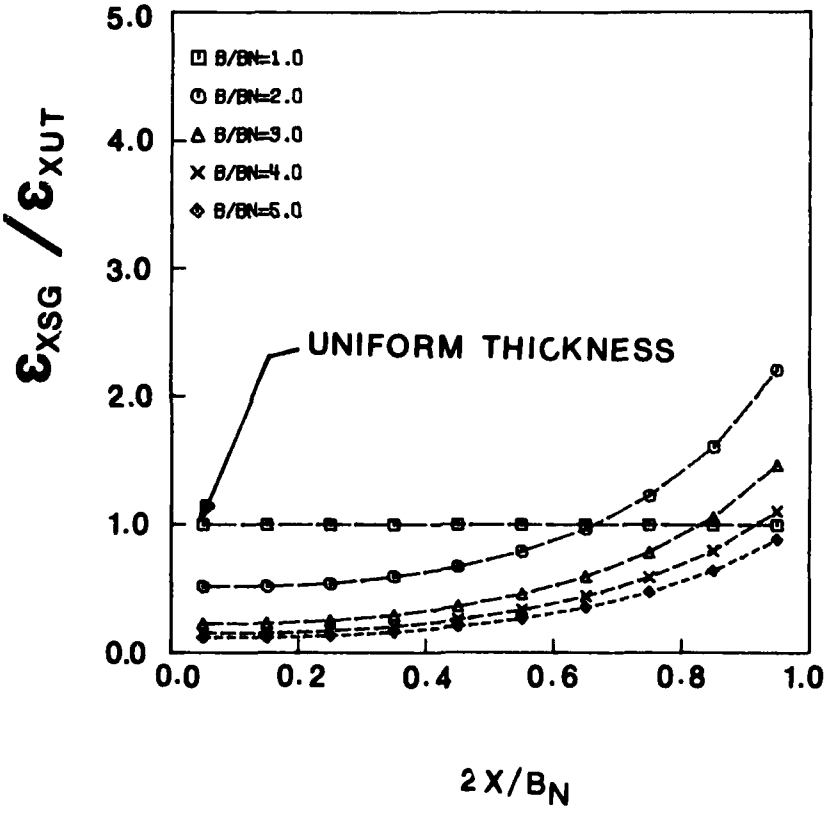

Figure 10 Effect of dimensionless side-groove root radius ρ/B_N on X-direction strain distribution (B/B_N = 4.)

$\rho/B_N = 0.5$. (The test retardation specimens had measured radii in the range $0.1 \leq \rho/B_N \leq 0.5$.) Note that results for the different side-groove depths (as expressed by B/B_N) indicate that the side-grooves effectively reduce the x-direction strain over a substantial portion of the specimen thickness. Moreover, conditions of plane strain ($\varepsilon_{XSG}/\varepsilon_{XUT} = 0$) are approached for the deeper side-grooves ($3 \leq B/B_N \leq 5$).

Figure 10 gives results for different notch radii ($\theta = 90°$, $B/B_N = 4.0$ for these cases). Note that although an order of magnitude change in groove root radius was considered ($0.1 \leq /B_N \leq 1.0$), strain distributions are considerably below the uniform thickness result ($\varepsilon_{XSG}/\varepsilon_{XUT} = 1.0$), except immediately at the notch root ($2x/B_N = 1.0$).

3. GAGE DESIGN CONSIDERATIONS

Since the preliminary analyses and experiments indicated that side-grooves promote plane strain conditions in thin sections, and are effective for reducing thickness dependent fatigue crack retardation, efforts next focused on designing a side-grooved crack growth gage.

The two basic designs shown in Figure 11 were considered. The double side groove (designated DSG) configuration shown in Figure 11a is a symmetric shape with side-grooves on both front and back surfaces. One face would be bonded to the structural member, leaving an unbonded length L_u. Since the fatigue crack retardation experiments indicated some difficulty in measuring crack lengths along the bottom of the side-grooves, the single side-groove (SSG) configuration shown in Figure 11b was also considered. In this case, the grooved side of the gage would be bonded to the parent structure, leaving the flat surface exposed for crack length measurement. It was hoped that the single side-groove gage would combine the plane strain advantages of the

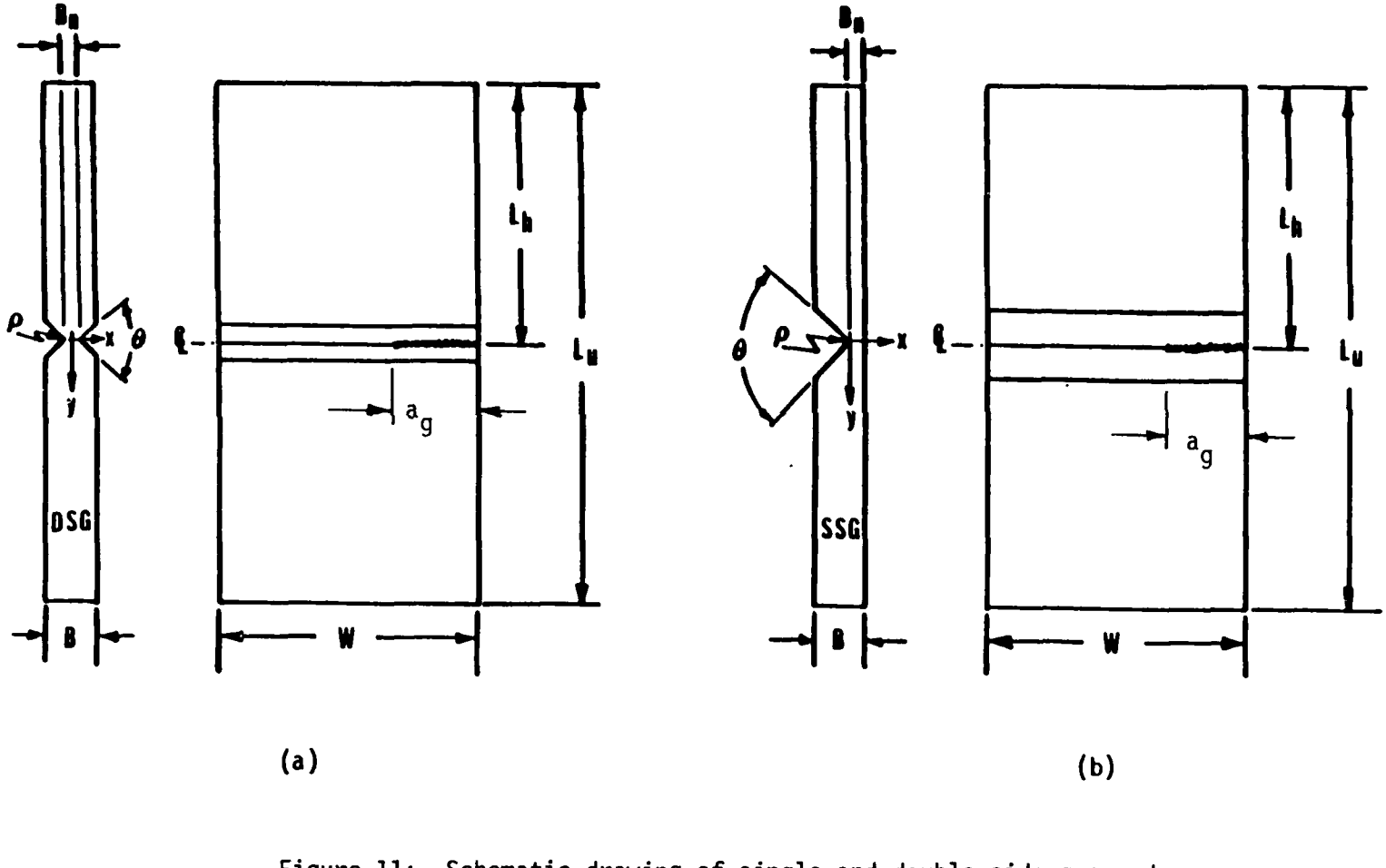

Figure 11: Schematic drawing of single and double side-grooved crack gages

side-grooves with the relative ease of crack detection associated with the flat surface, since the flat surface could be readily polished to aid crack length measurements. (Due to other difficulties described later, the single side groove geometry did not perform satisfactorily in the crack gage tests). A few other configurations, employing combinations of semi-circular and V-notched side-grooves were initially considered as described in Reference 7, but eventually rejected.

The crack gage parameters shown in Figures 4 and 11 are the width W, unbond length L_u, total length L_t, net thickness after side-grooving B_N, original thickness B, groove root radius ρ, and side-groove angle θ. For simplicity, it was decided to employ an edge crack (length a_g) for the gage flaw. The finite element model described in the previous section was used to study the effect of various gage parameters as summarized in Tables 1 and 2. The gages were assumed to be uncracked for these analyses, since the main goal was to determine the effect of side-groove parameters on promoting plane strain conditions. In addition, the coupons were assumed to be loaded in remote tension at this stage of the design. The effect of load transfer through the adhesive and the influence of the unbond length were considered later.

Typical strain distributions were described earlier in Figures 9 and 10; additional results are provided in Reference 7. The results of this parametric study indicate that the side-groove depth B/B_N and root radius ρ/B_N are the main terms which influence gage behavior. Plane strain conditions are approached as $B/B_N \geq 3.$ and $\rho/B_N \geq 0.5$. As discussed later, the unbond length L_u also has a significant role. The flank angle θ had little effect over the range considered. Similar observations are reported in References 17 to 20.

Table 1: Matrix of double side grooved gages modeled by finite element method (ρ/B_N = 0.5)

B/B_N	45°	60°	90°	120°
2.		+	++	+
3.		+	++	+
4.	+	+	++	+
5.		+	++	+

++Analyses were also performed for single side grooved gages.

Table 2: Matrix of side grooved gages modeled by finite element method (θ = 90° and B/B_N = 4.)

ρ/B_N	single side groove	double side groove
1.00	+	+
.75	+	+
.50	+	+
.25	+	+
.10	+	+
.05	+	+
.01	+	+

Practical considerations led to selecting the specimen width W as 2.0 in. and the net thickness B_N as 0.03 in. Experience with the preliminary side-groove retardation tests indicated the dimensionless root radius would fall in the range $0.1 \rho/B_N \leq 0.5$. The gages were to be made from a 0.125 in. thick sheet of 7075-T6 aluminum. It was decided to manufacture and test two variations of the double and single side-groove geometries, leading to the four configurations designated below.

SSG2 - single shallow side-grooved gage ($\frac{B}{B_N} \approx 2$).

SSG4 - single deep side-grooved gage ($\frac{B}{B_N} \approx 4$).

DSG2 - double shallow side-grooved gage ($\frac{B}{B_N} \approx 2$).

DSG4 - double deep side-grooved gage ($\frac{B}{B_N} \approx 4$).

Eventually, based on experiments with adhesively bonded crack gages described in the next section, only the SSG4 and DSG4 configurations were examined in detail.

4. CARRIER EXPERIMENTS

Extensive tests were conducted with side-grooved crack growth gages mounted to simulated structural components. The goal of these tests was to determine the relationship between the gage and structural flaws as functions of gage geometry and specimen loading. The description and results of those tests are briefly summarized in the remainder of this section. Additional details and results are reported in Reference 7.

a. Compact Carrier Tests

Five preliminary tests were conducted with single side-grooved specimens bonded in pairs to the front and back of dogbone shaped carrier specimens as shown schematically in Figure 12. The carrier specimens,

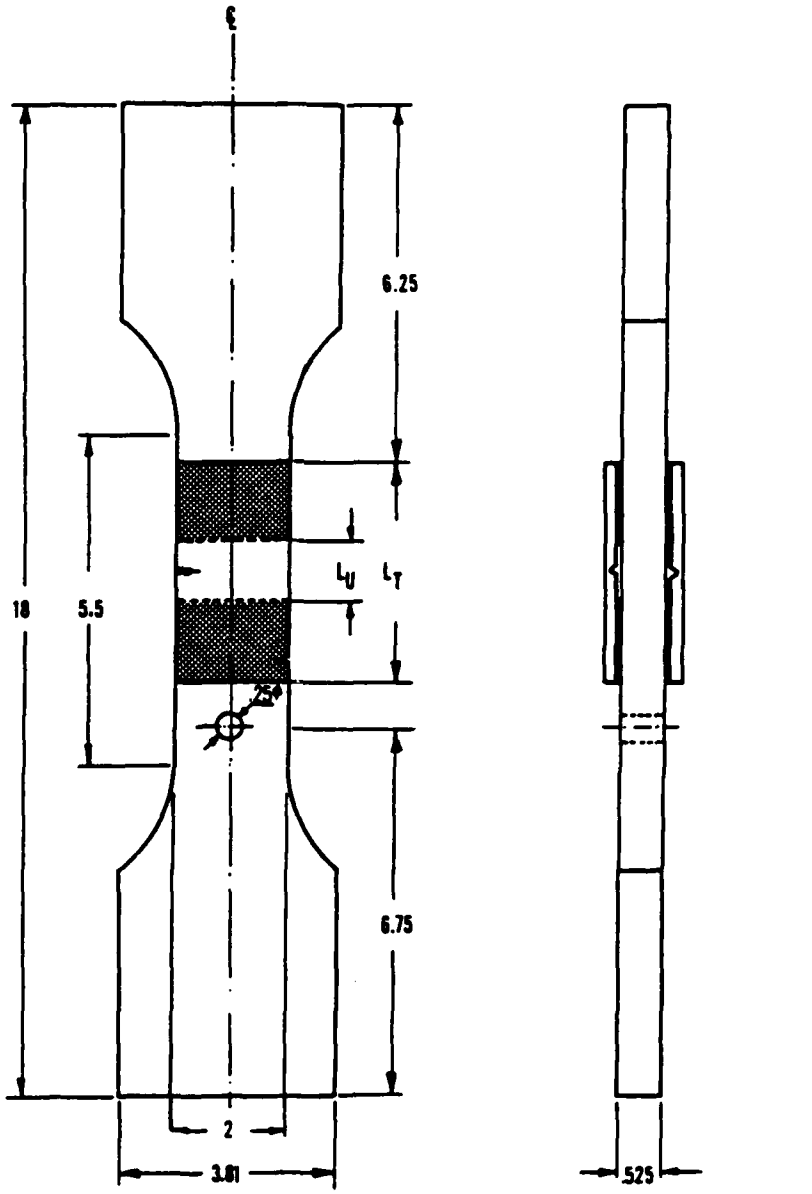

Figure 12: Compact carrier specimen with two single side-groove crack gages bonded to front and rear surfaces.

which were intended to simulate a structural member loaded in remote tension, had a 2.0 x 0.525 in. test section and were 18 inches long. As reported in Reference 7, the gages were bonded to the carrier with Thermoset 103 adhesive and employed various unbond lengths and B/B_N ratios. Since the objective here was to gain experience with testing side-grooved crack gages, the testing was preliminary in nature, and only the side-grooved coupons were precracked. Although considerable practical experience was gained from these tests, difficulties encountered with the adhesive prevented detailed quantitative analysis of the results. Typical crack growth curves are discussed in Reference 7.

b. Large Carrier Developmental Test Program

The main test program involved experiments with the large carrier specimens shown schematically in Figures 13 to 15. As indicated, the simulated structural members were 32 in. long, 3.9 in. wide, and 0.375 in. thick. All carrier specimens were made from 7075-T651 aluminum and contained a nominal 0.03 in. precrack emanating radially from a 0.375 inch diameter open hole. The hole was located offset from the centerline so that crack growth tended toward a symmetric configuration when a remote cyclic tensile force was applied. These carrier specimens were prepared by the University of Dayton Research Institute (UDRI) and were similar to those tested in their companion program [27].

Four side-groove crack growth gages were bonded in pairs to the front and back of the carrier specimens as shown in Figures 13 to 15. Most tests were conducted with the symmetric pairs of SSG4 and DSG4 crack gages shown in Figure 15, although a few specimens employed the thinner SSG2 and DSG2 crack gages. All side-groove coupons were precracked by

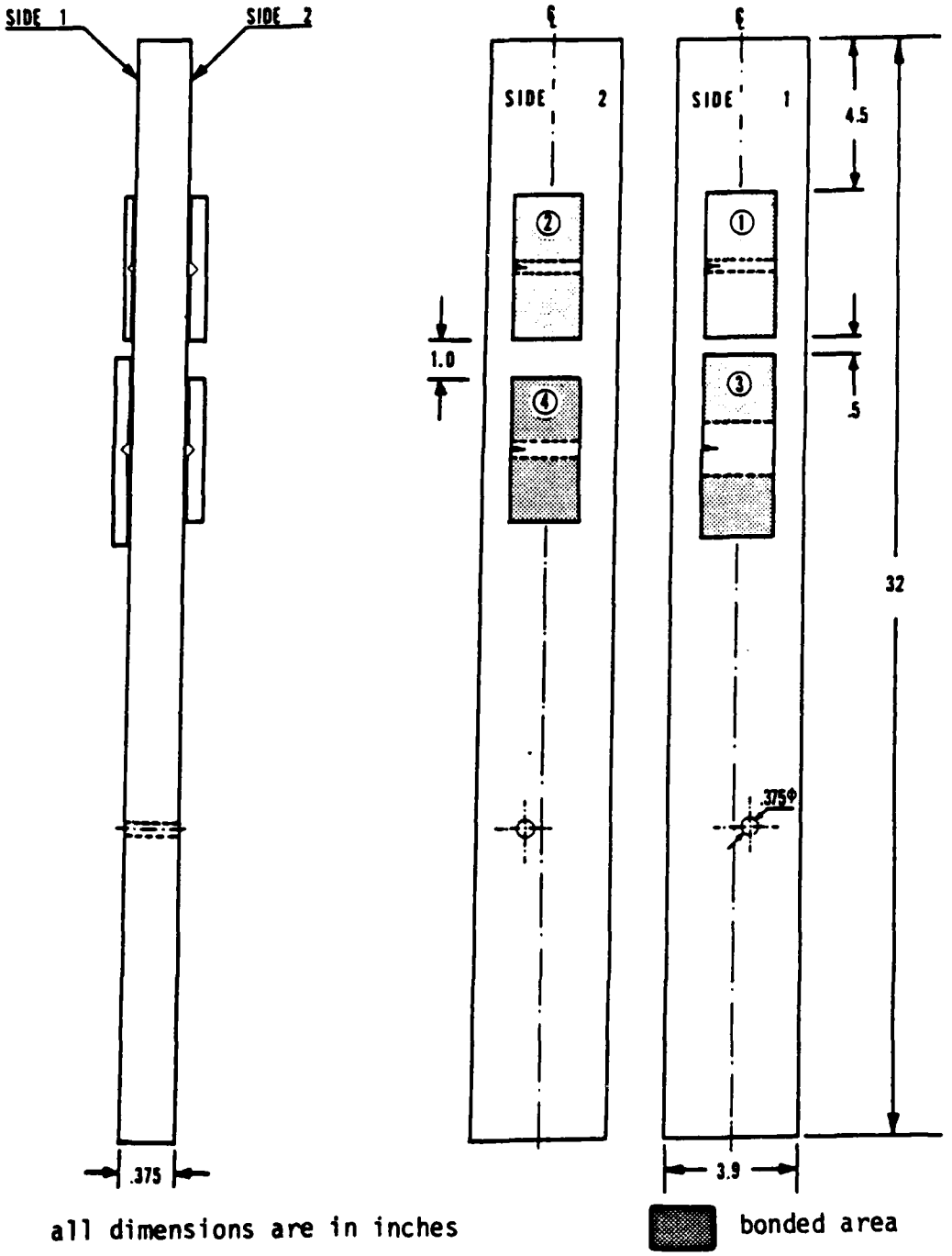

Figure 13: Large carrier specimen with four different single side-grooved crack gage configurations, typical of Tests 29 and 49.

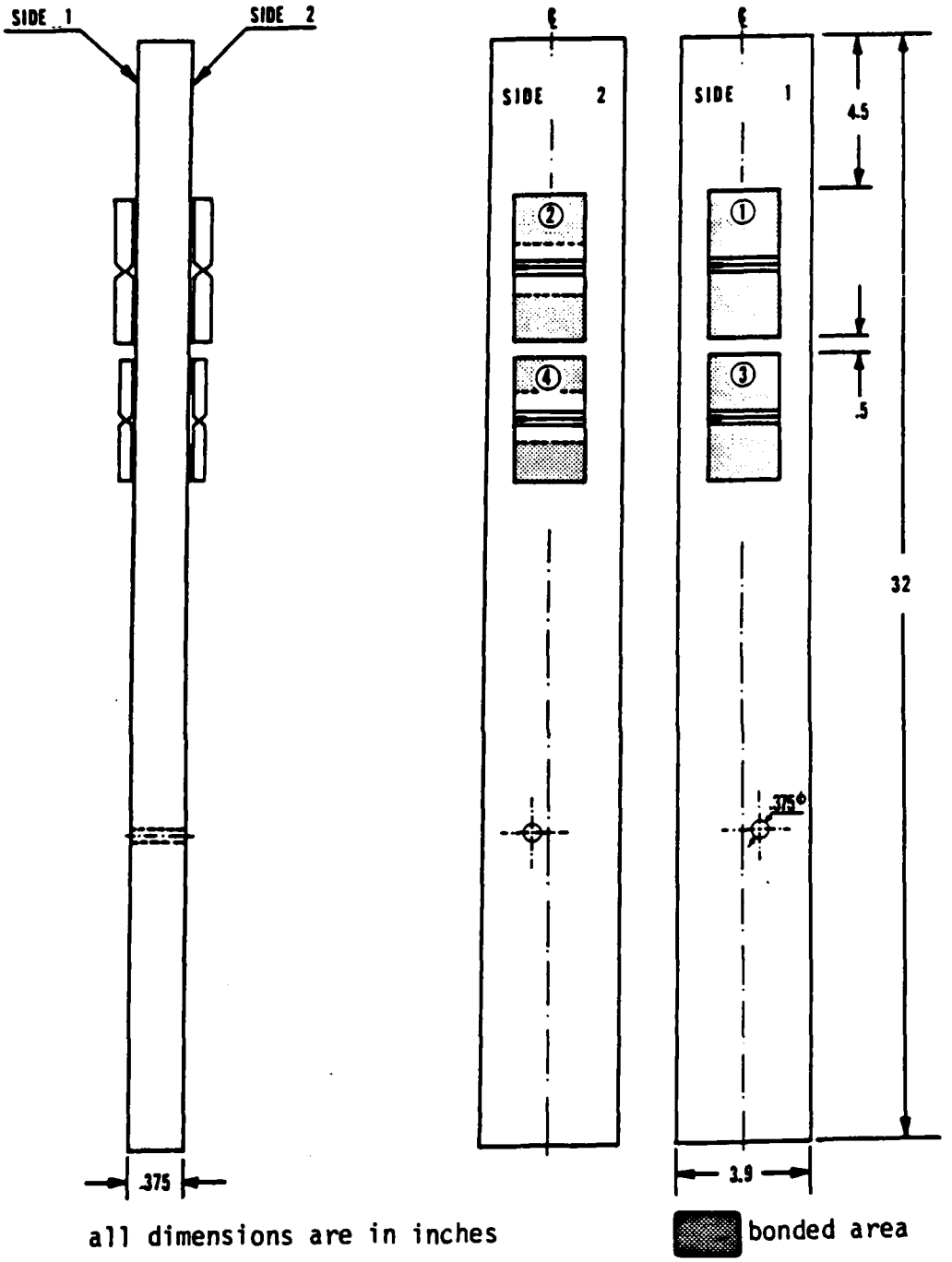

Figure 14: Large carrier specimen with four different double side-grooved crack gage configurations, typical of Tests 28 and 48.

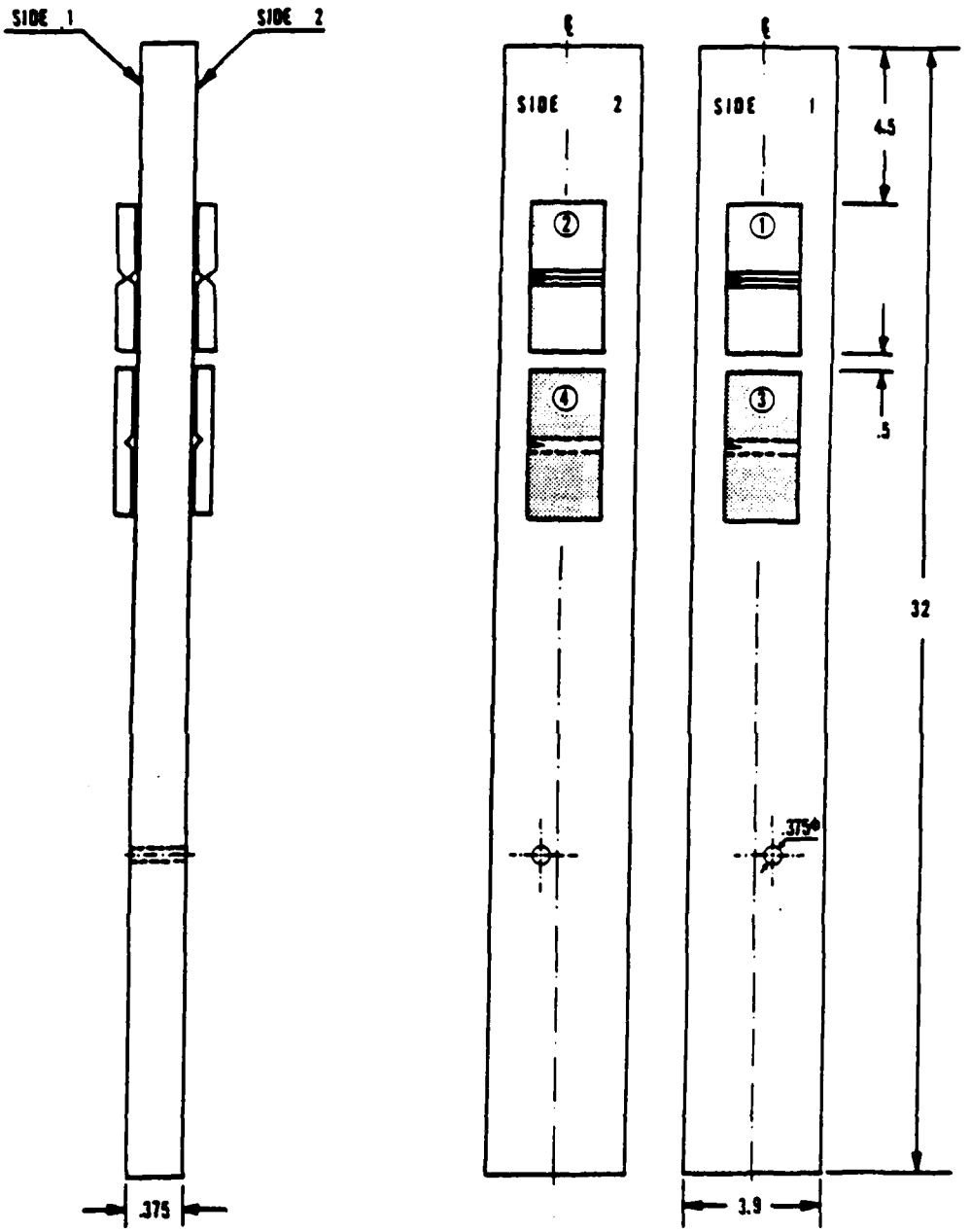

Figure 15: Large carrier specimen with two double and two single deep side-grooved gages (DSG4 and SSG4)

Purdue University, with special care taken to slowly reduce test loads to avoid crack retardation during precracking. The crack gages were then shipped to UDRI, who bonded them to the precracked carrier specimens. All large carrier specimen bonding employed the FM-73 adhesive and followed carefully controlled procedures [27].

Eighteen of these large carrier specimens were tested following the loading matrix given in Table 3. Here seven specimens were subjected to constant amplitude cyclic loading at either a 16 or 25 ksi maximum stress at one of three mean stress values (R = -0.1, 0.1, or 0.3). Two specimens were tested at the 22 ksi, R = 0.1 condition. Companion specimens were also subjected to similar constant amplitude loadings, except that 50 percent tensile peak overloads were applied to determine the effects of fatigue crack retardation on the crack gage/structural flaw response. Three specimens were subjected to variable amplitude load histories chosen to represent typical spectra expected to be seen by a fighter aircraft [27].

With the exception of the three variable amplitude tests,which were conducted by the University of Dayton Research Institute, all carrier specimens were tested at Purdue University with a 55 kip MTS electrohydraulic test machine. The specimens were loaded through hydraulic actuated grips and illuminated with a fiber optics light source. Travelling microscopes were mounted on moveable fixtures on each side of the specimen and, at periodic cyclic intervals, used to measure the six crack lengths (four gage cracks and front and back side of the cracked hole structural flaw). A photograph of the test apparatus is given in Figure 16. The structural specimen and the single side-groove gages were polished to aid in crack

Table 3 Summary of Large Carrier Tests with Side-Grooved Crack Gages

Loading	Spectra Tests	16 Ksi Max Stress			22 Ksi Max Stress			Load Transfer (uncracked)	
		R = -.1	.1	.1	R = -.1	.1	.3		
constant amplitude		27	28	29	30	31A, 31	32	33	34
50% overload		47	48	49	50	51	52		
T38-Mild	55								
T38-Baseline	58								
T38-Severe	61								

Comments

1. Tests 28 and 48 employed all double side-grooved gages with various unbond lengths.
2. Tests 29 and 49 employed all single side-grooved gages with various unbond lengths.
3. All remaining tests employed 1 pair of double-side groove gages and 1 pair of single side-grooved gages with fixed unbond lengths.
4. Spectra tests 55, 58, 51 were conducted by the University of Dayton Research Institute.

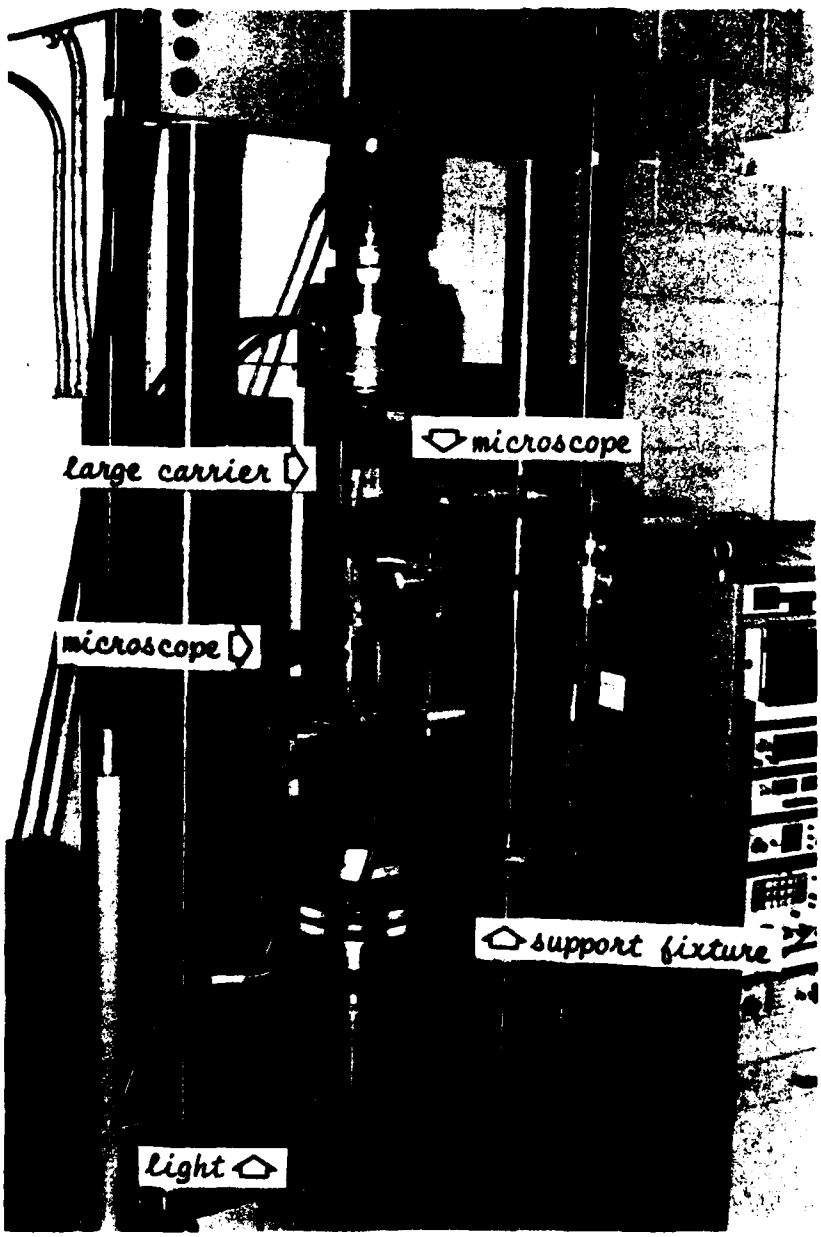

Figure 16: Photograph of carrier specimen test apparatus

length measurements, while, as discussed previously, a dye penetrant was used to assist crack length measurement in the double side-groove specimens. The total time required to measure and record all six crack lengths, including application of dye penetrant, was approximately 15 to 20 minutes.

As indicated in Table 3, Specimens 33 and 34 were used for load transfer measurements, and the side-groove coupons were not precracked. The parent structure and bonded coupons were instrumented with strain gages as shown in Figures 17 and 18, and subjected to a series of static tensile loads. The strain gage readings verified that uniform tension was applied to the large carrier specimens, and also provided an experimental measure of the force transferred into the side-groove coupons through the adhesive bond. Different unbond lengths (L_u), ranging from 0.375 in. to 3.0 in., were used for these series of tests to determine the effect of unbonded length on the crack gage load.

The results of these load transfer tests are given in Figure 19. Here the measured strain in the particular crack gage is divided by the measured strain in the structure (average strain at structure locations 5 and 6) and is presented as a function of remote load applied to the test specimen. The legend given in Figure 19 defines the strain gage location, type of crack gage (SSG2, SSG4, etc.), and gage unbond length (LH = half the unbond length = L_u / 2 and is given in inches). The negative strain ratios presented for some of the single side-groove gages (Figure 19a) resulted from bending which occurred in this nonsymmetric configuration. Note in Figure 19b that the double side-groove gages give a load transfer ratio which is independent of applied load. Recall that the adhesively bonded coupons were uncracked for load transfer specimens 33 and 34.

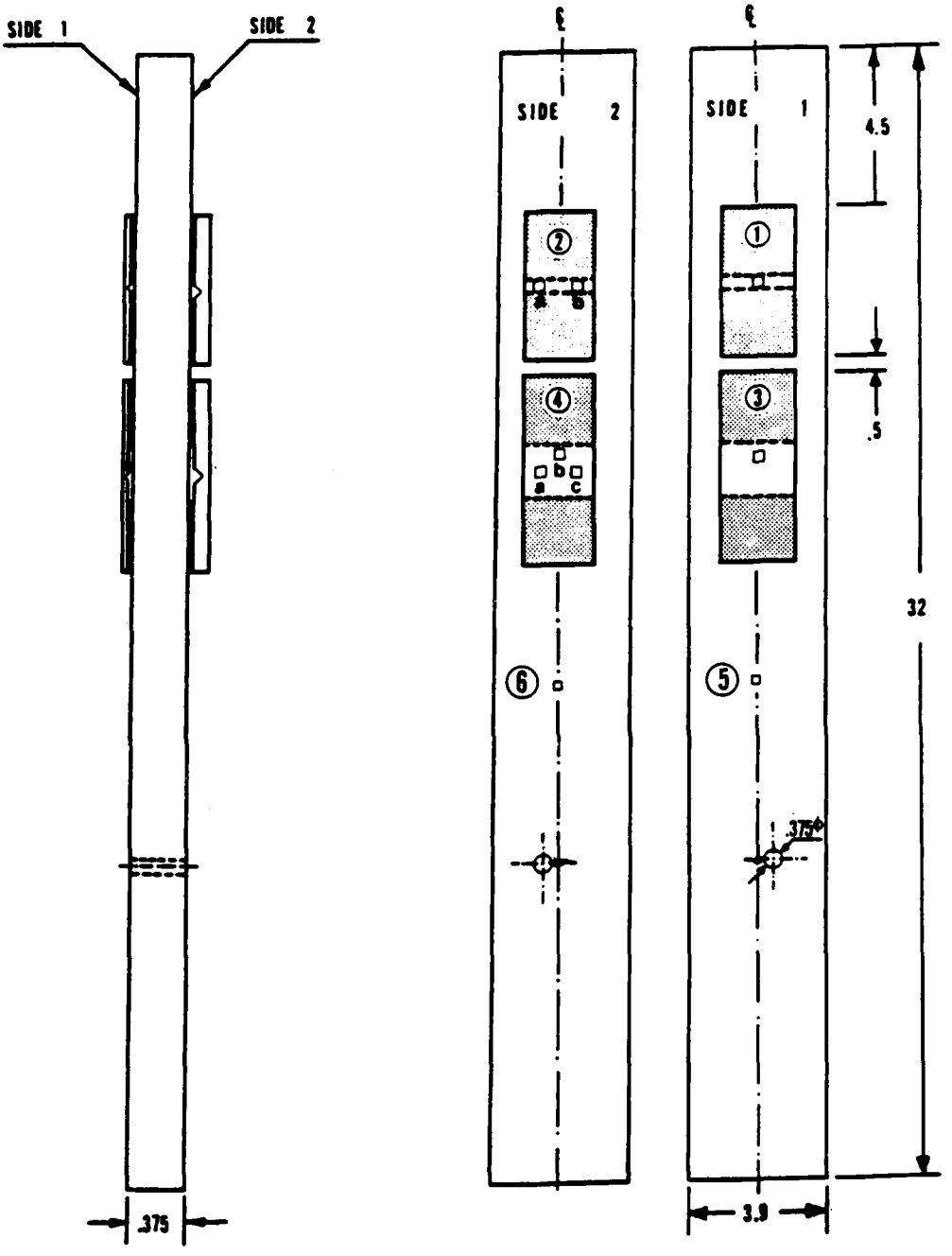

Figure 17: Load transfer carrier Specimen Number 33, showing location of strain gages and single side-grooved crack gages

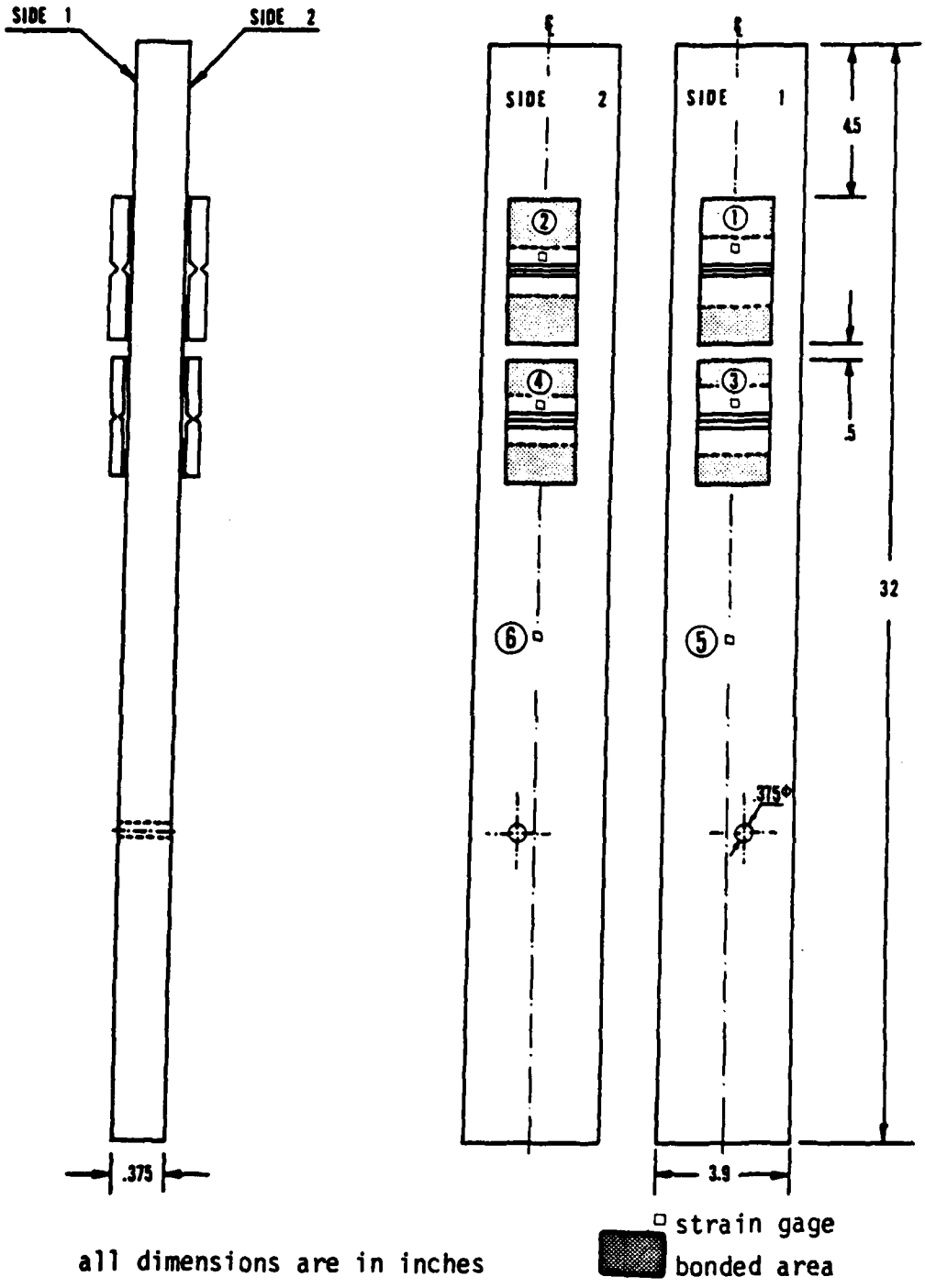

Figure 18: Load transfer carrier Specimen Number 34, showing location of strain gages and double side-grooved crack gages

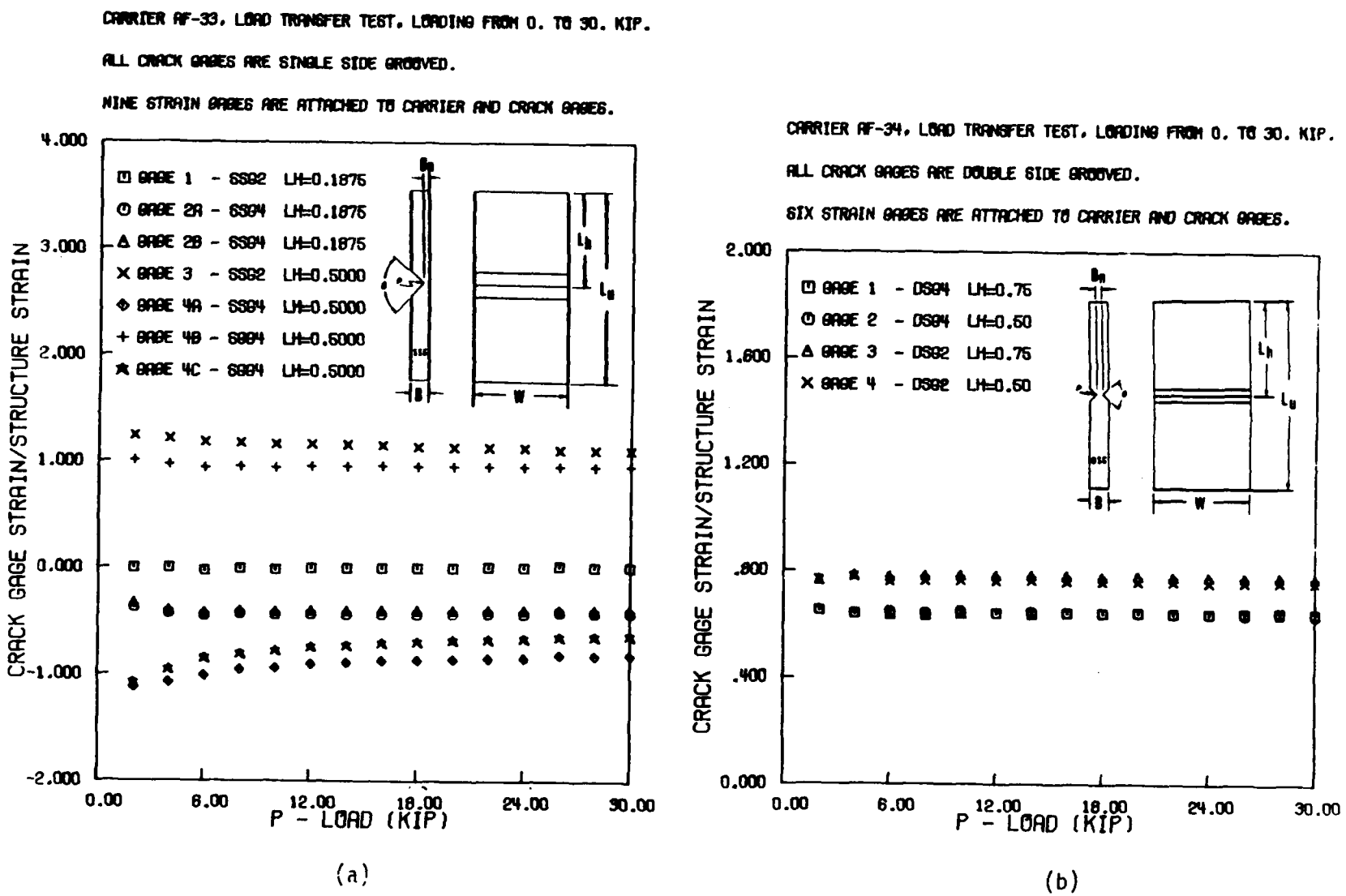

Figure 19: Dimensionless strain gage readings for load transfer tests 33 and 34

Sixteen large carriers were tested with four side-grooved crack gages attached to each carrier. Initially, carrier 31A (see Table 3) was tested with four double deep side-grooved crack gages. All gages had an initial flaw greater than 0.5 inch and a four inch unbonded length. This test was conducted at a 25 ksi cycle stress with R = .1 at a frequency of three hertz. Unfortunately all gages fractured almost immediately due to a higher than expected load transfer. In order to obtain more experience with the bonded side-grooved gages, the compact carriers test plan described in section 3.4.a was established prior to testing any additional large carriers. After the compact carriers had been tested, it was decided that future large carriers would be tested in the following two groups.

(1) Preliminary Tests with Different Gage Geometries

This preliminary group of large carrier tests included specimens 28, 48, 29, and 49. Specimens 28 and 48 (see Figure 14) contained various double side-groove gage configurations, while carriers 29 and 49 (see Figure 13) examined different single side-groove geometries. The results of these initial four tests led to selection of the DSG4 and SSG4 configurations for further testing. (Crack growth curves for this group of preliminary tests are given in Appendix A, and additional discussion of their results is reported in Reference 7).

(2) Verification Tests with a Common Gage Design

The remaining tests summarized in Table 3 employed matched pairs of double side-groove gages (DSG4) and single side-groove gages (SSG4) bonded to the carrier specimen bonded to the carrier specimen as shown in Figure 15. The crack gage unbond length L_u was set at 0.375 in. for these experiments, and different load histories were applied as indicated in Table 3.

The loading variables included mean stress, maximum stress, peak overloads, and variable amplitude cycling.

c. Large Carrier Crack Gage Results

Typical fatigue crack growth curves for the large carrier tests are described in this subsection. Corresponding results for the remaining carrier tests are given in Appendix A.

As discussed previously, crack length measurements were made at periodic intervals for both sides of the structural hole crack and for the four crack growth gage flaws (see Figures 13 to 15). Typical results for Specimens 31 and 51 are given in Figures 20 and 21. The maximum applied stress was 22 ksi (R = 0.1) for both tests. Specimen 31 employed simple constant amplitude loading, while Specimen 51 was subjected to a 50 percent tensile peak overload (see Table 3).

Following a consistent format, Figures 20a and 21a present crack growth measurements for the structural flaw, Figures 20b and 21b give the crack growth curves for the crack gages, 20c and 21c present cross plots of the structural crack size versus the double side-grooved gage flaw (corresponding to the same cyclic life), and Figures 20d and 21d present similar structural crack versus gage flaw size data for the single side-groove coupons. Each figure contains a legend which summarizes the carrier specimen number, the applied load, the measured laboratory temperature and humidity, and identifies the particular crack location and/or gage type. In addition, the gage half unbond length LH is also given (LH = half total unbond length = $L_u/2$). Complete crack gage dimensions are summarized for all of the tests in Reference 7. Some structural crack versus gage crack plots also

contain a solid line defining predictions based on Equation 7. These predictions are discussed in a later section.

5. DISCUSSION OF SIDE-GROOVED GAGE EXPERIMENTS

First consider the typical results obtained from carriers 31 and 51 (see Figures 20 and 21). Carrier 31 was subjected to a 22 ksi applied stress with R = 0.1. The gage cracks propagated at constant rates, with both double side-grooved gages producing the same crack growth rate. The single side-grooved gages revealed a large variation in crack growth rate, and also produced a long and narrow plastic zone ahead of the crack tip. One gage fractured early in the test, while the other SSG crack propagated at the same rate as the double side-grooved gage cracks. Another unexpected behavior occurred when one single side-grooved gage initiated a second crack at the opposite (uncracked) edge of the gage. This crack propagated slowly along the gage centerline. (This phenomenon was repeated in single side-grooved gages mounted to carriers 27, 30, and 50). The structure and gage crack growth data are shown in Figures 20a and 20b. The transfer functions relating gage and structure crack lengths are shown in Figures 20c and 20d for the double and single side-grooved gages respectively.

Carrier 51 was tested under the same conditions as carrier 31, except that a 50 percent peak overload (R_{01} = 1.5) was applied during the test. The overload was applied after a constant crack growth was established in all gages. The overload delayed the structure crack growth for 1500 cycles, while the gage delay was 2000 cycles. The behavior of both double side-grooved gages was identical and consistent with the carrier 31 gages. The single side-grooved gages, again

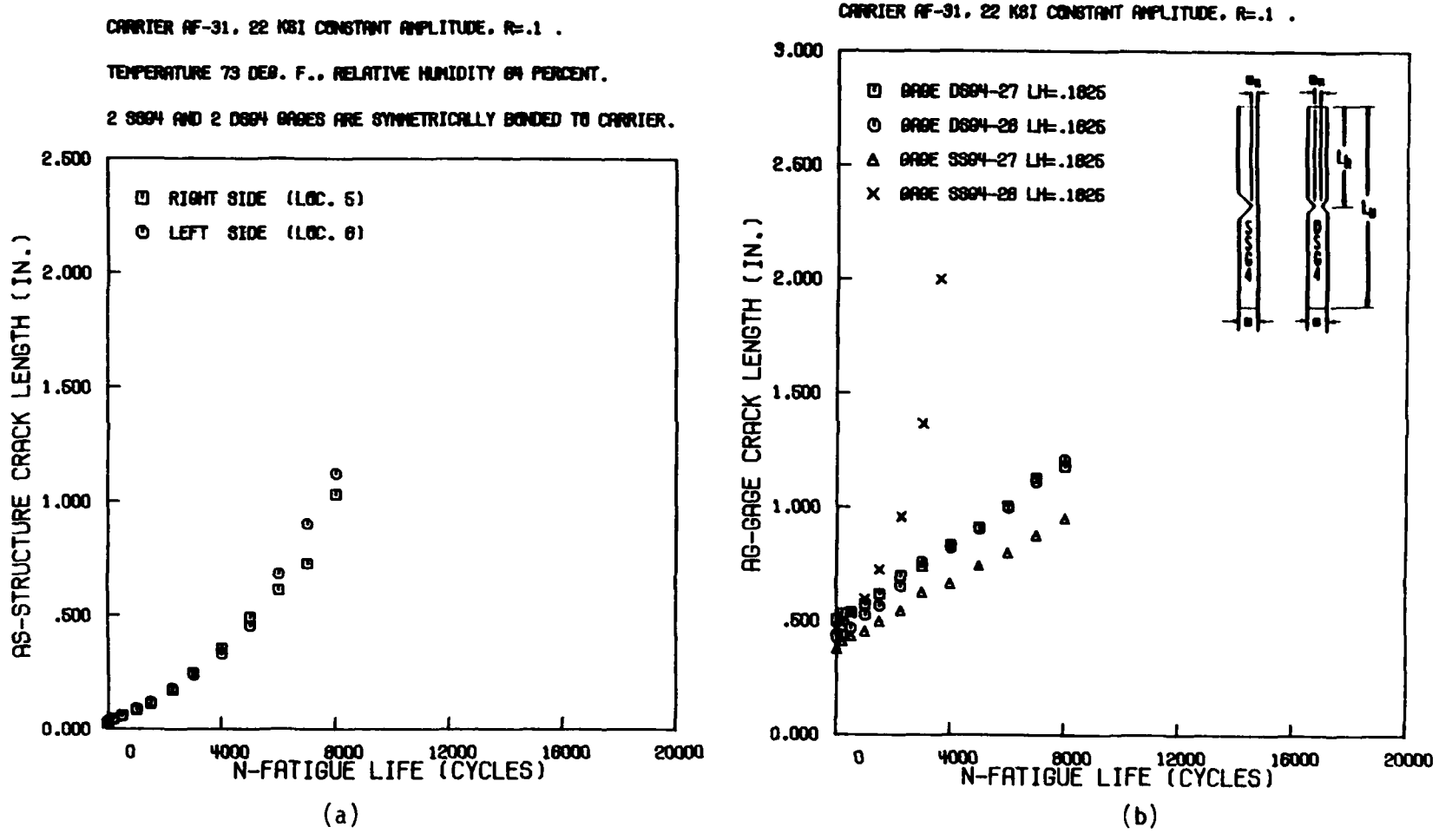

Figure 20: Crack growth data for carrier 31

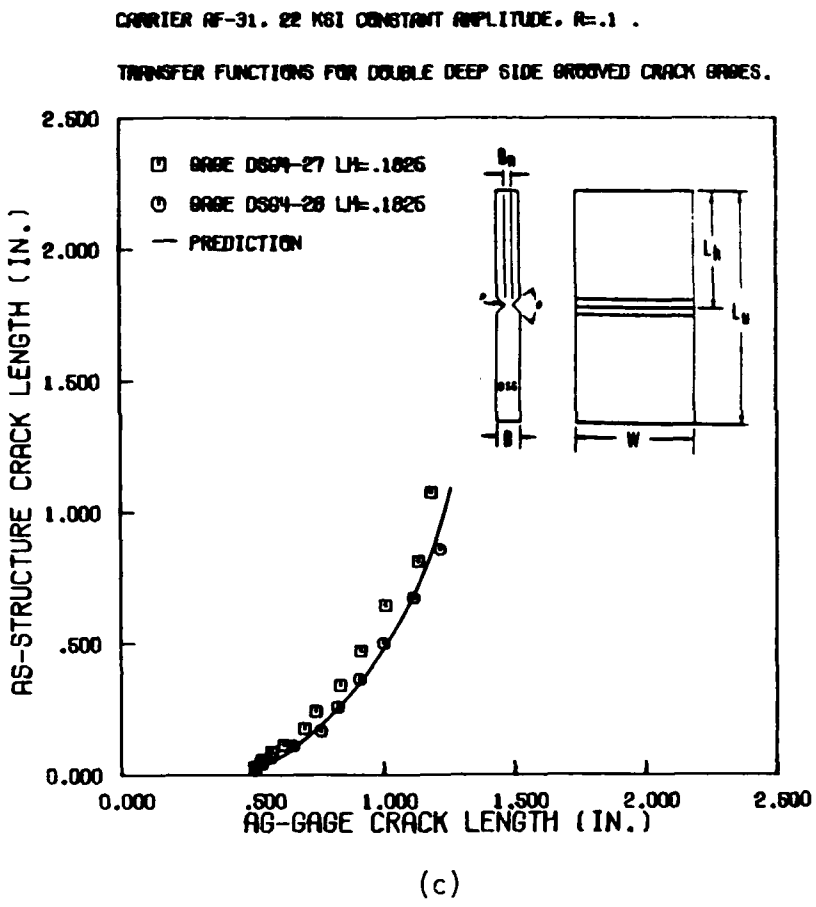

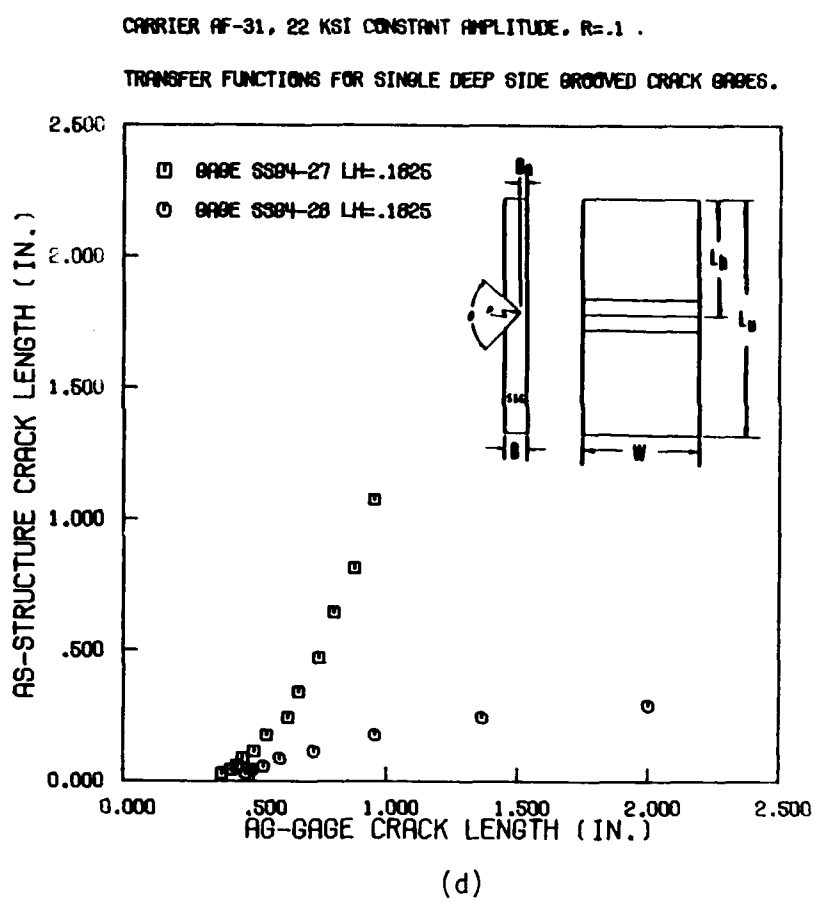

Figure 20: continued

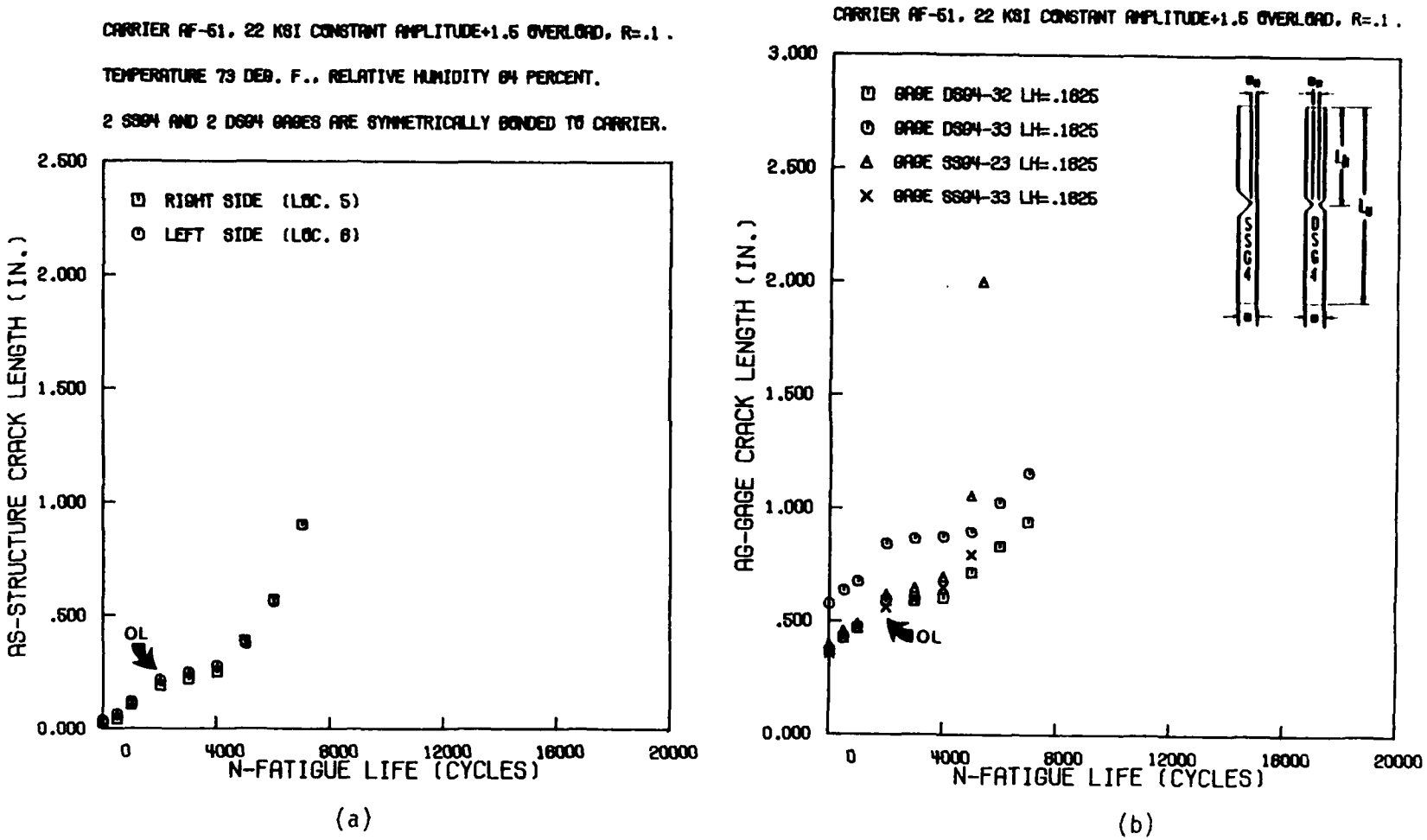

Figure 21: Crack growth data for carrier 51

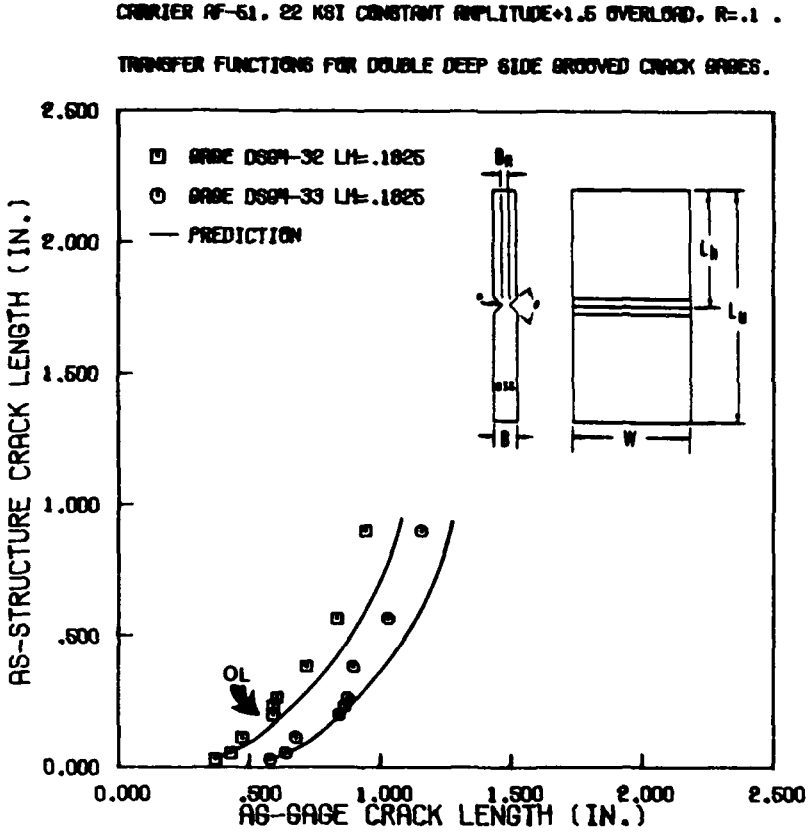

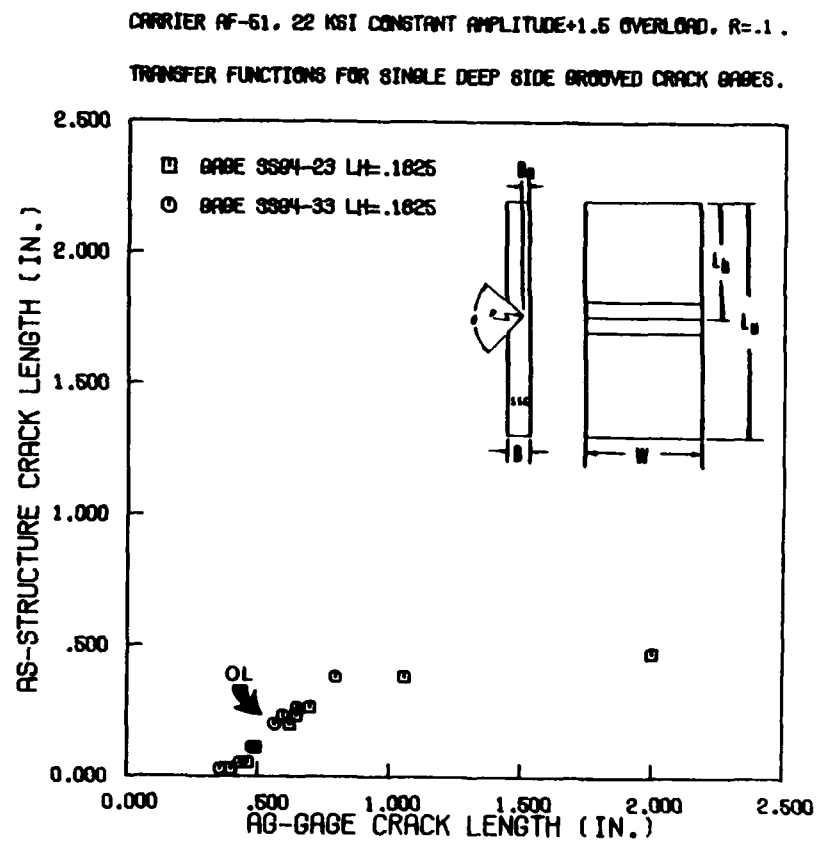

Figure 21: continued

produced inconsistent crack growth rates, further verifying that their behavior was not reproduceable. The structure and gage crack growth data are shown in Figures 21a and 21b, while the transfer functions are shown in Figures 21c and 21d for the double and single side-grooved gages.

a. Repeatability of Side-Grooved Gage Behavior

It is important to demonstrate that the crack gage behavior is reproduceable. Due to the complexity involved with the bonding procedure and gage manufacturing, it was considered essential to show that factors such as unbonded length, bonding thickness, adhesive and cohesive properties, gage positioning, gage geometry, etc. are controllable and a repeatable gage response can be produced.

The single side-grooved crack gage behavior in Figures 20 and 21 and in Appendix A indicates that SSG gages mounted on the same carrier produced large variations in crack growth rate. Since this behavior occurred in several of the large carrier tests, it was concluded that further investigation of the single side-grooved gages was unwarranted. The inconsistent gage behavior could be related to the large plastic zones formed by the gage bending.

The double side-grooved crack gage behavior, for specimens 27, 47, 30, 50, 31, 51, 32, 52, 55, 58 and 61, however, reveals the required repeatibility in gage properties. One sees that most double side-grooved gages produced very repeatable crack growth curves. The only exceptions were the gages mounted on carriers 30 and 50. For carrier 30, the variation in DSG gage crack growth rates was due to an unintentional difference in their unbonded lengths. For carrier 50, both gages produced the same crack growth rate prior to applying the peak overload, but once the peak

overload was applied and crack propagation was resumed, the steady state crack growth rate for one gage slowed down, while the rate in the other remained unchanged. When the gages were removed from the carrier, a slight difference was noticed in the bonding area, which may have affected the gage crack growth rate.

Following the anomalies observed in specimens 30 and 50, the bonding procedure was reviewed with the technician who performed the bonding. It was found that during bonding, the gause used as an adhesive carrier, was always cut shorter than the required bond length and then placed approximately 0.125 inch from the side-groove to allow the excess glue to flow outside. As a result, a small part of the bonding area sometimes had poorer adhesive contact, and may have led to a slight adhesive separation in the region close to the side-groove. It is expected that using a gause length equal to the required bonding length will prevent bonding irregularities.

Based on the test results discussed above, it is concluded that the double side-grooved crack gage (DSG4) behavior is reproduceable, and that the two exceptions (out of 22) were explained by irregular bonding. Furthermore, it is concluded that the single side-grooved gage does not have the required crack gage properties in that its crack growth response was not repeatable.

b. Effect of Overloads on Side-Grooved Gage Transfer Function

Since the original goal of the side-grooved crack gages was to obtain "thick section" fatigue crack retardation behavior in a "thin section", it is necessary to compare results obtained under the same loading conditions with and without overloads. For comparison purposes, the transfer

functions obtained under the same loading conditions, with and without an overload, are plotted together in Figure 22. Note that except for carriers 30 and 50, the overload transfer functions agree well with the non overload results. Since the irregularity in carriers 30 and 50 has already been discussed and explained, these results indicate that the side-grooves reduce thickness dependent retardation effects in the crack growth gages as desired.

c. Effect of Gage Manufacturer

The constant amplitude tests were conducted with either a 16 or 22 ksi maximum stress. When comparing fatigue crack growth curves for similar crack gage configurations, it was noticed that the 16 ksi tests gave faster growth rates than the 22 ksi loading. This effect may be noted in Figure 22, where the composite 16 ksi transfer functions show significantly faster relative growth in the flaw than in the structural crack. After checking several factors in an attempt to explain this paradox [7], the problem was traced to the source of gage manufacturer. It was noted that although all gages were made from the same sheet of material, all double side-groove gages tested at 16 ksi were manufactured at Purdue University, while the 22 ksi and T-38 spectrum tests employed gages manufactured by the University of Dayton Research Institute. In addition, a detailed examination of the gage precracking records indicated that the Purdue manufactured gages had a consistently shorter fatigue initiation life (the preloading histories were identical).

These findings led to the conclusion that since the raw material was the same in all cases, and uniform thickness gages from both manufacturers had very similar baseline crack growth rates, the cause for different

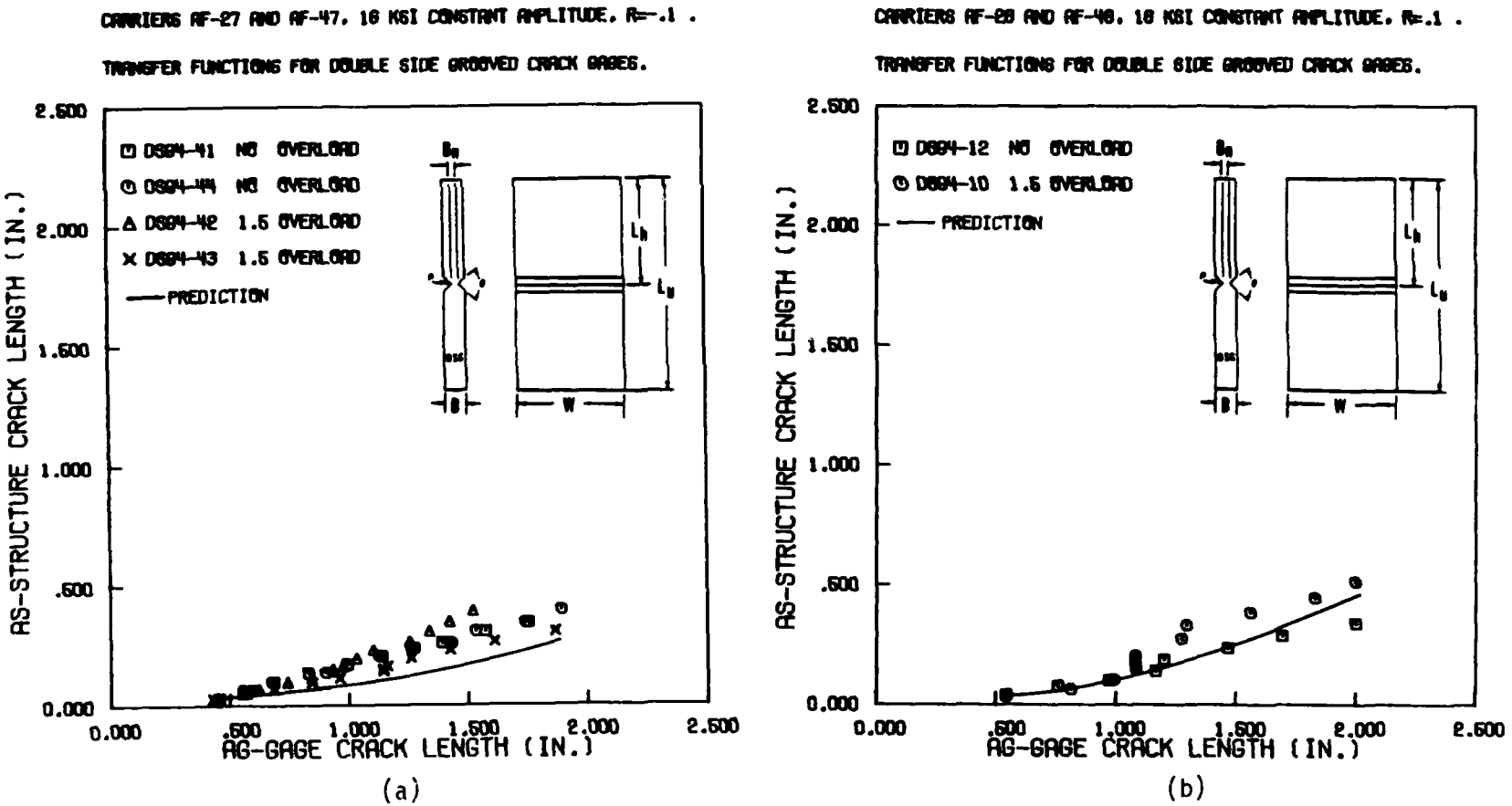

Figure 22: Comparison of flaw growth transfer functions for tests with and without peak overloads

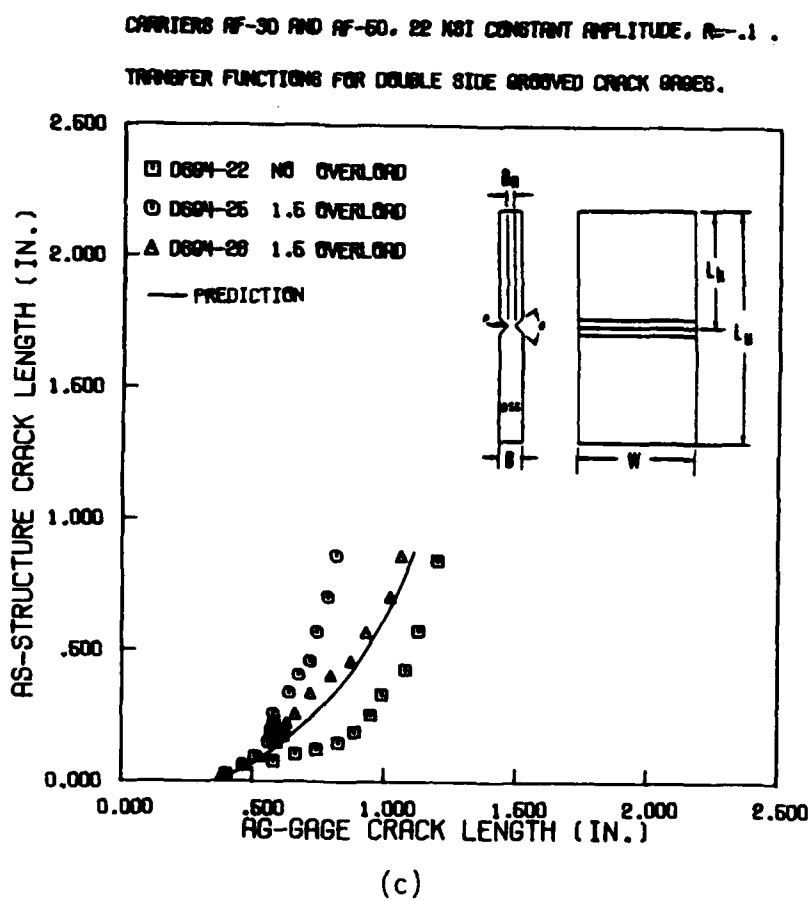

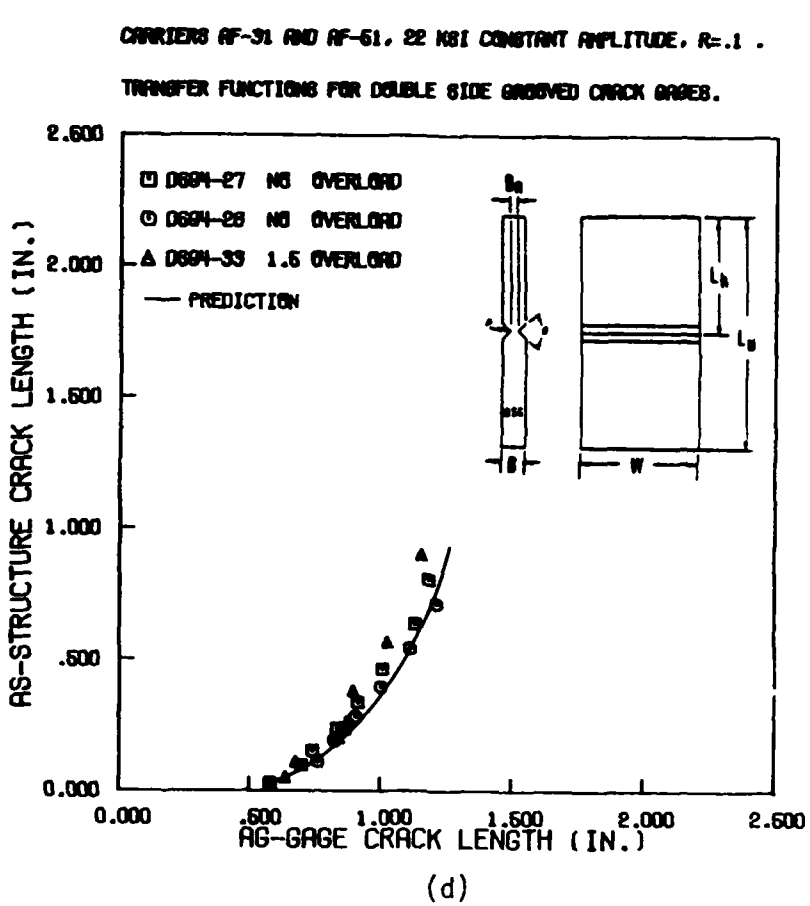

Figure 22: continued

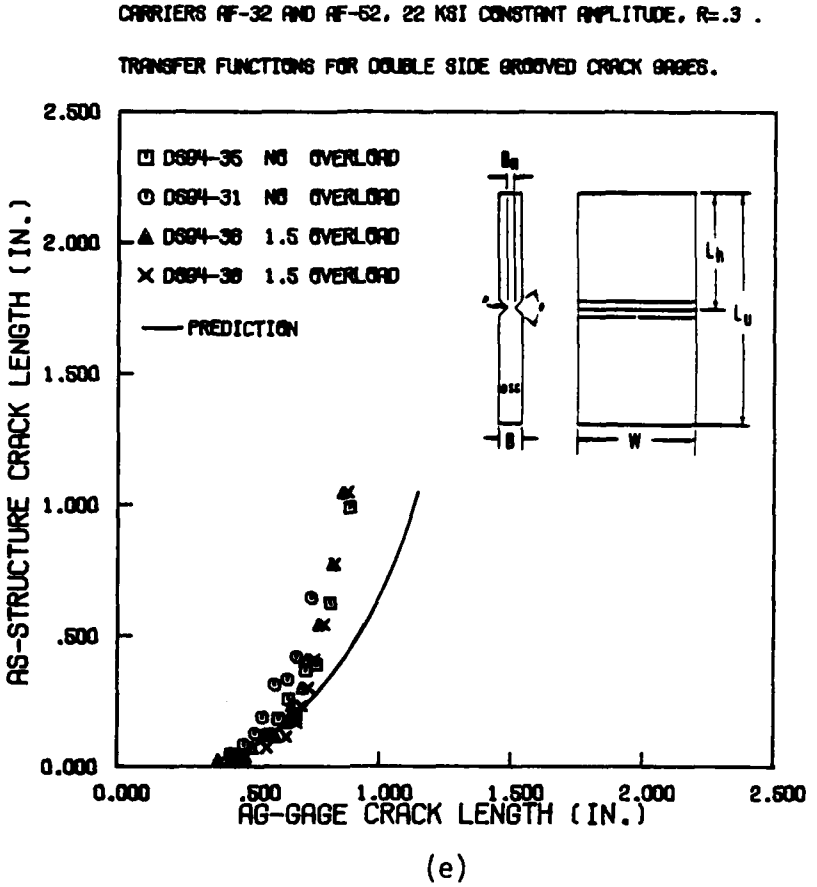

(e)

Figure 22: continued

side-grooved gage fatigue behavior must lay within the side-groove manufacturing procedures. Checking the equipment and procedures used by each manufacturer showed that better control was available with the UDRI equipment. It is believed plastic deformation, resulting in tensile residual stresses, could have occured during side-groove gage manufacture and influenced the crack growth rate. In order to avoid possible residual stress effects on the side-grooved gage fatigue behavior, future manufacturing should consider anealing and heat treatment after completion of the machining, or using well controlled machining operations such as chemical milling.

d. Effect of Load History

The effect of load history on the structure flaw/gage crack transfer function for the double side-grooved gages may be studied by examining the 22 ksi and T38 spectrum tests. (Recall that all of these gages were manufactured by UDRI and employed the same unbond length.) Composite transfer function plots for the 22 ksi tests are given in Figures 22c, 22d, and 22e, while the T-38 results are summarized in Figure 23. Figures 23a and 23b give average fatigue crack growth curves for the structural and gage flaws resulting from the three variable amplitude loadings: mild spectrum (M), baseline spectrum (B), and severe spectrum (S). (The original data are provided in Appendix A.) Note that the fatigue crack growth curves show a significant dependence on the load history, with the severe spectrum giving the shortest lives, and the mild spectrum providing the longest life as expected. When the T-38 crack gage transfer functions are compared in Figure 23c, however, the effect of load history is much less pronounced. The predictions indicated by solid lines in Figures 20 to 23 are discussed in the next subsection.

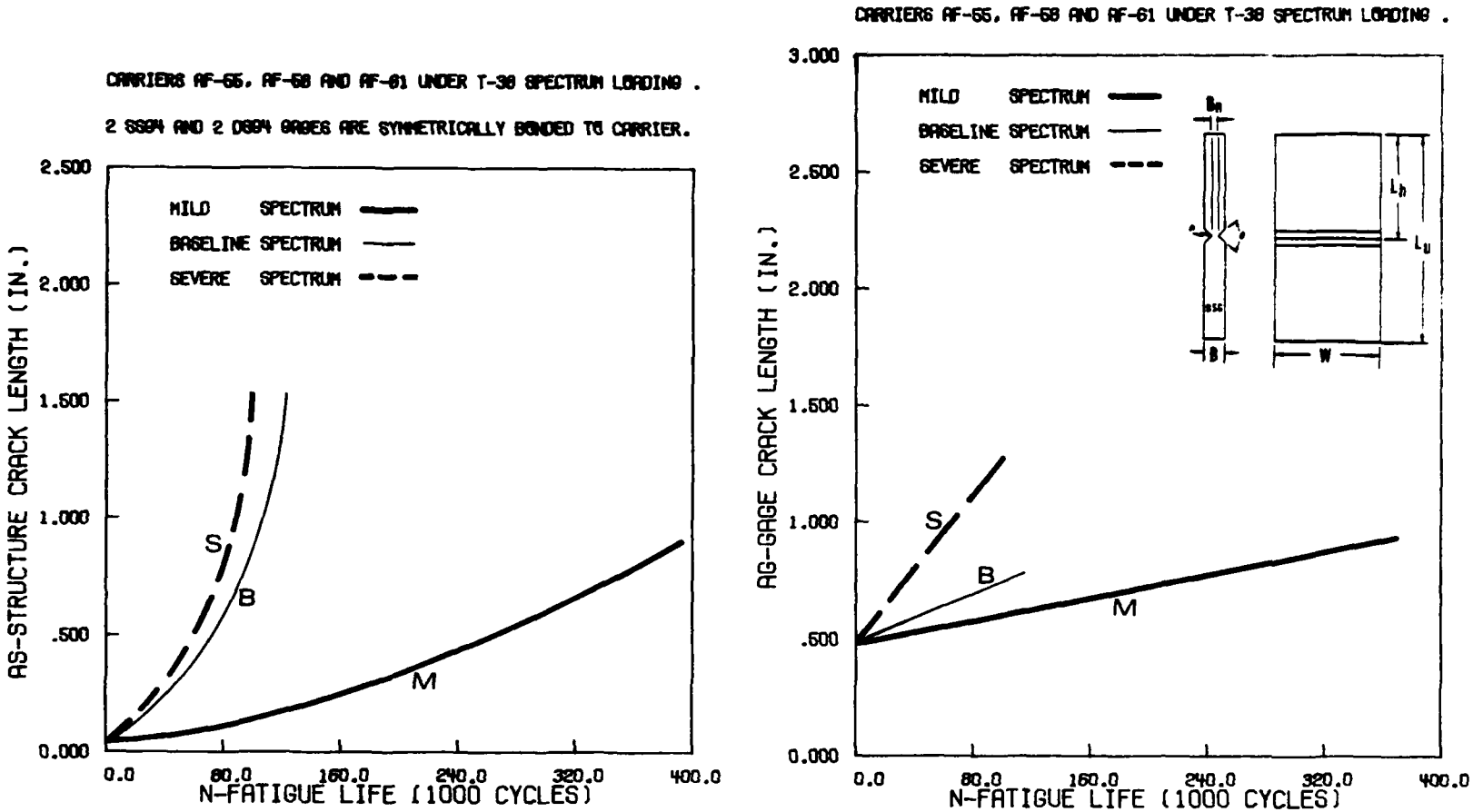

a. Structure flaw average

b. Gage flaw average

Figure 23: Composite crack growth data and transfer functions for variable amplitude tests

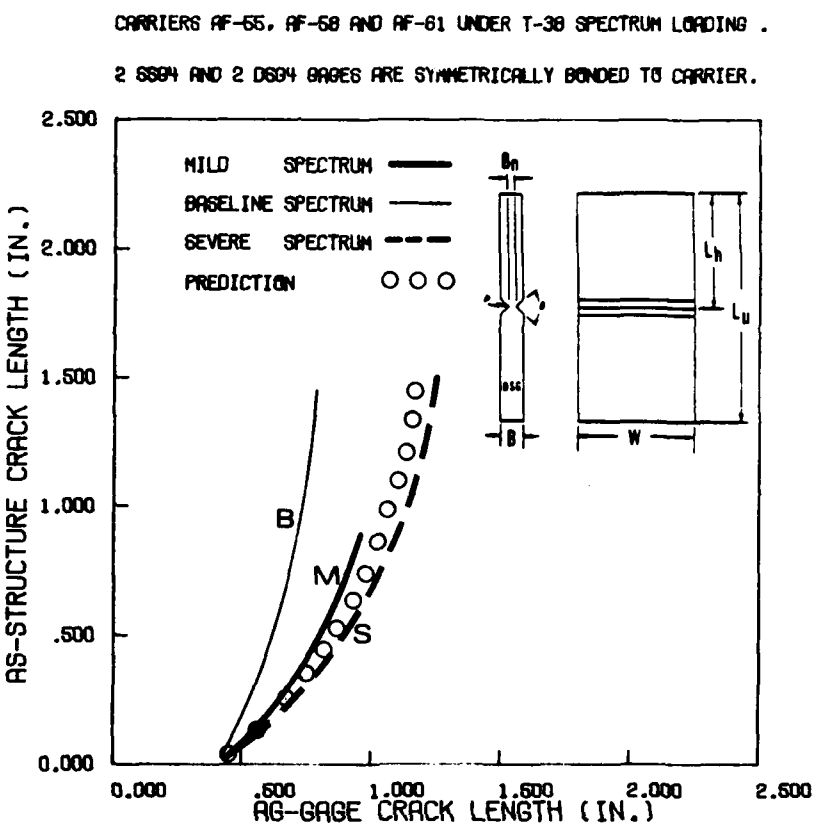

c. Composite transfer functions

Figure 23: continued

The transfer function for all seventeen of the 22 ksi and T-38 tests are combined in a composite plot in Figure 24. Note that although many different loads were applied to the carrier specimens (3 variations of the T-38 spectra, 22 ksi loading at 3 R-ratios, and the occasional inclusion of overloads), the transfer function data fall into a distinct band. These composite transfer function data are compared with numerical predictions and discussed in more detail in the following subsection.

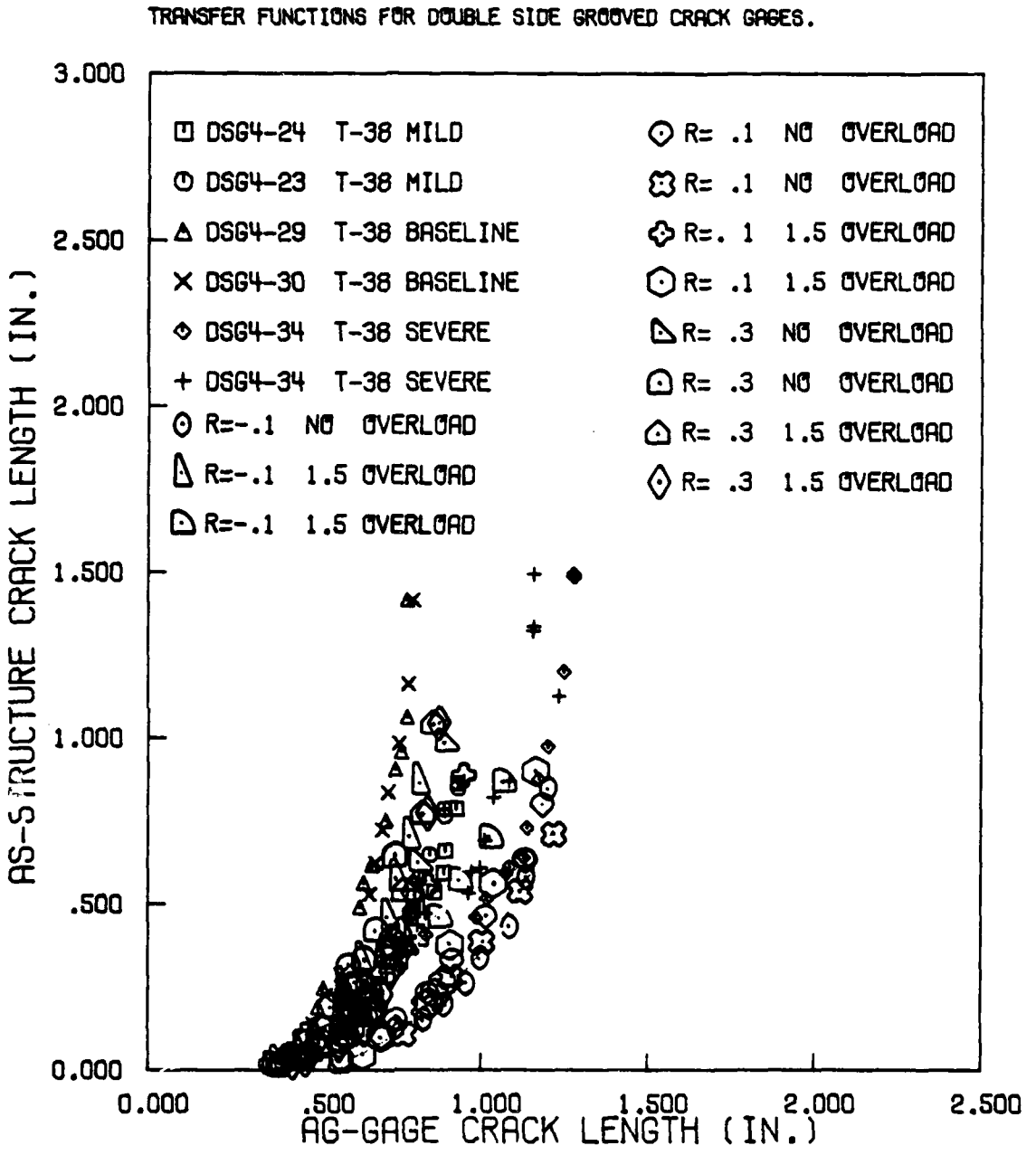

Figure 24: Composite plot of crack gage transfer function curves obtained from 22 ksi and T-38 spectrum experiments.

6. ANALYSIS OF SIDE-GROOVED GAGE EXPERIMENTS

This subsection summarizes the side-grooved crack gage analyses. Procedures for computing the crack gage stress intensity factor and for predicting the structural crack size as a function of gage crack length are briefly described. Additional details are given in Reference 7.

a. Side-Grooved Gage Stress Intensity Factor

Since the crack gage ends are adhesively bonded to the structural member, the crack gage is subjected to displacement controlled boundary conditions. Moreover, the unbond length is relatively short for the gage configurations considered here. Ignoring the side-grooves and the load transfer through the adhesive for a moment, one may examine the expected character of the side-groove stress intensity factor K by looking at the solution for an edge crack in a wide strip of length L [28].

$$K = \frac{E\nu_o}{\sqrt{(1-\nu^2)L}} \tag{9}$$

In Equation 9, ν_o is the applied displacement and L is the length of the strip, which is assumed to be in plane strain, E is the elastic modulus and ν is poisson's ratio. Note that K is independent of crack length in Equation 9, but is an inverse function of $L^{1/2}$.

The stress intensity factor for the side-grooved crack growth gage is complicated by the three-dimensional stress field around the side-groove and by load losses through the adhesive bond. As described in References 17, 23, and 29, the effect of the side-grooves is to reduce

the stress intensity factor in the side-grooved member in comparison to another similiar member with a uniform thickness equal to the net side-groove thickness B_N. This side-grooved stress intensity factor is given by

$$K_{true} = K^* \left[\frac{B}{B_N}\right]^{n-1} \tag{10}$$

where

$$K^* = \left[\frac{P}{B_N W}\right] \sqrt{\pi a} \quad \beta \tag{11}$$

Here K_{true} is the stress intensity factor for the side-grooved member, B is the original thickness without the side-grooves, B_N is the net thickness remaining after side-grooving, P is the applied load, W is the specimen width, a is the crack length and β is the conventional dimensionless stress intensity factor coefficient. The exponent n is an empirical constant in the range $0.5 \leq n \leq 1$. Note that K* is the stress intensity factor for a specimen of uniform thickness B_N. If the empirical exponent n = 1, the side-groove stress intensity factor $K_{true} = K^*$. If $n < 1$, the actual stress intensity factor K_{true} is less than K*.

The fact that side-grooves reduce the stress intensity factor for the present results is seen from the baseline fatigue crack growth data given in Figure 25. Here a conventional plot of fatigue crack growth rate $\frac{da}{dN}$ versus cyclic stress intensity factor ΔK is given for the 0.03 in. 7075-T6 aluminum crack gage material. Note that shallow side-groove (DSG2-7 and DSG2-8) and 0.03 in. uniform thickness specimens (RT-01 and

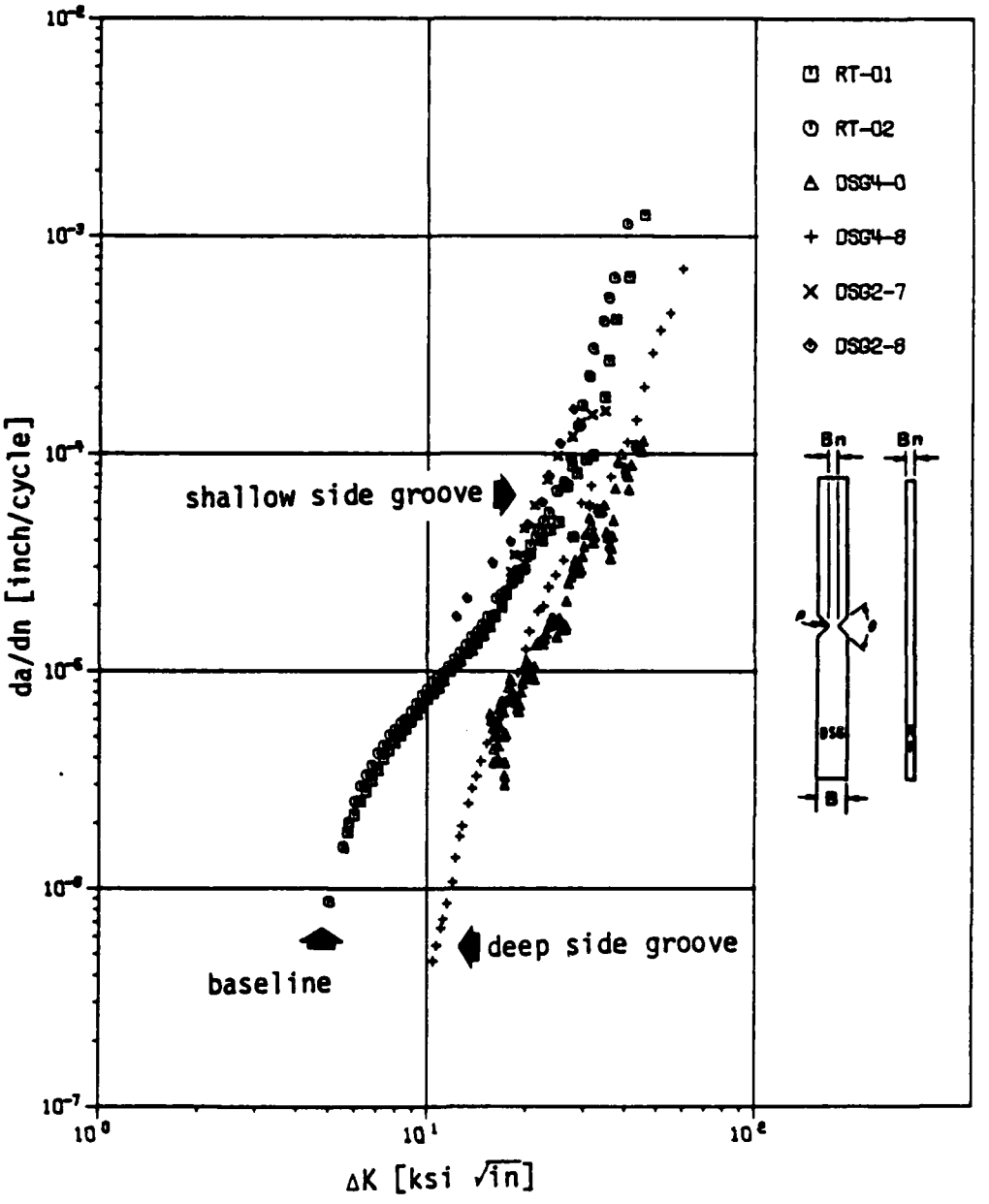

Figure 25: Crack growth rate test results for reduced thickness and double side-grooved specimens, machined from the 7075-T6 aluminum crack gage material.

RT-02) give essentially the same $\frac{da}{dN}$ versus ΔK relationship, while the deep side-groove members (DSG4-0 and DSG4-8) yield an apparently slower crack growth rate. The slower fatigue crack growth rates in the deep side-grooved specimens indicate the actual stress intensity factor K_{true} is less than K* ($\Delta K = \Delta K^*$ in Figure 25), as suggested by Equation 10.

The remaining factor which influences the side-grooved gage stress intensity factor is the load transfer through the adhesive bond. As indicated in the load transfer measurements reported for uncracked, but adhesively bonded coupons reported earlier in Figure 19b, the measured strain in the gage coupon is less than that in the parent structure. A detailed analysis for the load transfer function f is described in Reference 7. That analysis is based on the compliance approach described in References 4 to 6, and includes the various side-groove gage parameters.

As discussed in Reference 7, the final side-groove gage stress intensity factor K_{SG} for the DSG4 configuration studied here is given by

$$K_{SG} = 1.4\ \sigma_s\ D \tag{12}$$

where

$$D = f\ \phi \tag{13}$$

Here σ_s is the remote stress applied to the structural member, f is the load transfer term (a constant dependent on the particular side-groove

gage geometry and adhesive system), and ϕ is an empirical side-groove correction factor modeled after Equation 10. The constant ϕ is determined experimentally from a single constant amplitude crack growth rate test. The final constant factor D for the DSG4 side-grooved gages ($B/B_N = 4$, $B_N = 0.03$ in., $L_u = 0.375$ in.) is D = 1.41 $(in.)^{1/2}$ for the UDRI manufactured crack gages, and D = 2.19 $(in.)^{1/2}$ for the Purdue manufactured gages. (Recall that gages from the two sources gave different fatigue crack growth rates.)

Thus, as indicated by Equation 12, the side-groove gage stress intensity factors are independent of crack length, similiar to the Equation 9 solution for a displacement loaded strip. This crack length independence may be observed from the gage fatigue crack growth curves described earlier in Section 3.5. Recall that the gage cracks were observed to grow at constant rates during the constant amplitude fatigue tests, consistent with the crack length independence of Equation 12. Additional experimental verification for the gage stress intensity factor analysis is provided by the crack length transfer functions discussed in the next subsection.

b. Side-Grooved Gage Transfer Function Prediction

Predictions were made for the structural crack size as a function of the corresponding gage crack length. These predictions employed the load independent transfer function analysis given in Equation 7. The stress intensity factor for the side-grooved crack gage is given in Equation 12 (Note that $f\sqrt{\pi a}\ \beta_g$ in Equation 7 corresponds to 1.4D in Equation 12), while K for the structural crack was computed by a width corrected version of the Bowie [30] solution for a through-cracked hole [7].

The material constants C_s, C_g and m were determined from conventional constant amplitude fatigue crack growth tests and are summarized in Table 4. Note that the different alloys did not yield the same exponent m when Equation 4 was least squares fit through the raw data. In order to employ the equal m assumption in Equation 7, the gage and structural exponents were averaged and new values obtained for C_s and C_g with this specified m. Since the structure and gage crack growth rate curves were very close to each other, representing both by a single power law was deemed more appropriate and practical. The constants C and m for the single power law were obtained by averaging the structure and gage constants. These modified crack growth constants, also recorded in Table 4, were found to represent the original fatigue crack growth rate behavior quite well over the range of stress intensity factors relevant to this study. Thus, it is felt that this modification procedure is justified for the present work. Note that the same type of modification was also used successfully in References 5 and 6.

The predictions for a_s as a function of a_g obtained by iterative solution of Equation 7 are given by solid lines in Figures 20, 21, 22, 26, and in Appendix A. The predictions are indicated by open circles in Figure 23c. Note that, in general, the crack length transfer functions are predicted quite well in comparison to the experimental values. Very good results are obtained for the R = 0.1 predictions (with and without overloads), although a slight deviation is seen in the R = -0.1 and R = 0.3 data. In addition, the Baseline T-38 spectrum results shown in Figure 23c do not agree as well as the other two variable amplitude load histories. Nevertheless all predictions are reasonable.

Table 4 Fatigue crack growth constants
for power law equations used to represent gage and structure materials

	structure 7075-T651	gage 7075-T6	average
C	3.006×10^{-9}	1.663×10^{-8}	0.982×10^{-8}
m	3.587	2.653	3.120

Note:

1. The power law equation is given by

$$\frac{da}{dN} = C\ \Delta K^m$$

where $\frac{da}{dN}$ is the fatigue crack growth rate and ΔK is the cyclic stress intensity factor.

2. Units of C and m are such that da/dN is given in inch/cycle and ΔK in units of ksi-in.$^{1/2}$.

3. Stress ratio R = 0.1 in all cases.

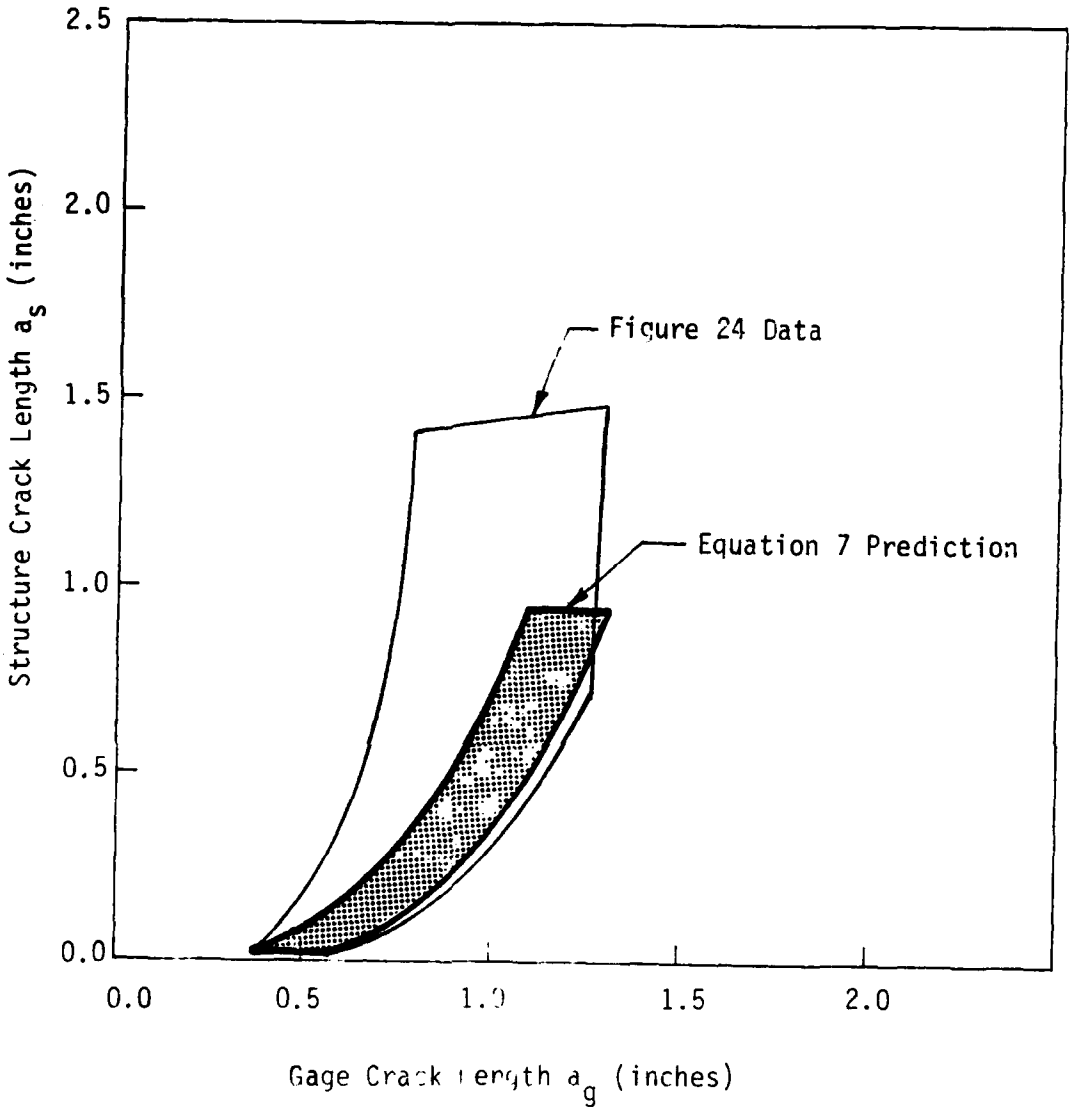

Figure 26: Comparison of predicted crack gage transfer functions with data obtained from 22 ksi and T-38 spectrum experiments.

It is significant to recall here that the predictions involve no knowledge of the actual load history, and depend only on geometric and material properties. Moreover, the only material constants employed were the R = 0.1 data reported in Table 4. The fact that reasonably good predictions were made in all cases by the load independent transfer function analysis of Equation 7 suggests that the load histories studied did not have a major influence on the side-groove crack gage response.

Figure 26 compares predicted transfer functions with experimental data for the 22 ksi and T-38 spectrum tests. The "data" band shown in Figure 26 encompasses the composite plot of data given in Figure 24. The "predicted" band shown on Figure 26 was obtained by employing the extremes in the initial (a_s, a_g) starting points observed in the tests. Although efforts were made to begin each experiment with the same initial combination of gage and structural flaw sizes, it was impossible to obtain the exact precrack lengths in all cases. One may interpret the predicted band width in Figure 26 to represent the portion of "scatter" in the experimental a_s versus a_g results due to the different starting conditions. The remaining variability in the composite transfer function data plot is typical of that commonly observed in fatigue crack growth rate testing. Virkler and Hillberry [31], for example, noted that a well controlled set of constant amplitude experiments with 68 identical specimens, gave fatigue crack growth lives which varied by as much as a factor of 1.45 to 1. Such variations in crack growth rate must be expected for the structure and gage flaws as well.

As a final comment regarding the composite transfer function given in Figure 26, it should be noted that the transfer function is steeper than desired, in that the structural crack grows at a faster

rate than the gage crack. It would be preferable in most cases for the gage crack to grow faster, so that it would "amplify" the expected structural flaw size. Increased gage crack growth rates are readily achieved by a simple design change. As discussed in Reference 7, the crack gage stress intensity factor is a function of the unbonded gage length L_u, with longer lengths giving larger K's. The unbonded length was only 0.375 in. for the results reported in Figure 24, and may readily be increased. It is suggested that future efforts with the double side-grooved gage DSG4 configuration studied here employ slightly longer unbond lengths (on the order of 0.5 in.), to increase the gage K and yield faster crack growth rates in the side-grooved coupon.

Section 4

DOUBLE GAGE MODEL

1. BACKGROUND

Recall that the objective of this task was to develop an alternative to the structure/gage crack transfer function given by Equation 7. A key assumption in that transfer function is that crack growth in both gage and structure materials is described by the simple power law relationship of Equation 4. When this assumption is met, the crack transfer function is <u>independent</u> of stress (see Equation 7). Although the load independent analysis of Equation 7 gave good predictions for the side-grooved gage results described in Section 3, and performed well for experiments reported in References 5 and 6, the simple Equation 4 power law assumption may not be appropriate for all cases, and the load independent analysis of Equation 7 may not always be valid.

An alternative approach, designated as the double gage model was developed here to provide an improved crack transfer function. The double gage model employs two independent crack gages to yield a load dependent transfer function. The basic premise lies in introducing an additional degree of freedom to the computational scheme through information obtained from a second crack gage. This additional information allows calculation of the effective stress $\bar{\sigma}_{eff}$ seen by the structure, and provides means to employ more general fatigue crack growth laws in the numerical model. Since two crack gages are mounted to the structural component as shown schematically in Figure 3, they see the same number of load cycles as the assumed structural crack. Conventional fracture mechanics

analyses determine the crack growth life N and relate the current gage crack lengths a_{g1} and a_{g2} with the structural flaw size a_s. The basic equations are summarized below.

$$N_{g1} = \int_{a_{i1}}^{a_1} \frac{da}{F_1(K)} \tag{14}$$

$$N_{g2} = \int_{a_{i2}}^{a_2} \frac{da}{F_2(K)} \tag{15}$$

$$N_s = \int_{a_{is}}^{a_s} \frac{da}{F_2(K)} \tag{16}$$

$$N_{g1} = N_{g2} = N_s \tag{17}$$

The terms in Equations 14 to 17 are defined below.

a_{i1} = initial crack length in gage 1
a_{i2} = initial crack length in gage 2
a_1 = current crack length in gage 1
a_2 = current crack length in gage 2
a_{is} = initial crack length in the structure
$F_1(K)$ = crack growth rate function for gage 1
$F_2(K)$ = crack growth rate function for gage 2
$F_S(K)$ = crack growth rate function for the structure

known quantities

$\bar{\sigma}_{eff}$ = system equivalent stress (a parameter in K)
a_s = current crack length in the structure
N = current cyclic life (subscripts 1, 2, and s refer to gage 1, gage 2, and structure respectively)

unknowns

As indicated above, the a_i are specified initial crack lengths in gages 1, 2, and the structure, and the F(K) are the appropriate fatigue crack growth laws $\left(\frac{da}{dN} = F(K)\right)$ for gages 1, 2 and the structure. The unknowns are N, a_s and the effective stress $\bar{\sigma}_{eff}$, which is one of the parameters of the crack growth function F(K). It is assumed that the current gage crack lengths a_1 and a_2 are measured, the three initial crack lengths are specified, and the stress intensity factor calibration and fatigue crack growth model (including material constants) are known for the crack gages and structural flaw. In addition, it is possible to relate the effective stress $\bar{\sigma}_{eff}$ with the actual stress in the crack gages and the structural component (as per Equation 1).

2. BOEING CRACK GAGE DATA

The double gage model was evaluated with crack gage data obtained by G. Cassatt of the Boeing Company and reported in Reference 10. Before describing the solution procedure and results, the baseline data used to evaluate the solutions are briefly described.

The Boeing crack gage experiments consisted of six large carrier specimens, which contained 10 crack gages (5 on each side) as shown schematically in Figure 27. There were also 5 structural flaws in each specimen: corner cracked holes at locations 1 and 2, through-cracked holes at locations 3 and 4, and a center crack at location 5. These specimens were subjected to various constant amplitude and variable

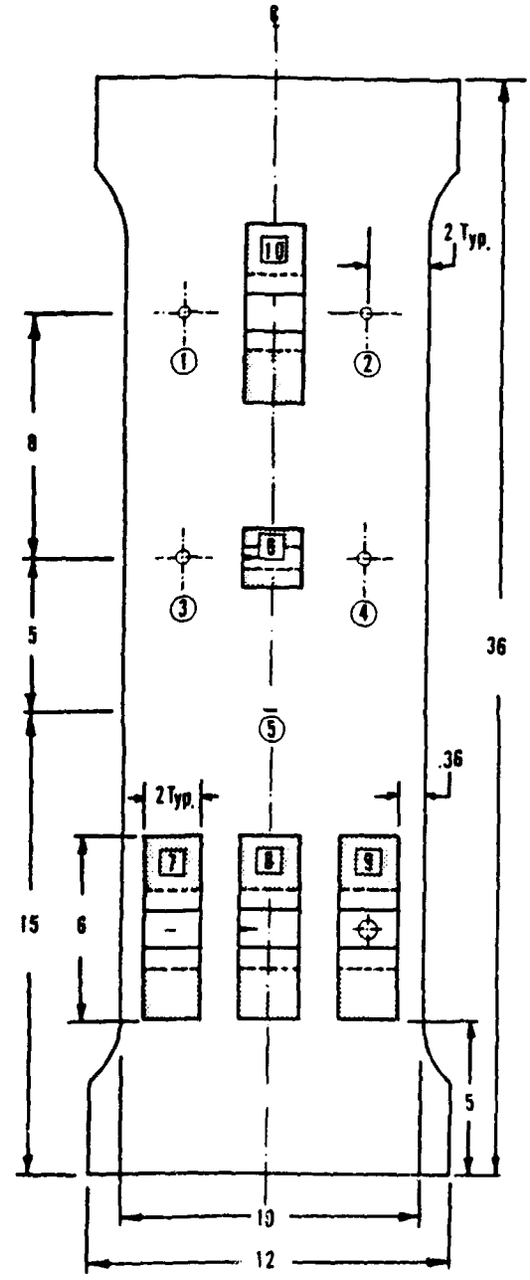

Figure 27: Crack gage evaluation specimen

amplitude loadings as summarized in Table 5. Several crack gage configurations were employed; those considered here are summarized in Table 6. (Additional specimen details are reported in References 7 and 10.)

Typical fatigue crack growth data for specimen AFCG-5 are reproduced here in Figures 28 and 29. The original crack growth data are given in Figures 28a and 29a, while Figures 28b and 29b present crack growth curves which are shifted to a common origin. Since all the tests involved repeated load histories, the curves could be shifted along the cycle (or flight) axis. Although not necessary for the present purposes, this shifting to a common origin was helpful in determining repeatability of the crack gage behavior.

Note that since each specimen contained several different crack gages and structural flaws, and different load histories were applied to the specimens, many crack combinations were available to evaluate the double gage model. (The original crack growth data are presented in tabular form in Reference 10.) The numbering system described in Appendix B was employed here to identify particular crack growth results for subsequent use in the double gage model.

As described in Reference 7, a considerable amount of effort was directed at developing stress intensity factor solutions for the Boeing crack gages and modeling the baseline crack growth data for use here. It was decided to represent the baseline $\frac{da}{dN}$ versus ΔK data by straight line segments valid over individual ΔK ranges. Numerous life calculations were performed using the known specimen loads in order to verify that

Table 5 Test matrix for Boeing crack gages (based on Reference 10)

specimen and test number	constant amplitude [10 ksi]		spectrum loading		
	R = .05	R = .33	KC-135 wing (1)	fighter (2)	KC-135 fin (1)
AFCG-1	X				
AFCG-2		X			
AFCG-3			X		
AFCG-4				X	
AFCG-5	X				
AFCG-6					X

notes:

1. KC-135 5.1 hour tanker mission profile

2. fighter flight profile

Table 6 Boeing crack gages used for present analysis (based on Reference 10)

test	specimen	crack gage type at locations			
		7	8	9	10
1	AFCG-1	CC	EC	DCH	reference
2	AFCG-2	DCH	EC	CC	reference
3	AFCG-3	reference	EC	CC	CC
4	AFCG-4	EC	reference	CC	EC
5	AFCG-5	CC	EC	CC	reference
6	AFCG-6	CC	EC	CC	CC

CC = center crack through the thickness

EC = edge crack through the thickness

DCH = double cracked hole

Reference = uncracked coupon

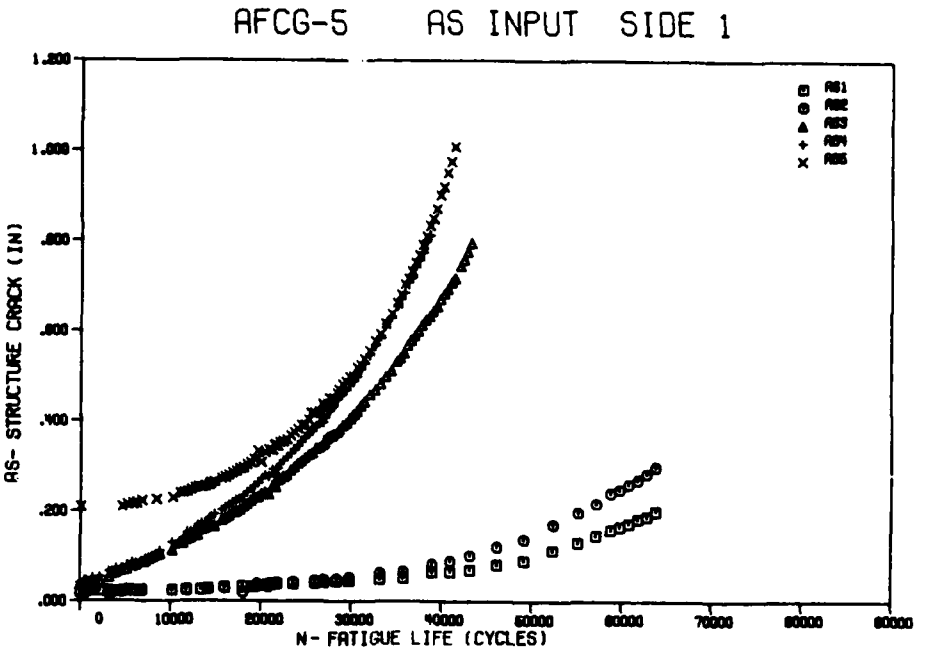

(a) original crack growth data

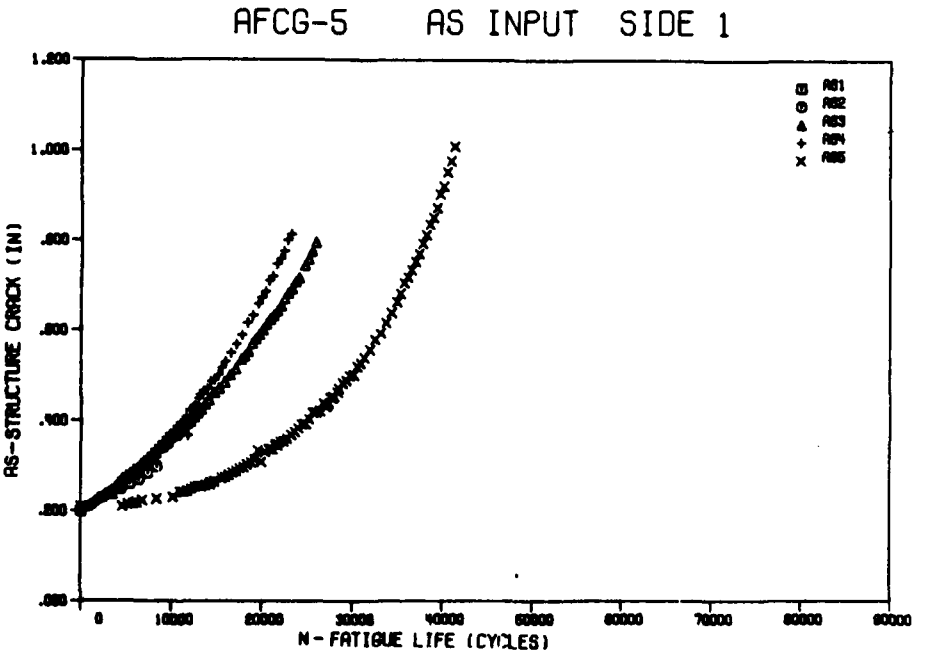

(b) shifted to common initial crack size

Figure 28: Typical structural member crack propagation data.

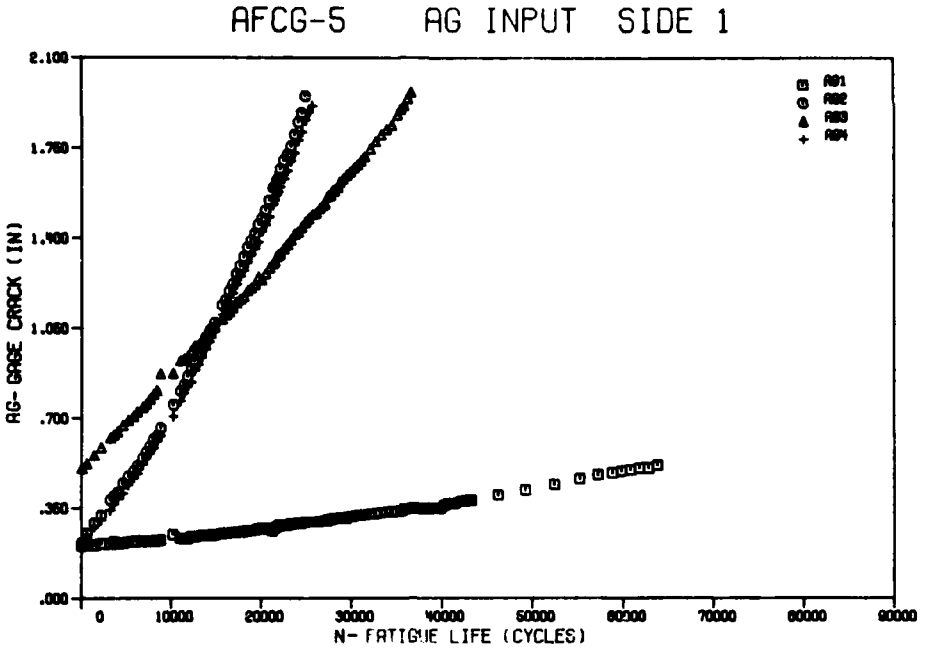

(a) original crack growth data

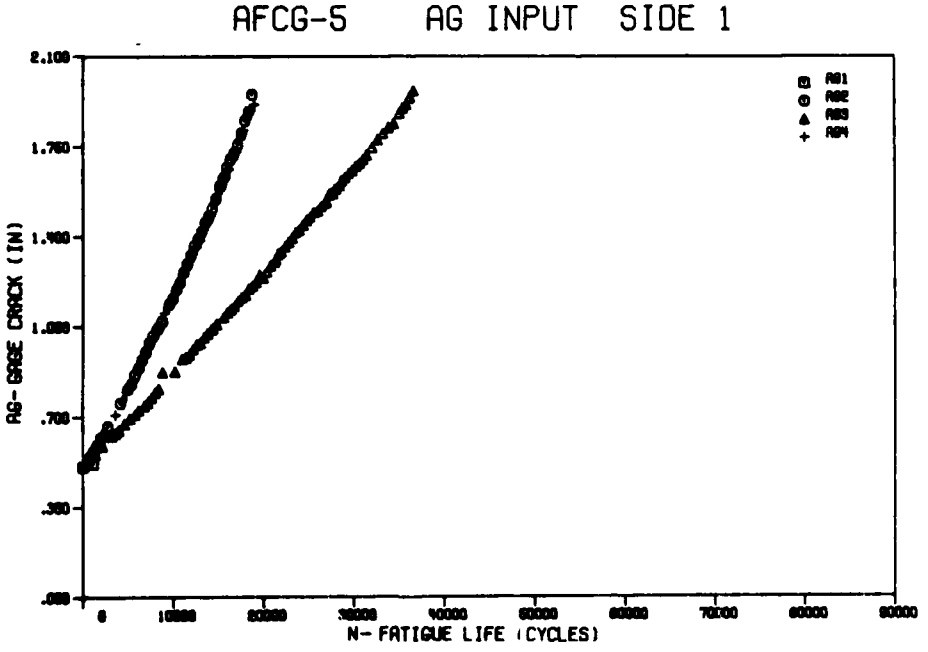

(b) shifted to common initial crack size

Figure 29 : Typical gage crack propagation data

accurate K solutions and crack growth models were available. The research was then directed toward developing and verifying the double gage model. The applied stress was now considered an unknown parameter to be determined during the analysis scheme.

3. DOUBLE GAGE MODEL SOLUTION TECHNIQUES

A computer program was written to iteratively solve Equations 14 to 17 for the effective structural stress $\bar{\sigma}_{eff}$ and the structural crack length a_s. Note that the approach is based on the concept that both crack gages and the structural flaw should yield the same cyclic life (Equation 17). Since fatigue crack growth data typically show considerable scatter, and since solving Equations 14 thru 16 involves numerical iterations, it is impractical to demand that all three flaws have the exact same life. Several different solution strategies were considered in the overall approach to reflect these variations in crack growth behavior.

a. Gage Integral Equations

First, assume variability in the predicted life for the crack gages, such that

$$N_{g1} = (1+V)N_{g2} \tag{18}$$

where $|V| \leq 0.6$, a typical variation seen in crack growth lives. Combining Equations 14 and 15 now gives

$$\int_{a_{i1}}^{a_1} \frac{da}{F_1(K)} = (1+V) \int_{a_{i2}}^{a_2} \frac{da}{F_2(K)} \tag{19}$$

The unknown in Equation 19 is the effective structural stress $\bar{\sigma}_{eff}$ (which is a parameter of K).

A series of calculations was performed to determine the optimum value for the variability factor V. As summarized in Table 7, various gage pairs were matched and used to predict the corresponding structural flaw size. In these calculations, V was allowed to vary between 10% and 60%. It was determined that a value of V = 28%, which corresponded to the actual average variation in crack gage lives, also gave the best double gage model results. (The pluses in Table 7 indicate configurations which were considered in this series of calculations.)

b. Structure Life Equations

Once the effective system stress $\bar{\sigma}_{eff}$ was obtained from Equation 19, the next step was to match the structural life integral (Equation 16) with one of the crack gage lives (Equations 14 and/or 15). Since the gages did not necessarily give the same life, and variation might again be allowed in the structural life, various methods for making this calculation were considered. The structural life N_s was assumed to be a function ℓ of the two gage lives N_{g1} and N_{g2}.

$$N_s = \ell(N_{g1} + N_{g2}) \tag{20}$$

Various forms for the function ℓ were examined.

(1) Linear Averaging

$$N_s = \frac{N_{g1} + N_{g2}}{2} \tag{21}$$

Table 7 Study of gages integral equation relative error effects

test	gage pair ID	structure location	structure crack type	gage integral equation relative error					
				10%	20%	28%	40%	50%	60%
AFCG1	A	3 4 5	SCH (2) SCH CC (3)	+	+	+ + +	+		
AFCG2	A	3 4 5	SCH SCH CC			+ + +			
AFCG3	A	3 4 5	SCH SCH CC			+ + +			
AFCG4	A	3 4 5	SCH SCH CC			+ + +			
AFCG5	A	3 4 5	SCH SCH CC			+ + +			
AFCG5	B	3 4 5	SCH SCH CC	+	+	+ + +	+	+	+
AFCG6	A (1) (1)	3 4 5	SCH SCH CC			+ + +			
AFCG6	B (1) (1)	3 4 5	SCH SCH CC			+ + +			

(1) - data is available for side "1" only

(2) - single cracked hole

(3) - center crack through the thickness

(2) Non Linear Averaging

$$a_s = \frac{a_{s1} + a_{s2}}{2} \tag{22}$$

where now the two structural crack sizes a_{s1} and a_{s2} are found from iterative solution to

$$\int_{a_{is}}^{a_{s1}} \frac{da}{F_s(K)} = N_{g1} \tag{23}$$

$$\int_{a_{is}}^{a_{s2}} \frac{da}{F_s(K)} = N_{g2} \tag{24}$$

(3) Minimum Life

$$N_s = MIN(N_{g1}, N_{g2}) \tag{25}$$

(4) Maximum Life

$$N_s = MAX(N_{g1}, N_{g2}) \tag{26}$$

The series of calculations summarized in Table 8 were performed to compare these various methods for computing the structural crack size. The Maximum Life calculation given in Equation 25, gave the most conservative predictions, and was selected for further evaluation.

Note that solution to Equations 23 and 24 involve iterative estimates of the unknown structural crack lengths a_{s1} and a_{s2}. A series of

Table 8 Study of techniques to estimate structure cycles

test	gages pair ID	structure location	structure crack type	structure cycles estimation method			
				linear	nonlinear	Min. life	Max. life
AFCG1	A	3	SCH (2)	+	+	+	+
		4	SCH	+	+	+	+
		5	CC (3)	+	+	+	+
AFCG2	A	3	SCH				+
		4	SCH				+
		5	CC				+
AFCG3	A	3	SCH				+
		4	SCH				+
		5	CC				+
AFCG4	A	3	SCH				+
		4	SCH				+
		5	CC				+
AFCG5	A	3	SCH				+
		5	SCH				+
		4	CC				+
AFCG5	B	3	SCH				+
		4	SCH				+
		5	CC				+
AFCG6	A (1)	3	SCH				+
		4	SCH				+
		5	CC				+
AFCG6	B (1)	3	SCH				+
		4	SCH				+
		5	CC				+

(1) - data is available for side "1" only

(2) - single cracked hole

(3) - center crack through the thickness

calculations were performed to determine the best increment in crack length Δa to be used in the solution scheme. An increment $\Delta a = 0.005$ in. was found to be sufficient.

c. Structure Integral Equation Error

Solving integral Equations 23 and 24 involves an iterative procedure. The decision when to stop the iteration depends on the allowable difference between the predicted fatigue life (based on an assumed structure final crack length) and the life determined by the crack gages. Since no bonding problems or other factors (irregularities, unbonded length, bonding thickness, etc.) are involved with structural cracks, one anticipates that solution to these equations will be performed with less relative error than that of the crack gage integral equations. The scatter in the structure crack propagation data was analysed and was found to vary between 5 to 12 percent of the fatigue life. The iterative procedure was repeated while changing the allowable error from 0.5 to 30 percent (the gages error) as indicated in Table 9.

d. Other Considerations

Solving the integral equations involves numerical integration by the Romberg technique [32]. Different values for the Romberg integration error were checked and it was found that an allowable integration error of 0.1 percent was sufficient. As described in Reference 7, other considerations in developing the double gage model included smoothing the inputted gage crack data (a_1 and a_2) prior to performing the double gage algorithm, and evaluating various methods for representing the baseline data. Details of these considerations are given in Reference 7.

Table 9 Study of structure integral relative error effect

test	gages pair ID	structure location	structure crack type	structure integral equation relative error					
				.5%	5%	8%	10%	20%	28%
AFCG1	A	3	SCH (2)		+				+
		4	SCH		+				+
		5	CC (3)	+	+	+			+
AFCG2	A	3	SCH		+				+
		4	SCH		+				+
		5	CC	+	+				+
AFCG3	A	3	SCH	+	+	+			+
		4	SCH		+				+
		5	CC	+	+		+	+	+
AFCG4	A	3	SCH						+
		4	SCH						+
		5	CC	+	+				+
AFCG5	A	3	SCH		+				+
		4	SCH		+				+
		5	CC	+	+				+
AFCG5	B	3	SCH		+				+
		4	SCH		+				+
		5	CC		+	+			+
AFCG6	A (1)	3	SCH		+				+
		4	SCH		+				+
		5	CC		+				+
AFCG6	B (1)	3	SCH		+				+
		4	SCH		+				+
		5	CC	+	+		+	+	+
AFCG6	C (1)	3	SCH						
		4	SCH						
		5	CC		+				

(1) - data is available for side "1" only
(2) - single cracked hole
(3) - center crack through the thickness

4. RESULTS OF DOUBLE GAGE MODEL

As reported in Reference 7, 210 Boeing crack gage/structural flaw combinations were examined in evaluating the double gage model. Measured crack lengths from a particular pair of gages were inputted into the model and used to predict the corresponding structural flaw size. Specimen load information was not entered into the calculation scheme, but was computed during the algorithm procedure as outlined previously. In addition to the parametric studies which determined the effect of various solution techniques as described in the last section, calculations were made for 45 different structural crack curves. For brevity, only a sample of those results are given here.

Typical sets of results are given in Figure 30 for each of the six carrier specimens. Here the structural crack length is plotted versus the gage flaw in the transfer function format employed earlier. The triangular points represent measured data taken from Reference 10, the circles are predictions obtained by the double gage model (DGM), and the square points (SGM) represent predictions made by the original load independent (or single gage model) transfer function given by Equation 7. The legend further indentifies the loading applied to the test specimen and the type and location of the crack gage pair and structural flaw.

Note that the double gage model provides, in general, a good estimate of the structural flaw size, and represents an improvement over calculations made by the original Equation 7 transfer function. The one exception, where both analysis schemes fail, is the fighter spectrum

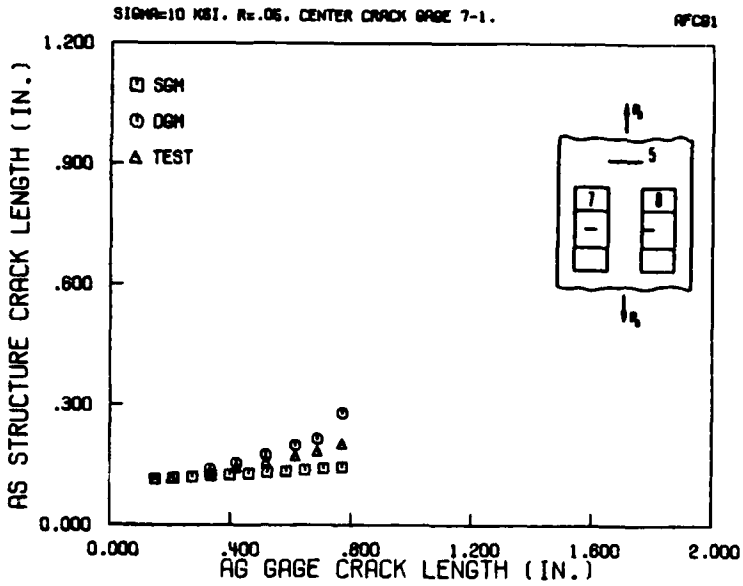

(a)

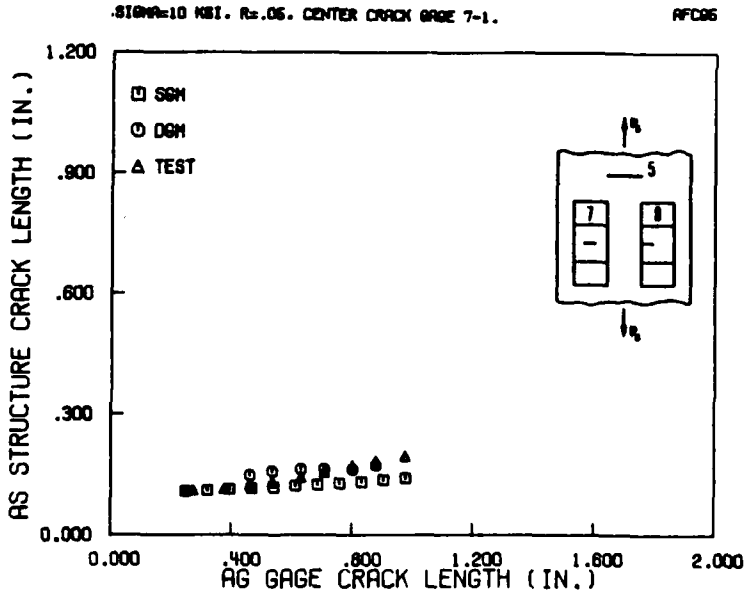

(b)

Figure 30: Comparison of DGM predictions with SGM predictions for various amplitude loadings.

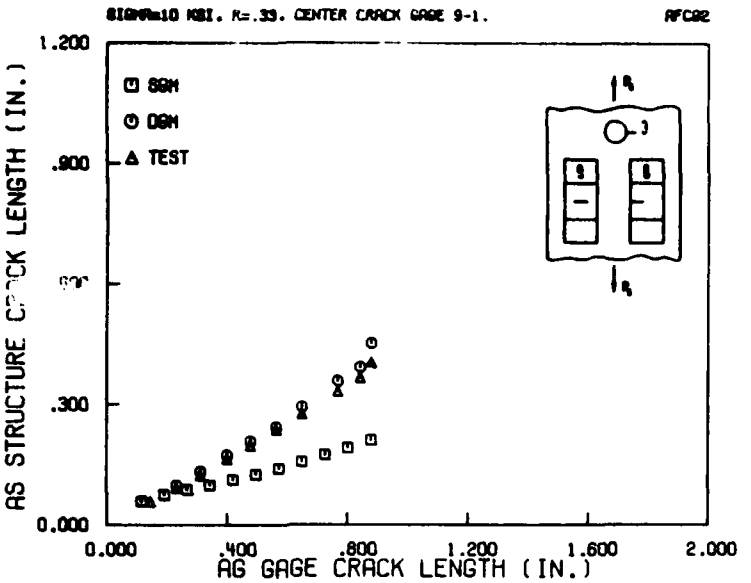

(c)

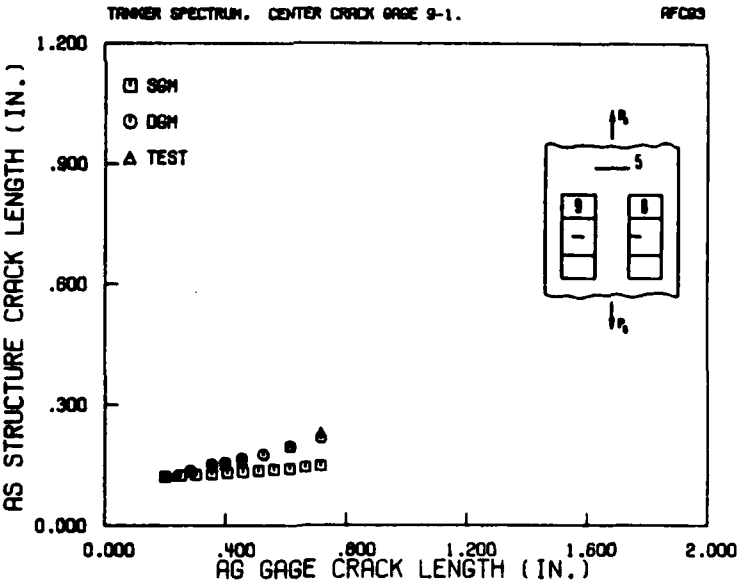

(d)

Figure 30: continued.

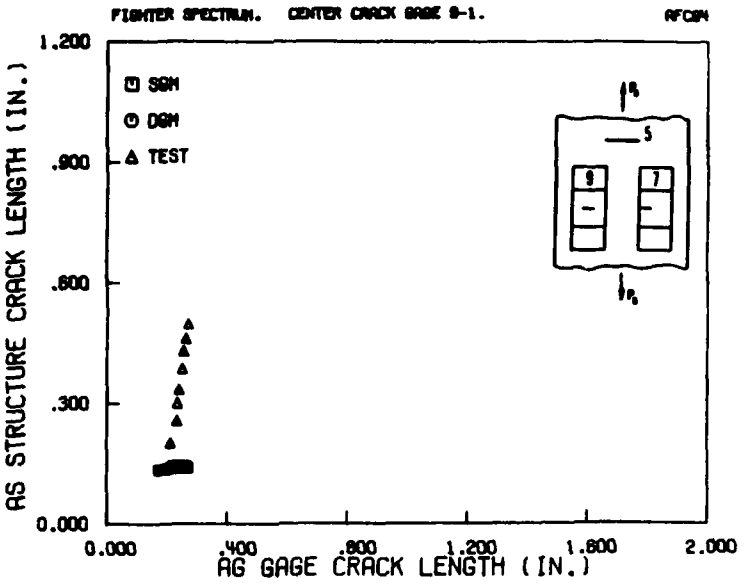

(e)

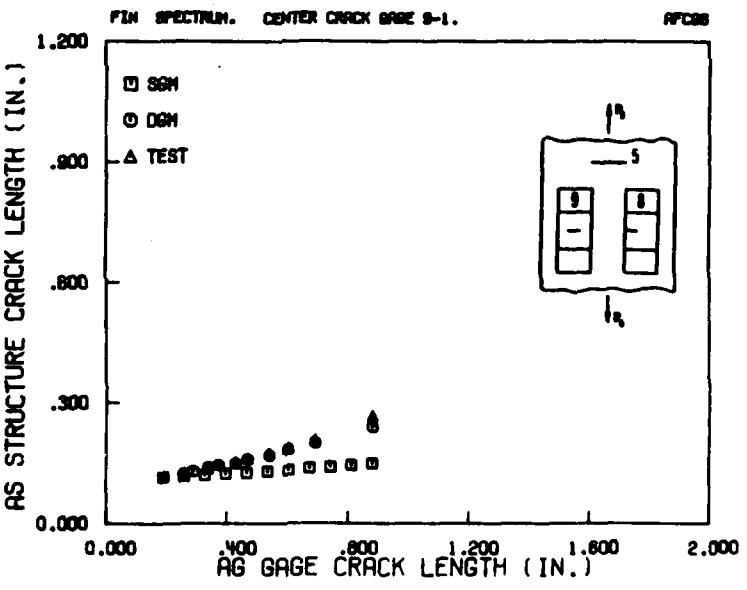

(f)

Figure 30: continued.

load history given in Figure 30e. The Boeing crack gages were of a stepped design, where the crack was placed in a section with a uniform 0.02 in. thickness [10]. Since the fighter load history contained large tensile overloads, crack retardation was more prevelant in the thin crack gage than in the thicker structural member, and, thus, the gage crack grew slower than predicted. (Recall that this thickness dependent retardation problem provided the motivation for the side-grooved gage research described in Section 3.) Although several other calculation schemes were investigated [7] to determine if the double gage model could make better predictions for the fighter spectrum, these efforts were largely unsuccessful. Nevertheless, good predictions were obtained by the double gage model for the other loadings given here and in Reference 7.

Since the double gage model predicts an effective stress σ_{eff} during the calculation scheme, it is interesting to compare the computed effective stress with the actual applied load. Several different stress representations were computed for the known spectrum loadings, including various root mean square characterizations [3]. Comparison of the computed effective stress from the double gage model revealed that the maximum peak to peak stress which occurs during the spectrum agreed best with the effective stress computed by the double gage model (see Table 10). The maximum peak to peak stress parameter $\Delta\sigma_{max}$ is defined as the difference between the largest and minimum stresses which occur during the repeated load history.

Table 10

Comparison of applied stress and effective stress computed by double gage model for Boeing Test results.

Test	Applied Stress (ksi)		Computed Effective Stress σ_{eff} (1)
	Constant amplitude σ_{max}, R	Spectrum $\Delta\sigma_{max}$	
AFCG 1	10, .05	0.95	10.07
AFCG 2	10, .3	0.7	6.88
AFCG 3 (Wing)		23.95	26.32
AFCG 4 (Fighter)		21.53	20.43
AFCG 5A	10, .05	0.95	10.80
AFCG 5B	10, .05	0.95	10.85
AFCG 6A (Fin)		16.54	17.00
AFCG 6B (Fin)		16.54	18.75

Notes

1. All double gage model calculations are based on R = 0.05 constant amplitude baseline data (da/dN versus ΔK).
2. A and B predictions for Tests AFCG 5 and AFCG 6 resulted from different gage pair combinations.

Section 5

SUMMARY AND CONCLUSIONS

The objective of this report is to summarize results of an investigation conducted to develop the crack growth gage concept as an advanced individual aircraft tracking technique. More detailed descriptions of the research are described in References 7 and 23. This particular program involved two major goals: (1) development of a thin side-grooved crack growth gage which would yield crack growth behavior which approximates that found in thicker structural components, and, (2) development of the Double Gage Model as an improved transfer function for relating gage and structural crack lengths. Results and conclusions from these two studies are summarized below.

1. SIDE-GROOVED CRACK GROWTH GAGE

The objective of this task was to develop a thin section crack gage coupon which would minimize thickness dependent crack retardation effects. The particular goal was to simulate plane strain conditions in a thin crack gage through use of deep side-grooves. This approach was based on the concept that if plane strain behavior could be induced in the thin crack gage by the side-grooves, the gage crack tip plastic zone would match that found in the thicker structural member (also in plane strain), and similiar crack retardation behavior would be experienced by both gage and structural flaws. Earlier investigations have suggested that thickness dependent retardation effects could cause crack growth in the thin coupon to yield an unconservative estimate of the structural flaw size.

A series of finite element stress analyses conducted on various side-groove configurations indicated that plane strain behavior could be induced in the thin test section, and helped evaluate the influence of various side-groove parameters on the crack gage design. Fatigue crack retardation tests were then conducted with side-grooved members, and confirmed that the side-grooves did, in fact, simulate thick section crack growth behavior by minimizing thickness effects on crack retardation.

Several side-groove configurations were considered for use with crack growth gages, including single and double side-groove geometries. Subsequent testing with crack gages bonded to large carrier specimens indicated that the double side-groove configuration performed well, while the single side-groove design gave erratic results. The large carrier specimens were subjected to several different load histories, including constant amplitude cycling with and without overloads, various mean stress levels, and three versions of a variable amplitude fighter spectrum. Although the results did depend on the source of gage manufacturer (there were two sources), consistency was obtained within each group. It is suggested that more stringent controls be placed on gage machining to avoid possible residual stress effects.

Composite plots of crack gage performance were prepared for gages with common design and manufacture. The results of seventeen similiar double side-grooved gages fell within a distinct band. Part of the scatter is due to the effect of load history on the relation between structure and gage flaws. The variation in remaining output was attributed to slightly different initial crack lengths, and to the normal scatter seen in fatigue

crack growth behavior. Predictions for the structure/gage crack transfer function agreed well with the original load independent analysis.

The side-groove gage does minimize thickness dependent crack retardation effects, although there is still some load dependence on the gage/structure crack transfer function. It is suggested that this design be given further evaluation. Future efforts should evaluate slightly longer gage lengths in order to increase growth of the gage crack in relation to the structural flaw.

2. DOUBLE GAGE MODEL

The objective of this task was to develop a general transfer function for relating structural and gage cracks. The original model employed in earlier work is based on the assumption that fatigue crack growth rates are a simple power law function of the cyclic stress intensity factor. When this assumption is met, the structure/gage relation is independent of the applied load, and depends only on geometric and material properties. Although the load independent model has performed well in earlier tests, and successfully predicted the side-groove crack gage behavior obtained in the current effort, it was hoped an alternate approach would allow more general fatigue crack growth relationships to be used in the analysis scheme. Attempts to incorporate other crack growth models in the original algorithm result in a single equation with two unknowns: structural flaw size, and applied load. Although the applied loading could be supplied by other means, the crack gage would no longer serve as a single monitoring device, having to be supplemented by an additional sensor.

The new approach, designated the double gage model, introduces an additional degree of freedom into the numerical algorithm by using crack length data from two separate crack gages located at the same control point. The information obtained from the two independent crack gages allows calculation of an effective system stress. This system stress is then used to compute the desired structural crack length. The advantage of the new procedure lies in the fact that all required information is obtained from the crack gages, and that arbitrary fatigue crack growth rate models may be used in the computation. This advantage is especially significant if either the structure or gage flaw is propagating in a region where the slope of the da/dN versus ΔK relation is changing (such as near the threshold and/or fracture portions of the fatigue crack growth rate curve).

A computer program was written to perform the double gage calculations. Crack gage data available from an earlier research effort conducted by the Boeing Company provided a convenient test bed to evaluate the computer program. Over 200 test cases were considered in evaluating various computational schemes.

In general, the double gage model provided good predictions for the structural flaw as a function of the gage crack lengths. One exception occurred when poor predictions were obtained for test results from a fighter spectrum. This poor correlation was attributed to the thickness dependent retardation problem addressed separately by the side-groove research (the other major goal of the current program). It was not possible to use the double gage model to predict the current side-groove

gage test results, since the approach requires crack length data from two different crack gage designs, and the well characterized side-groove coupons were quite similiar in shape.

In summary, the double gage model provided an effective means to correlate crack gage and structural flaws. Improved predictions were made in several cases, and the computed effective stress was determined to have a reasonable value in comparison to the applied loads. The approach does require, however, a fairly large amount of preliminary data to optimize various calculation strategies.

3. CONCLUDING REMARKS

This effort, along with the companion program described in reference 27, has considered the crack growth gage approach to Individual Aircraft Tracking. The eventual goal is to develop a sensor which records aircraft usage and responds with an output which can be related the crack growth life of structural components. Although it has been demonstrated that gage crack length can be related to extension of an assumed structural flaw, the crack size relationship is subject to variability. This "scatter" may be attributed to load history dependence, to initial crack size variation, and to inherent variability in the fatigue process. Since calculations discussed in Reference 27 indicate that crack length variations can magnify errors in the predicted structural life, the role of the crack gage in Individual Aircraft Tracking deserves closer examination. It may be possible to reduce the variability in the gage/structure crack relation caused by load history dependence through a more sophisticated analysis which employs data from an alternate source (perhaps a simple pilot log). In this context, the crack gage would not serve as a stand alone tracking device, but when

used in conjunction with another method, might still play a useful role in simplifying and improving the accuracy of the overall tracking system.

The remaining question regarding inherent variability in fatigue crack growth, however, has more significant implications, both from the standpoint of the sensor (the crack gage) and the monitored quantity (the structural crack growth life). Scatter in gage crack growth certainly can influence the predicted structural flaw size, although this disadvantage may be offset by the potential simplicity and economic advantages of the crack gage method. It must be remembered, however, that even a "perfect" tracking sensor could be developed - one that always responds in exactly the same way to a given load history - scatter in structural fatigue crack growth will still exist. The implications of this structural crack growth variability on the Individual Aircraft Tracking mission should be investigated further. Tests similar to those in the present program, where a sensor was mounted to a simulated structural component and both sensor output and structural crack growth were measured for various load histories, should be conducted with other tracking devices. In this manner, it may be possible to determine the influence of structural crack growth variability on the tracking ability of other devices as well.

APPENDIX A

SIDE-GROOVE GAGE CRACK GROWTH DATA

Individual crack growth curves for the side-grooved crack growth gage carrier tests are presented in this Appendix. The format for data presentation is similar to the examples discussed in Section 3. Results are given for the 16 ksi, 22 ksi, and spectrum loading tests summarized in Table 3.

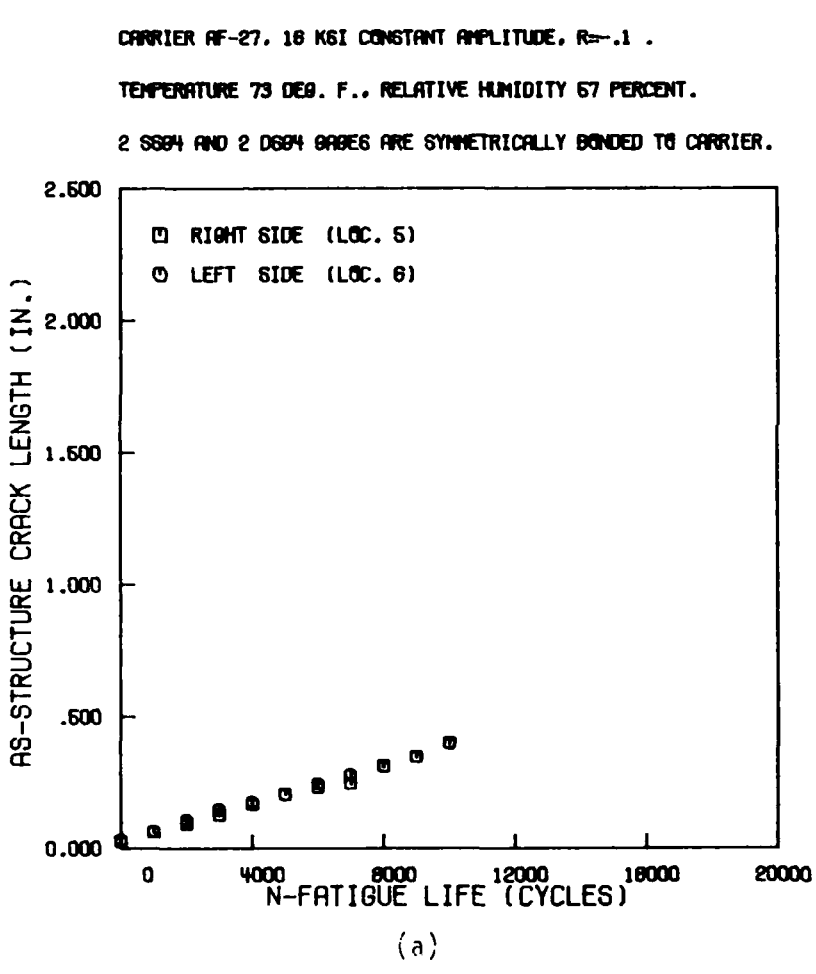

(a)

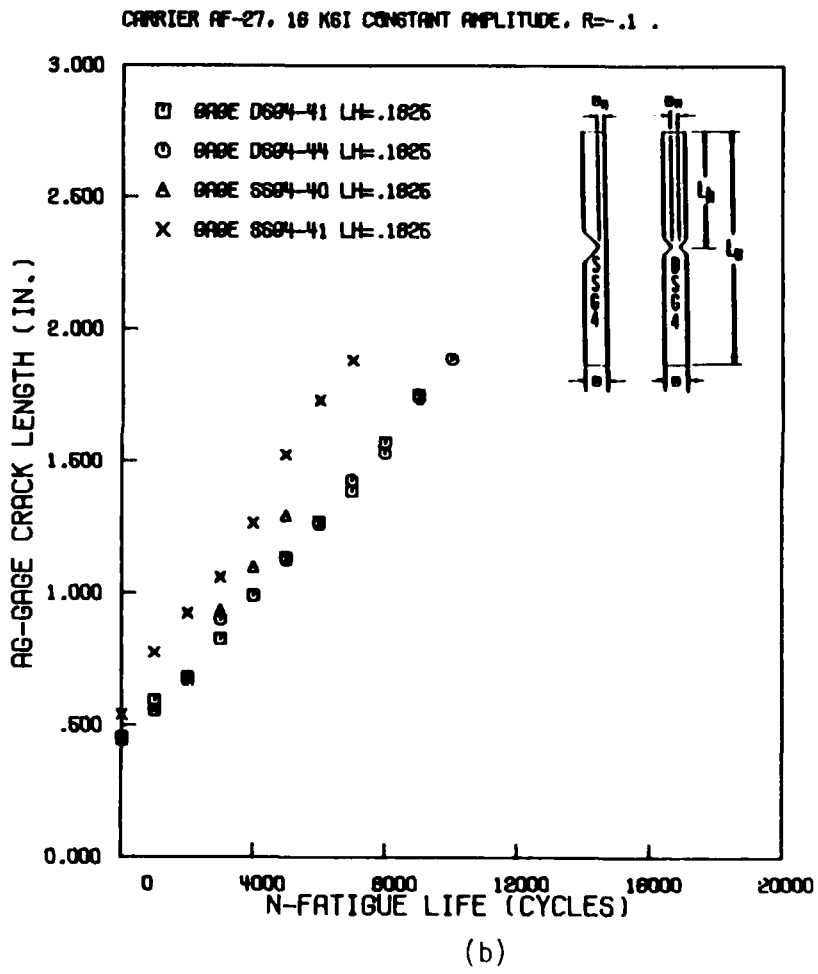

(b)

Figure A1 : Crack growth data for carrier AF-27

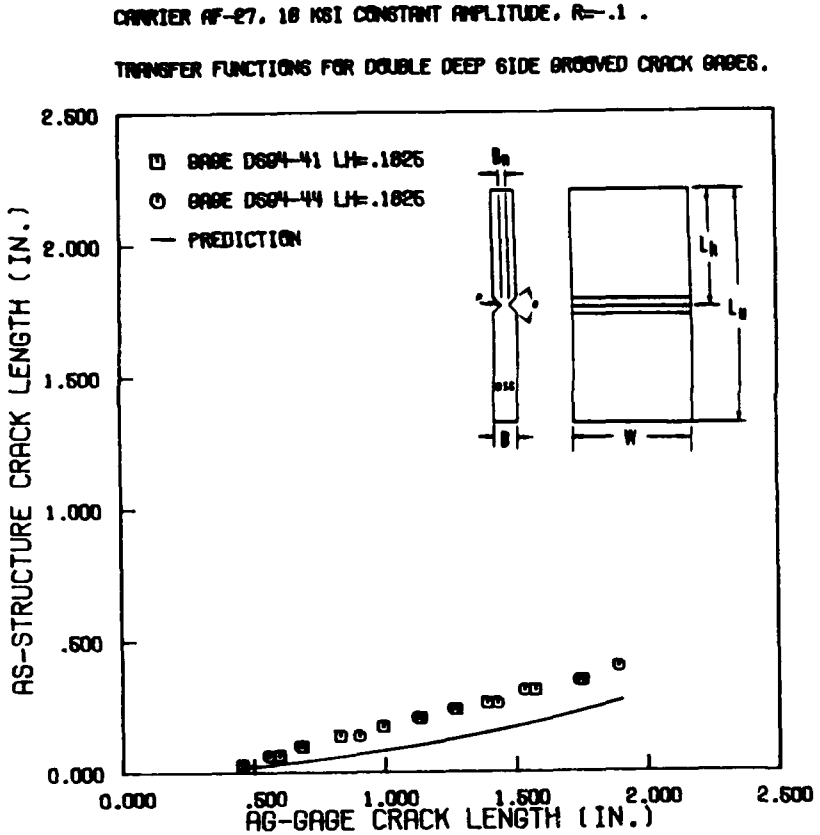

(c)

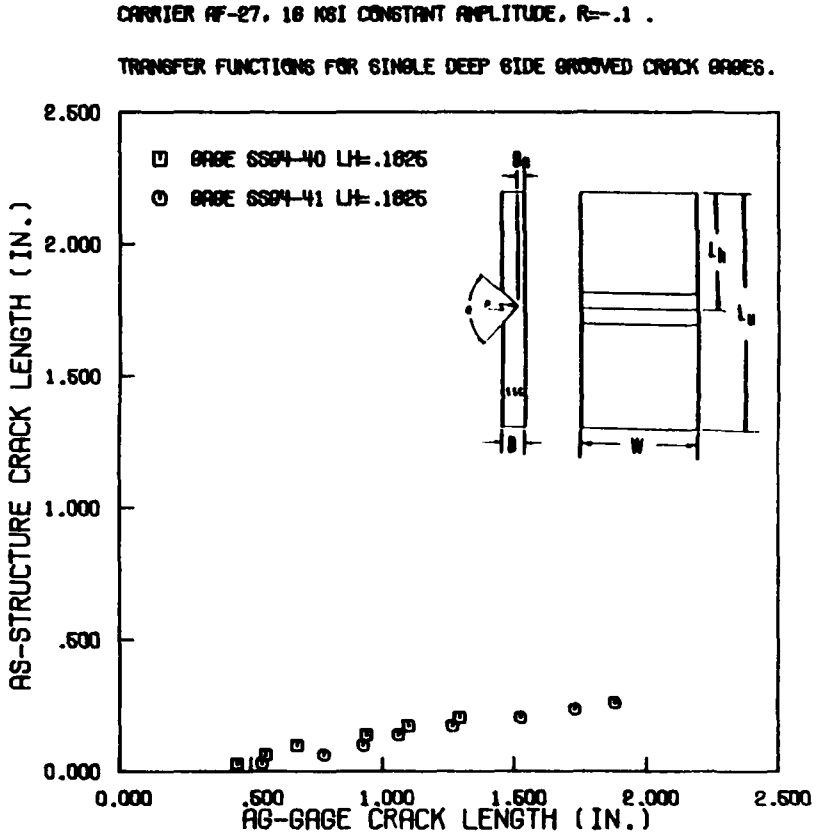

(d)

Figure A1, continued

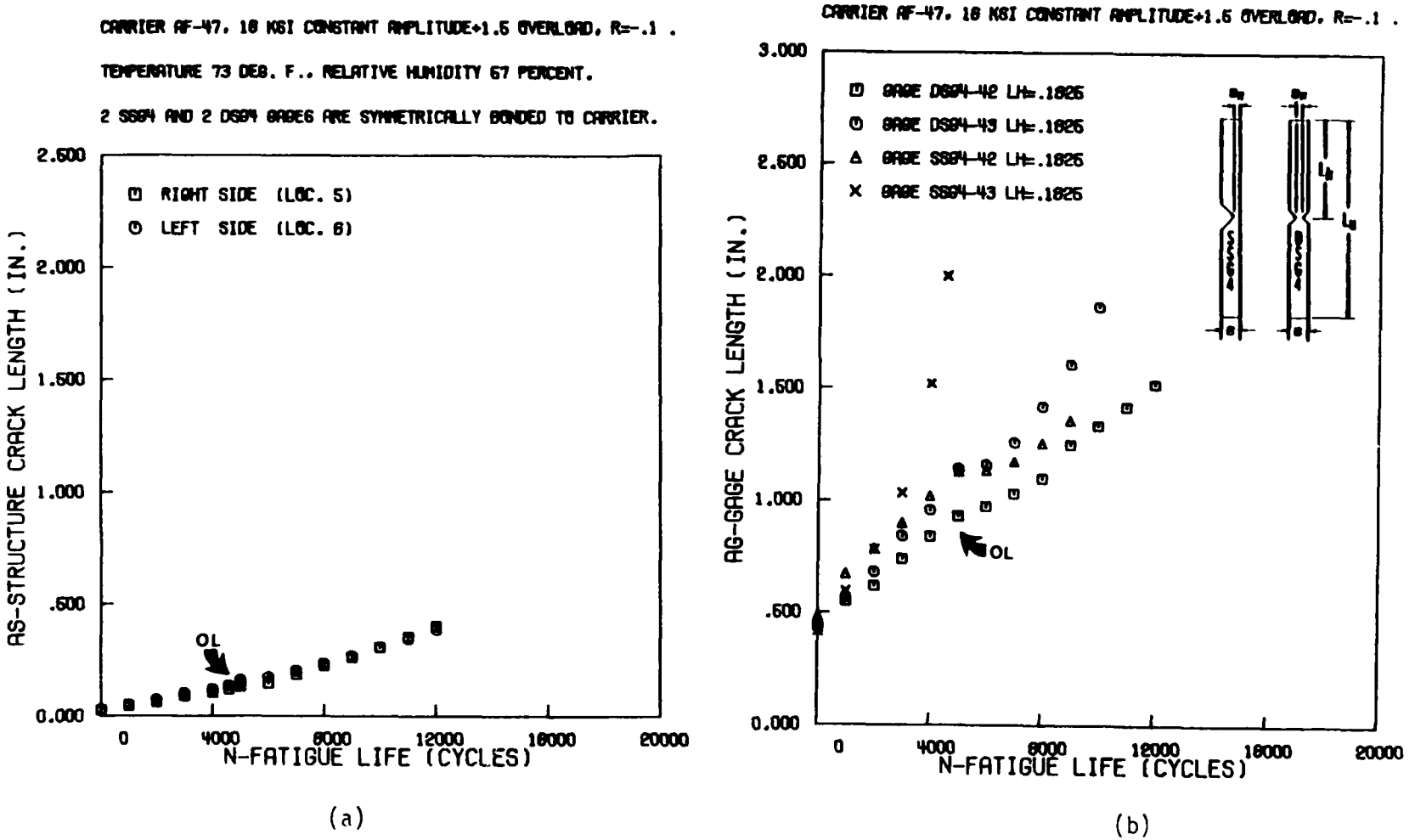

Figure A2 Crack growth data for carrier AF-47

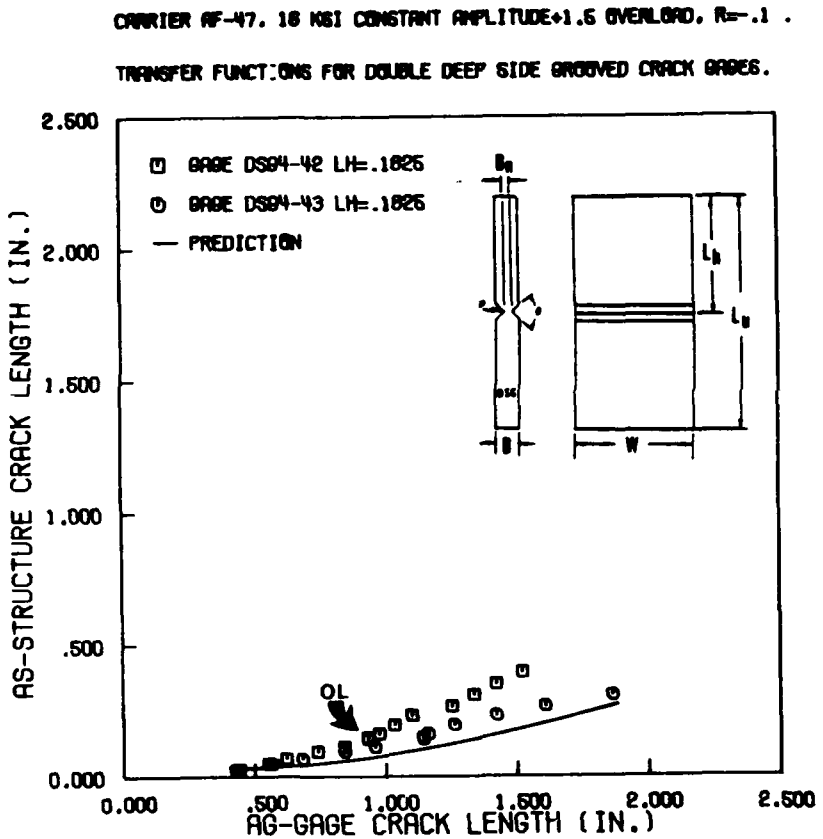

(c)

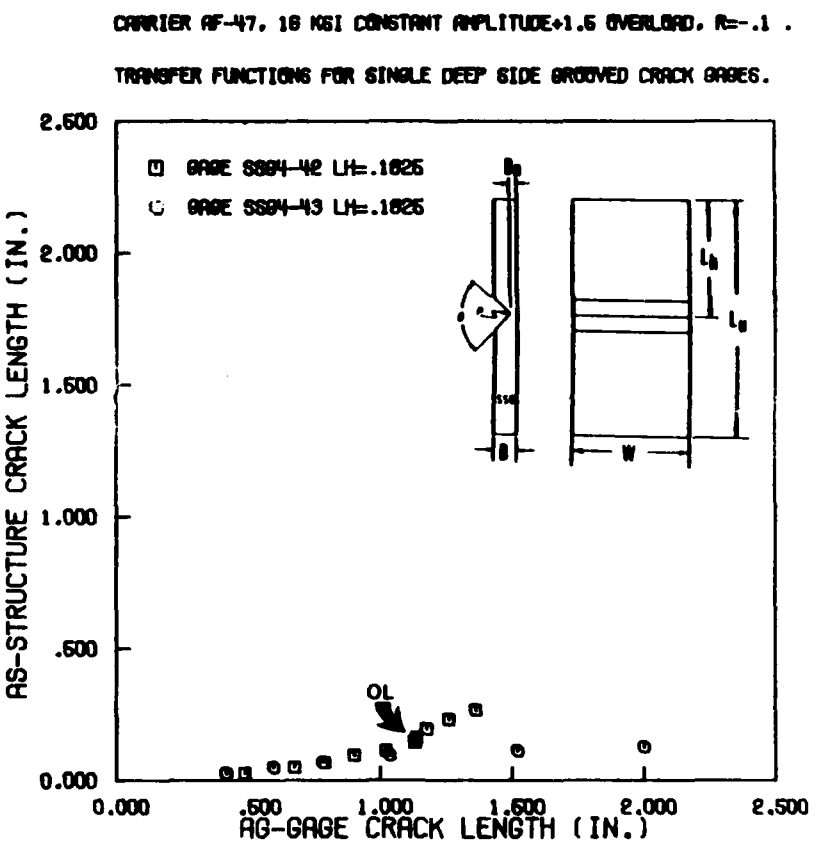

(d)

Figure A2, continued

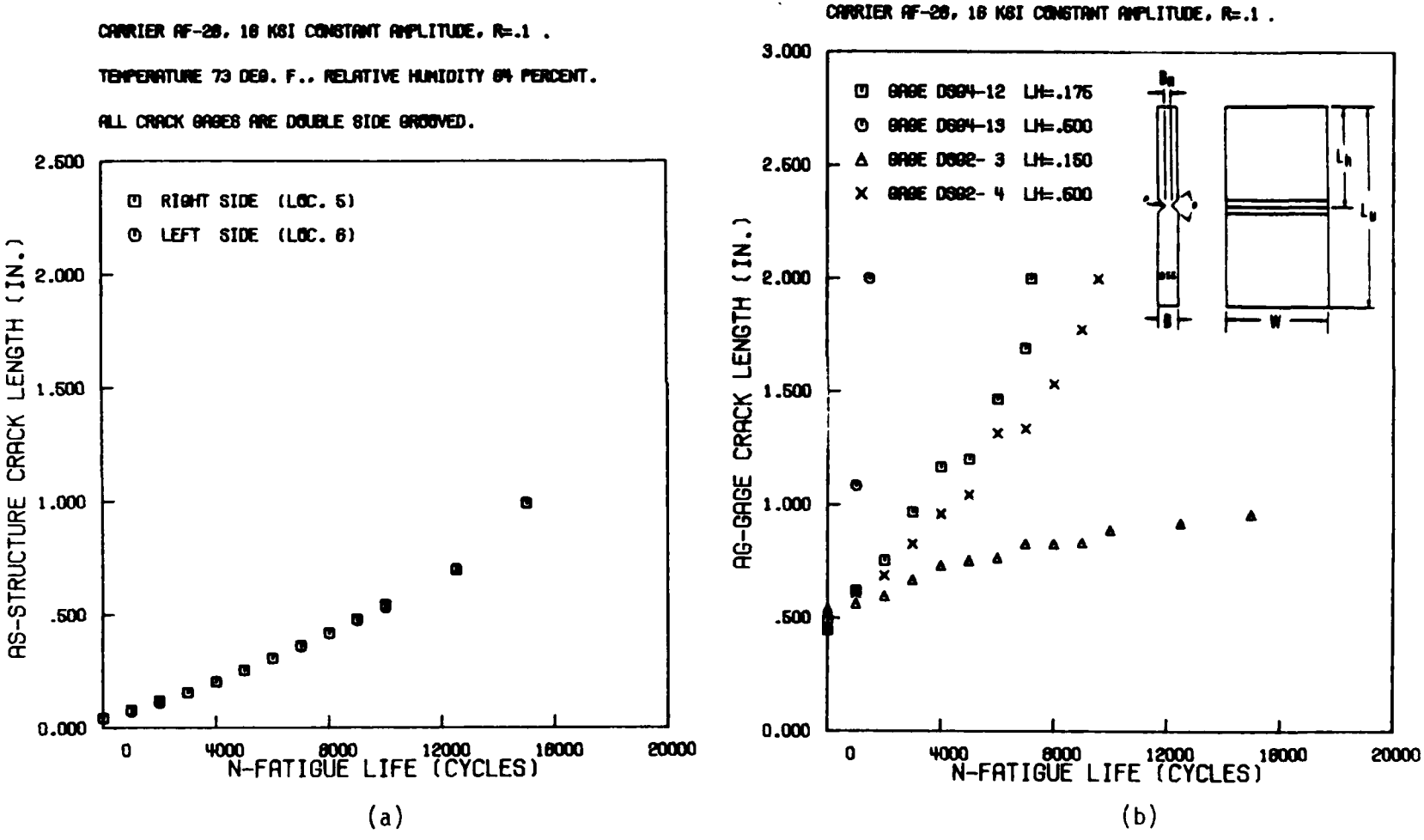

Figure A3 Crack growth data for carrier AF-28

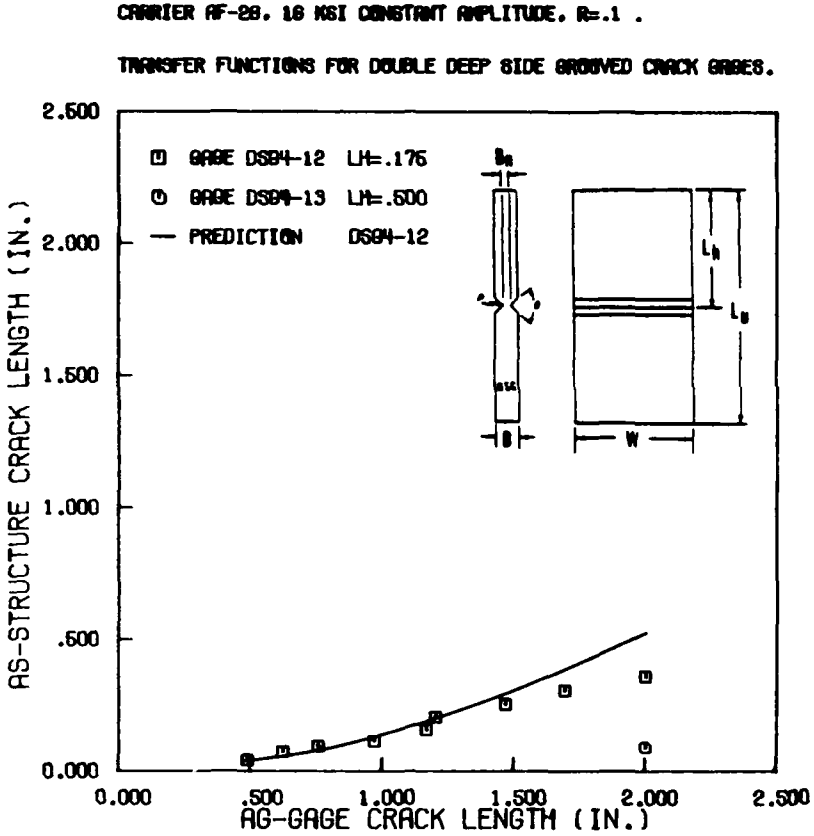

(c)

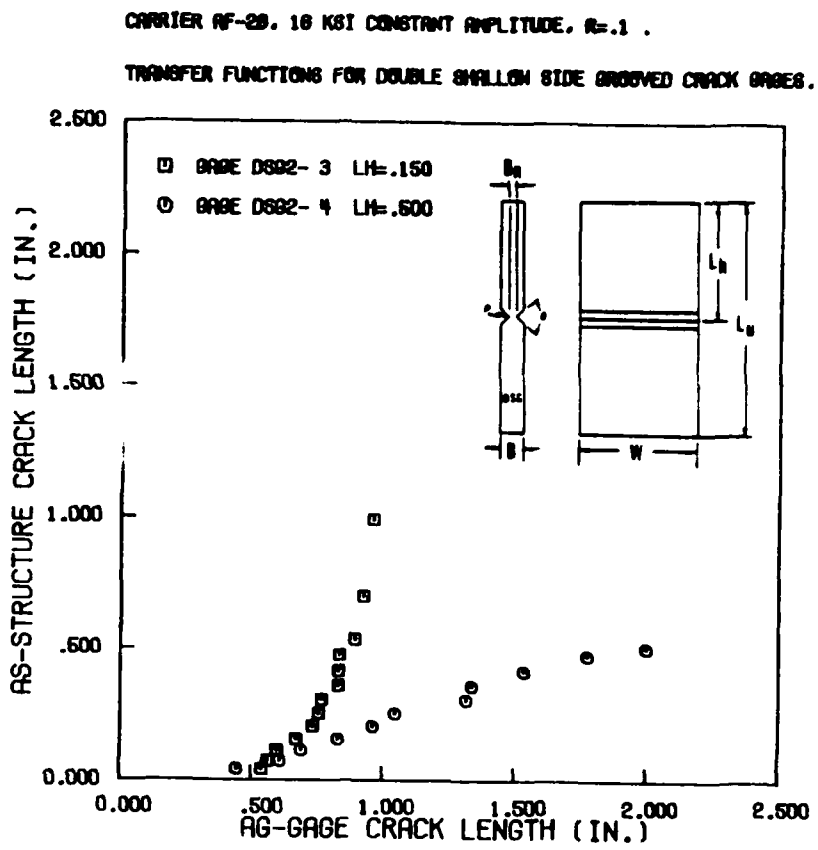

(d)

Figure A3, continued

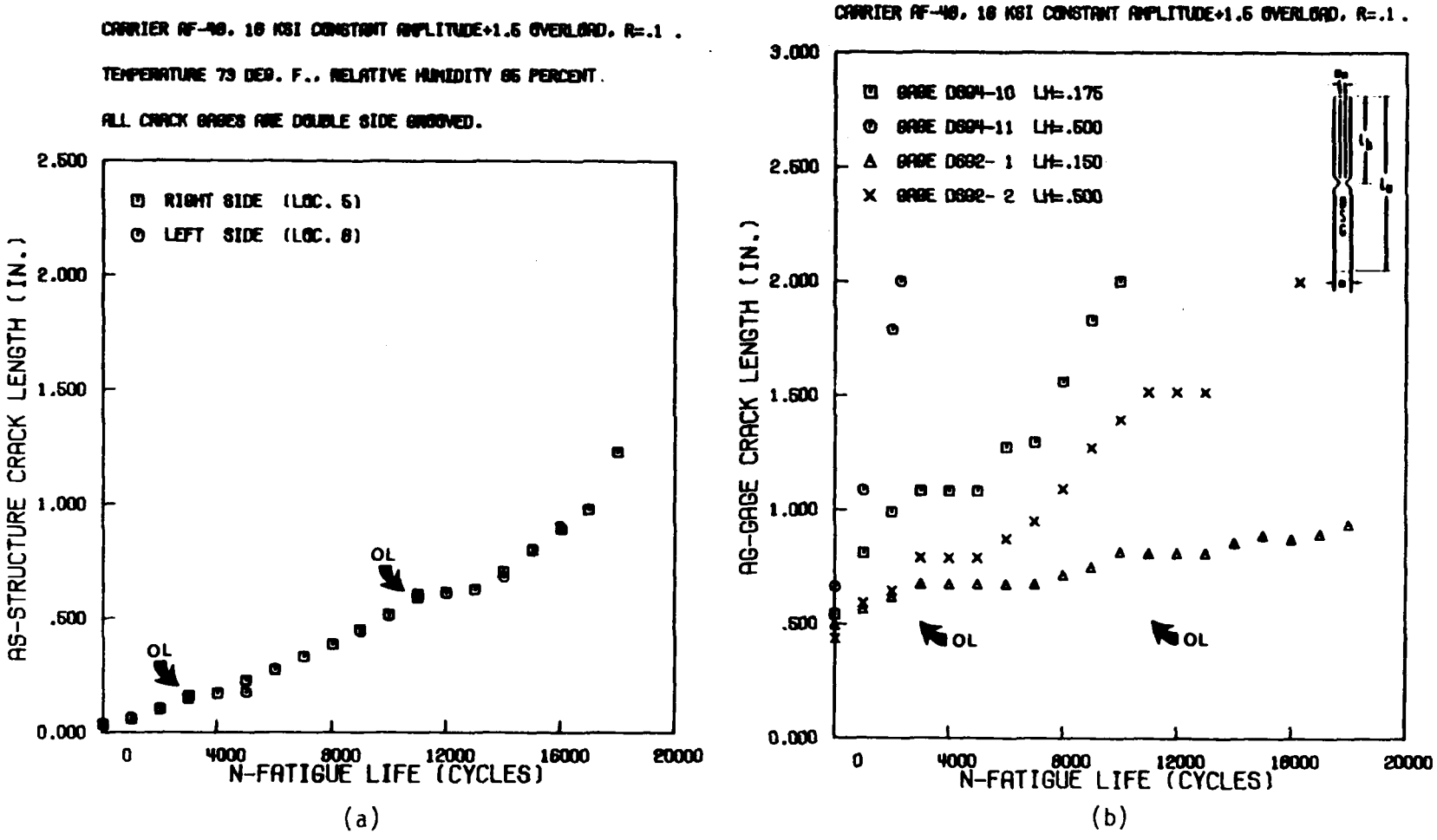

Figure A4 Crack growth data for carrier AF-48

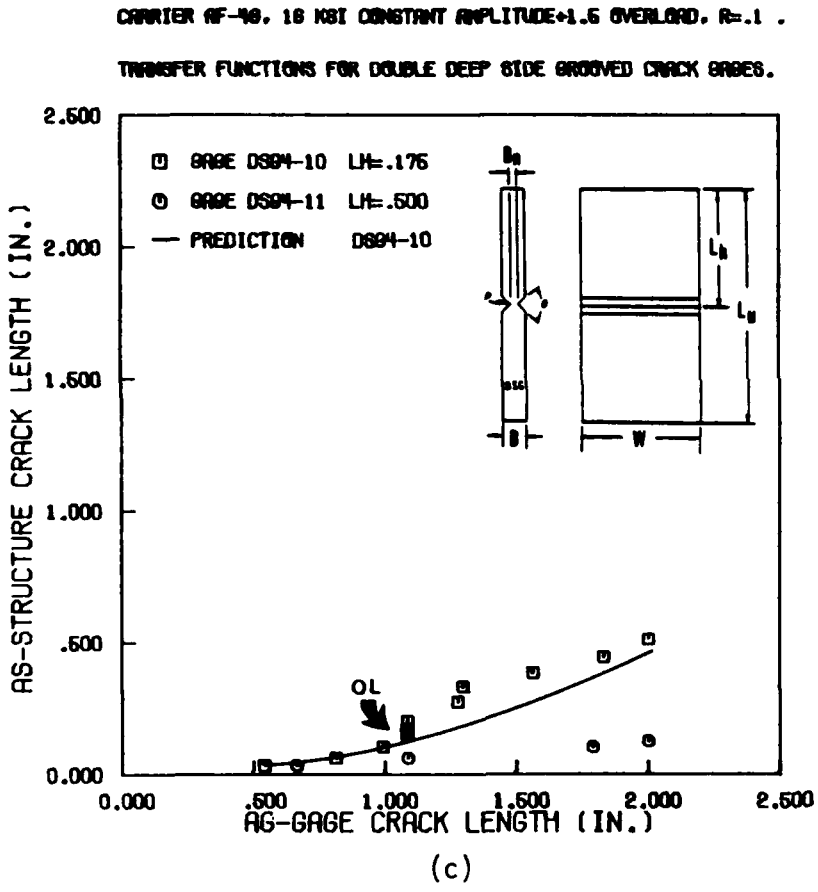

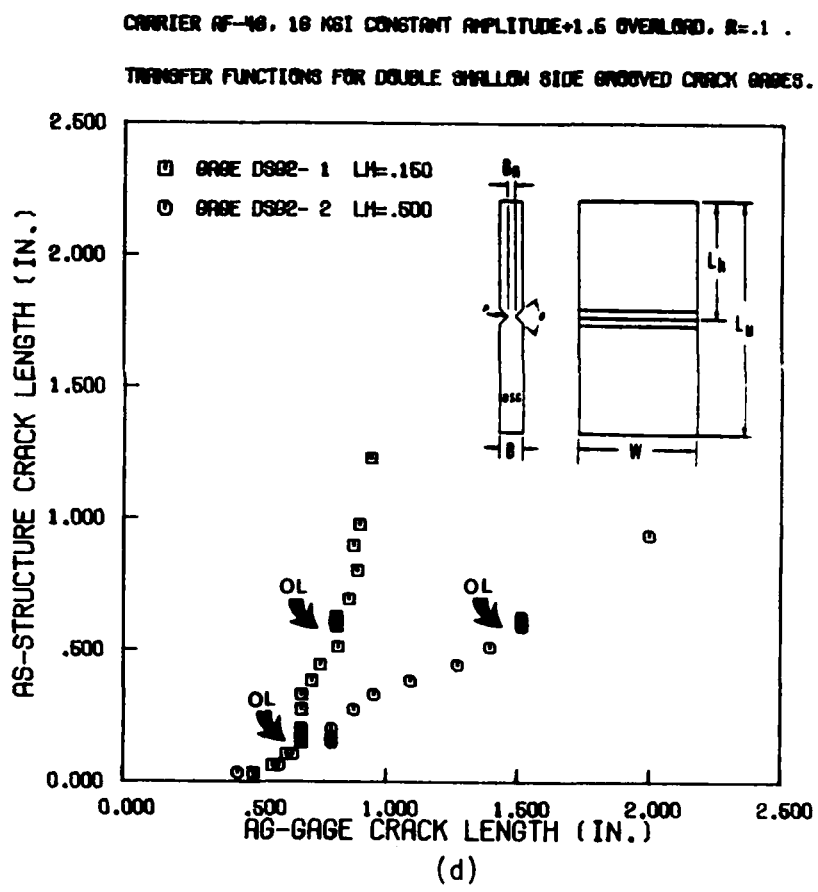

Figure A4, continued

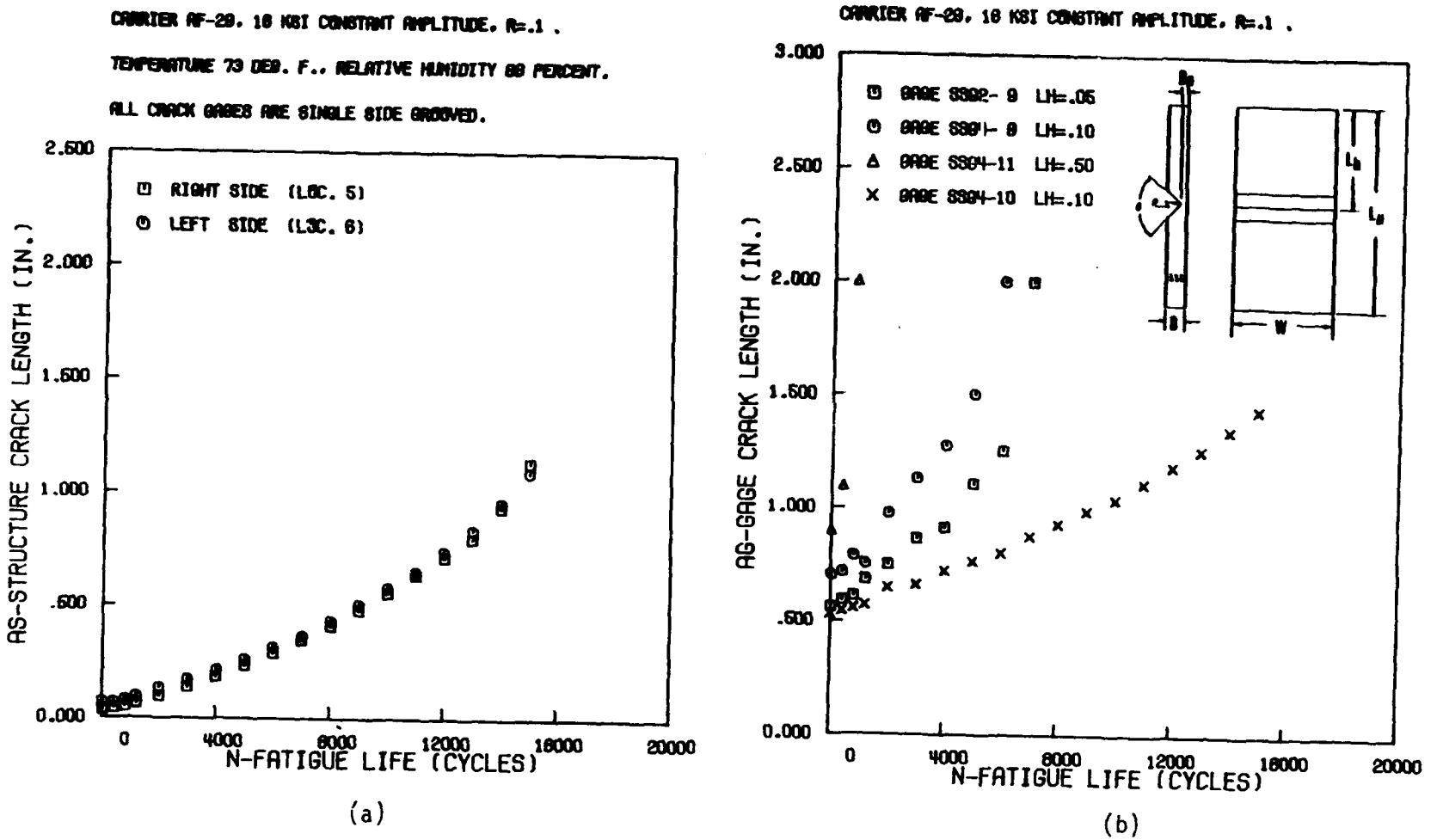

Figure A5 Crack growth data for carrier AF-29

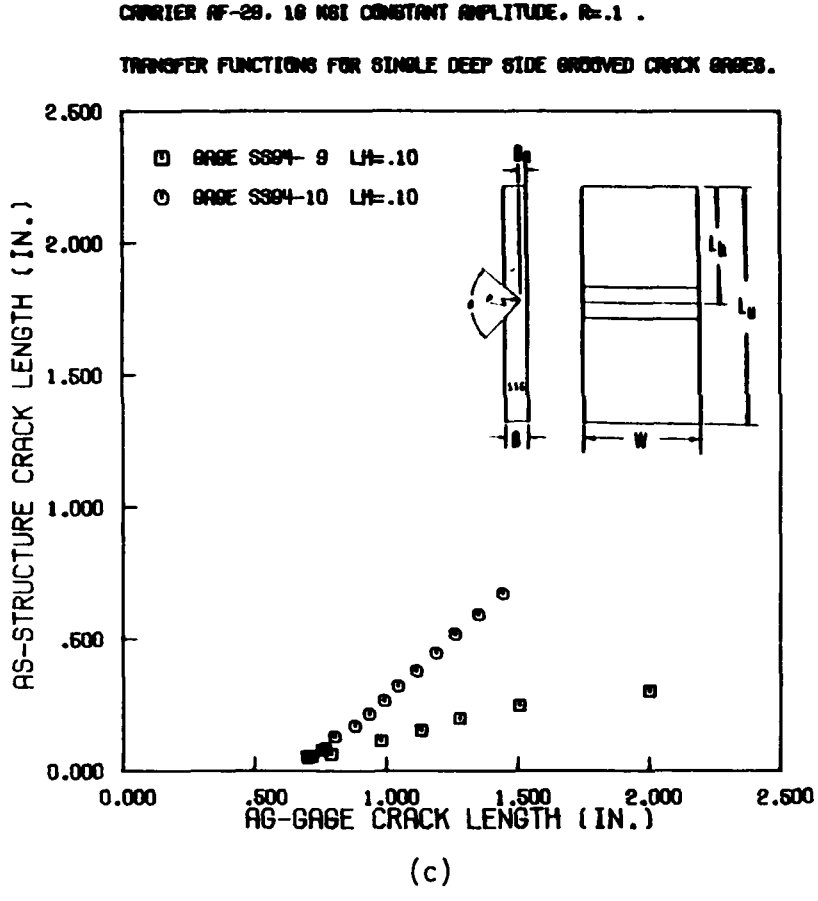

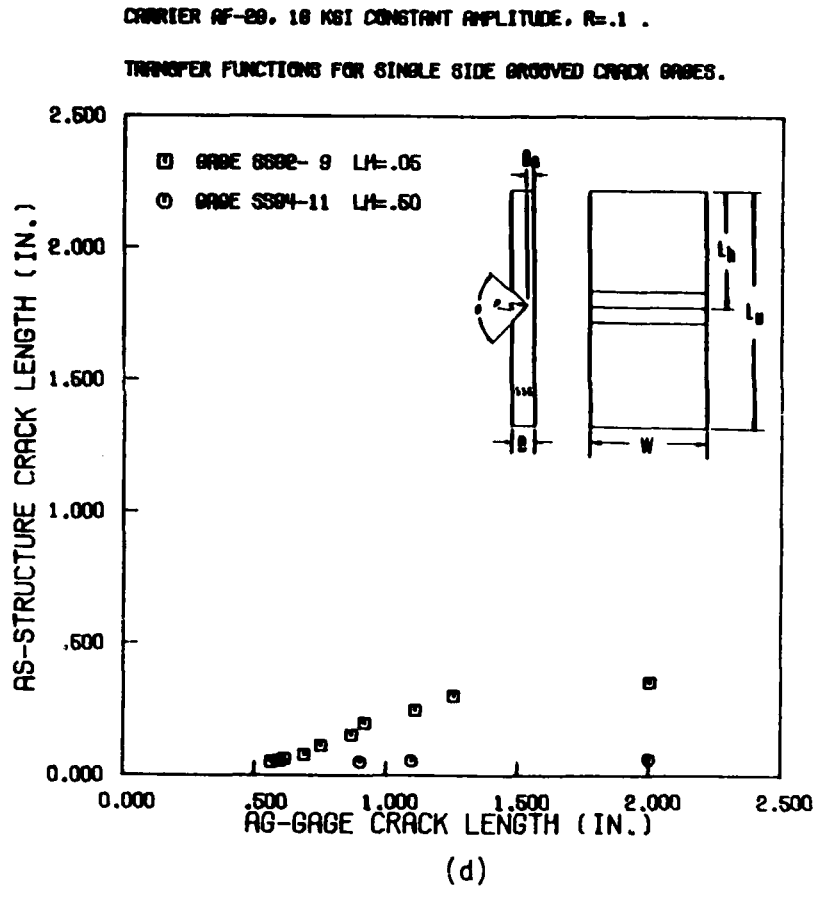

Figure A5, continued

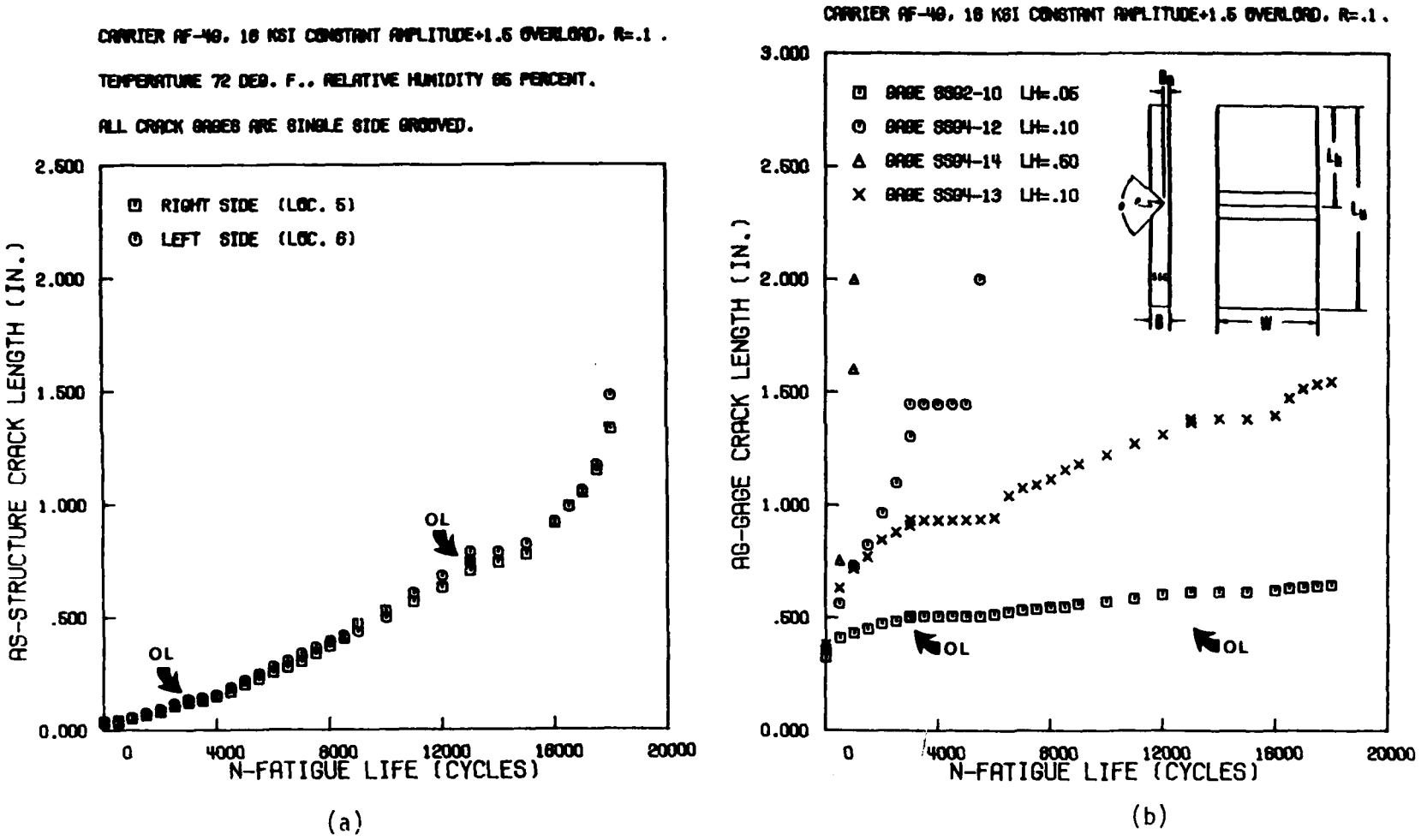

Figure A6 Crack growth data for carrier AF-49

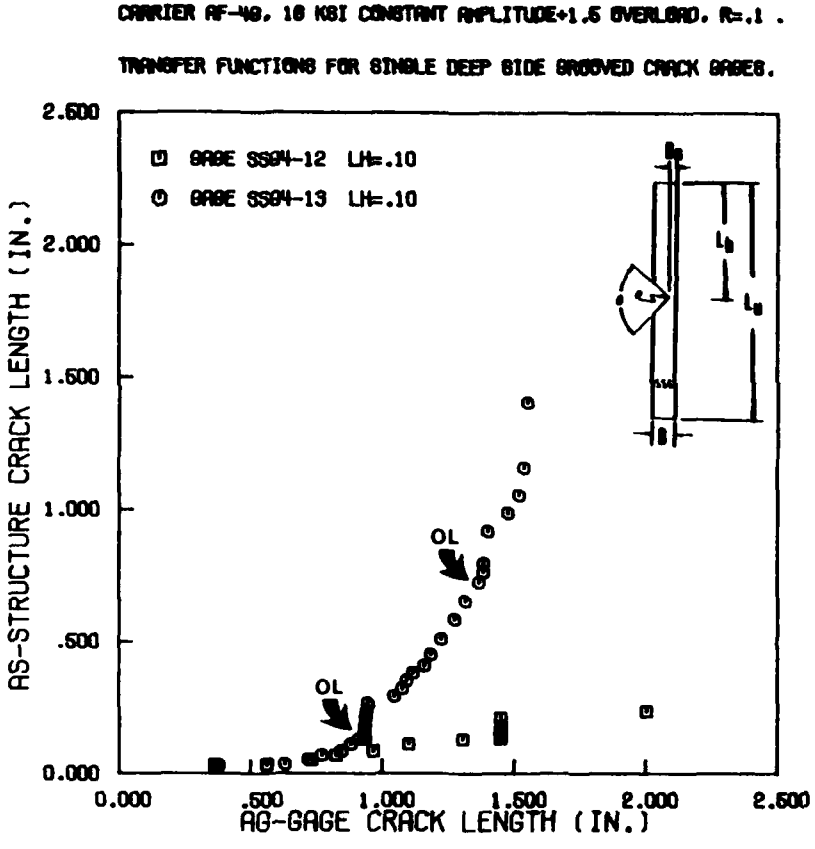

(c)

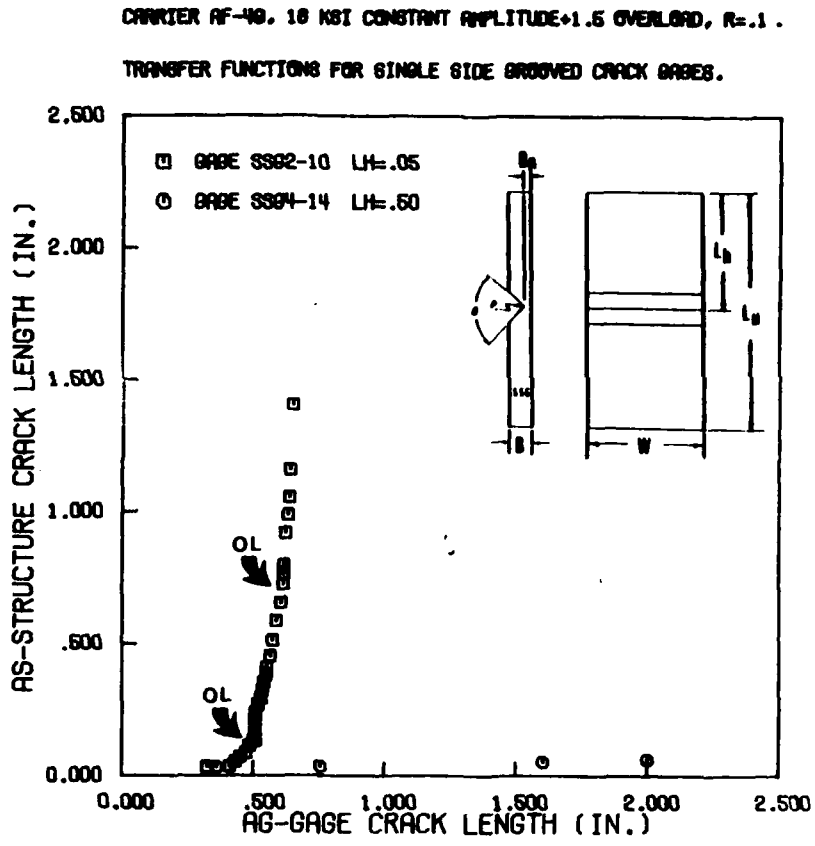

(d)

Figure A6, continued

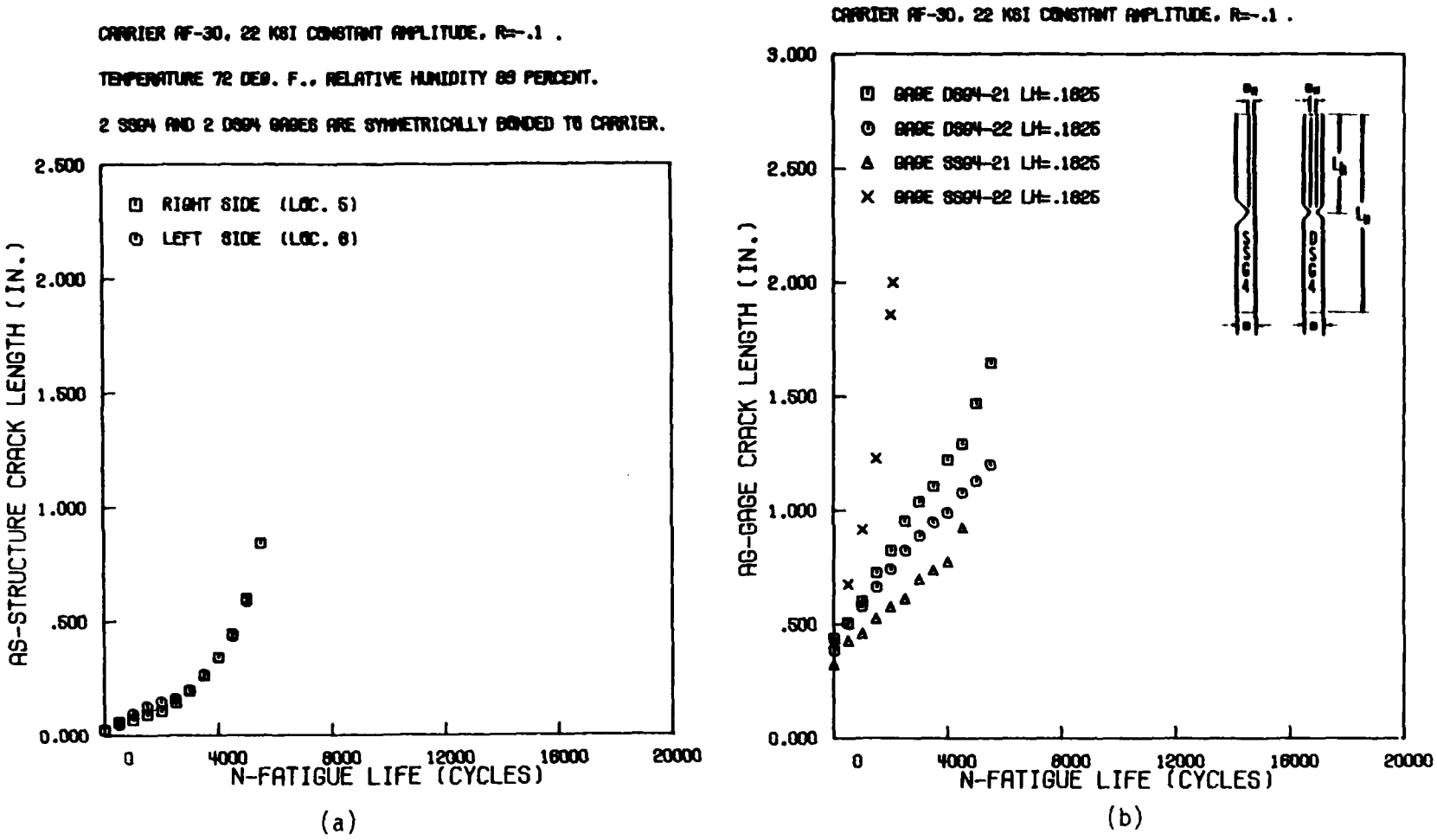

Figure A7 Crack growth data for carrier AF-30

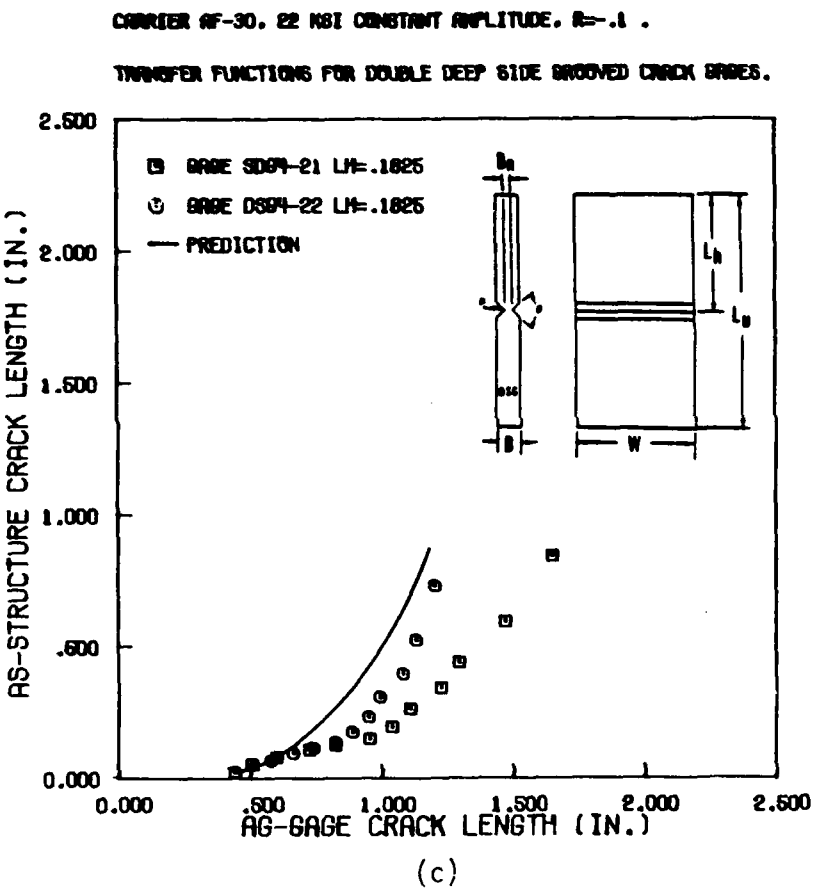

(c)

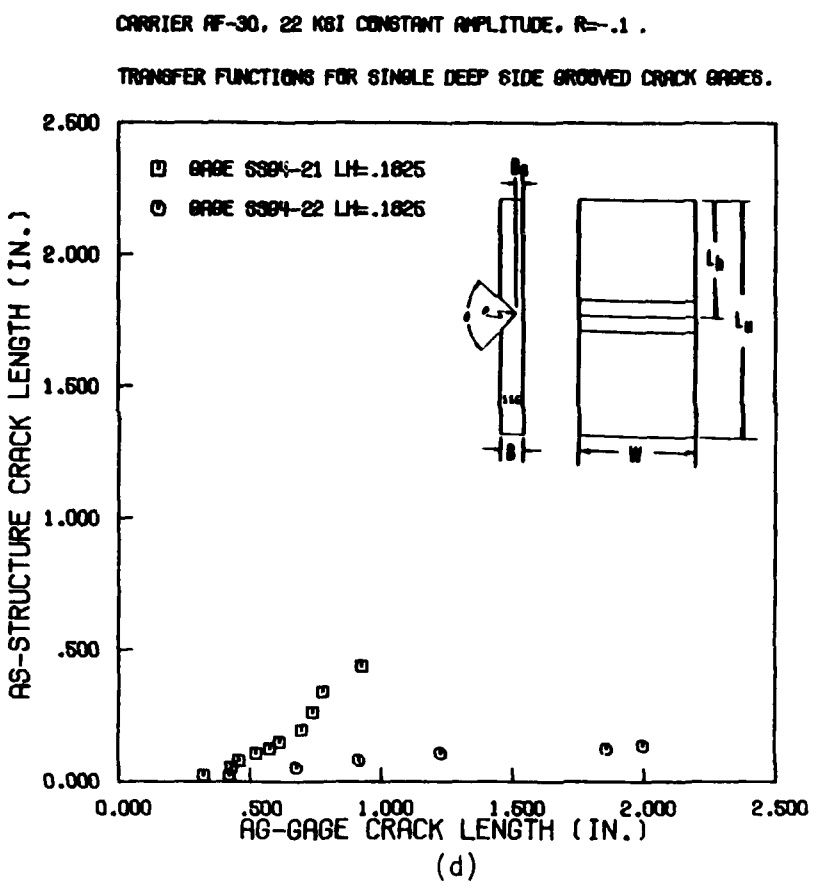

(d)

Figure A7, continued

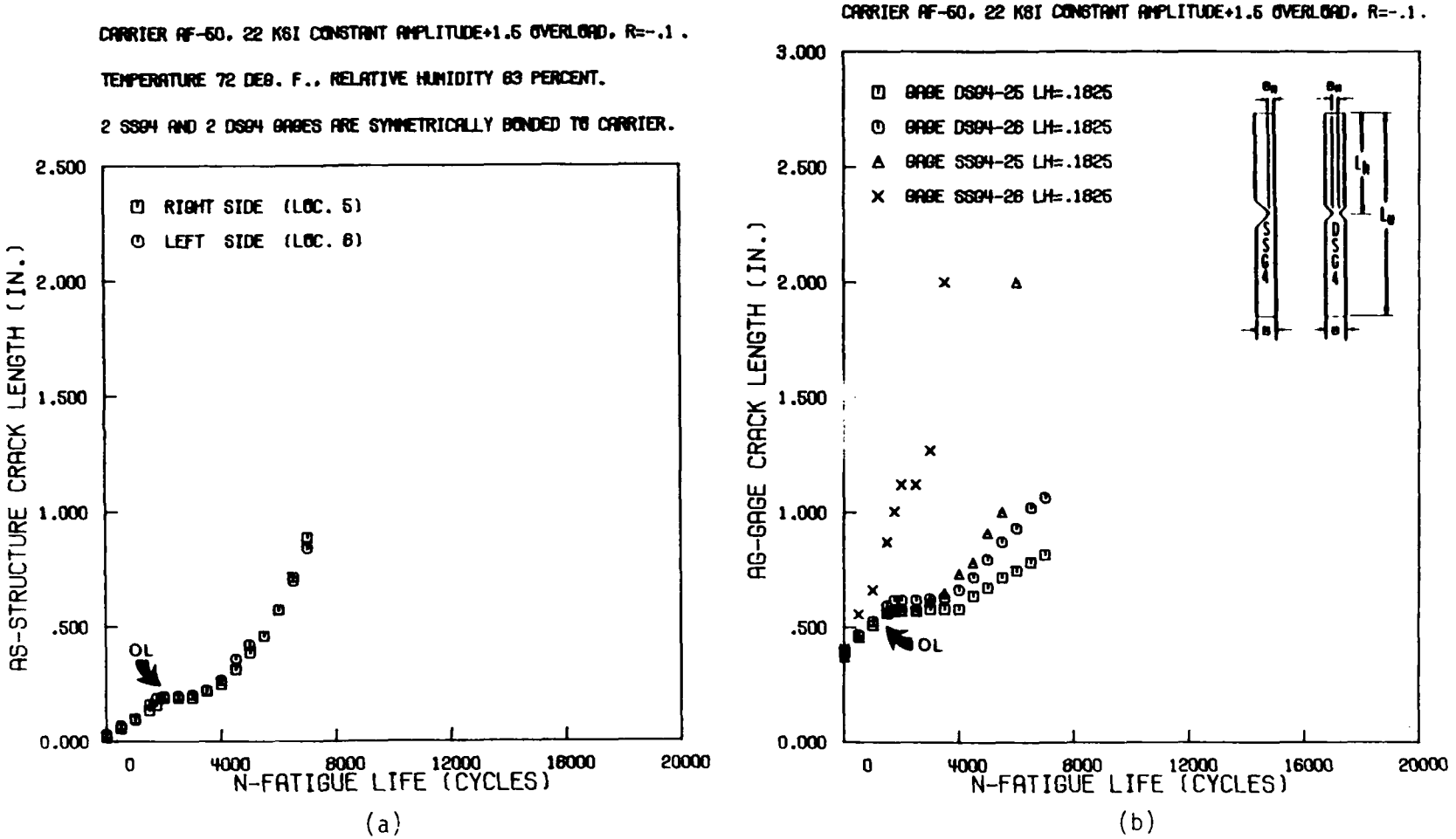

Figure A8 Crack growth data for carrier AF-50

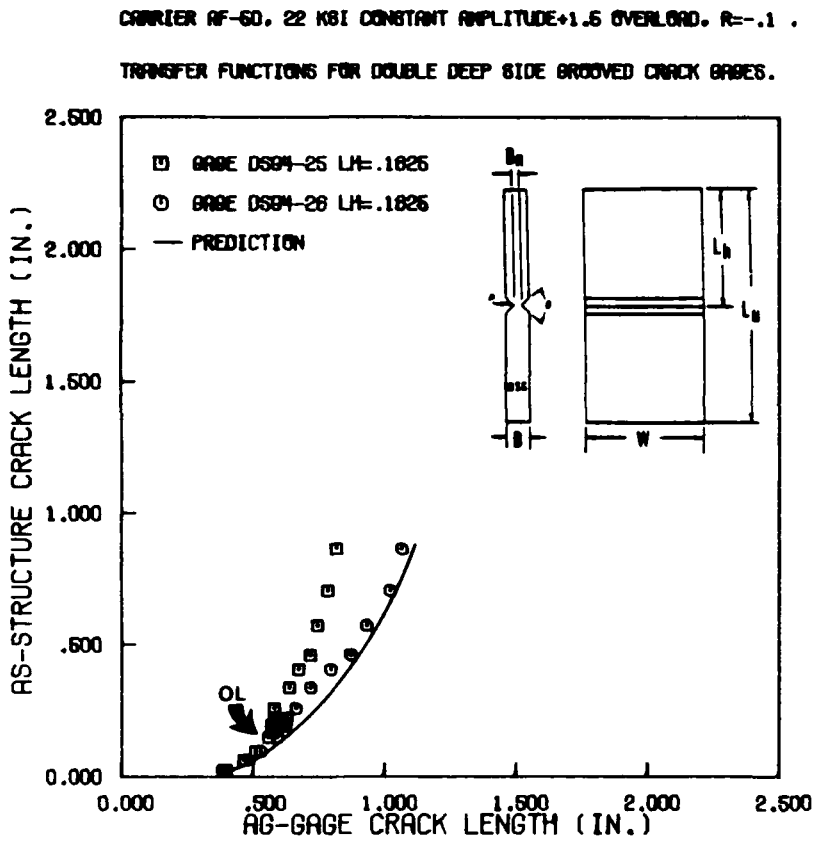

(c)

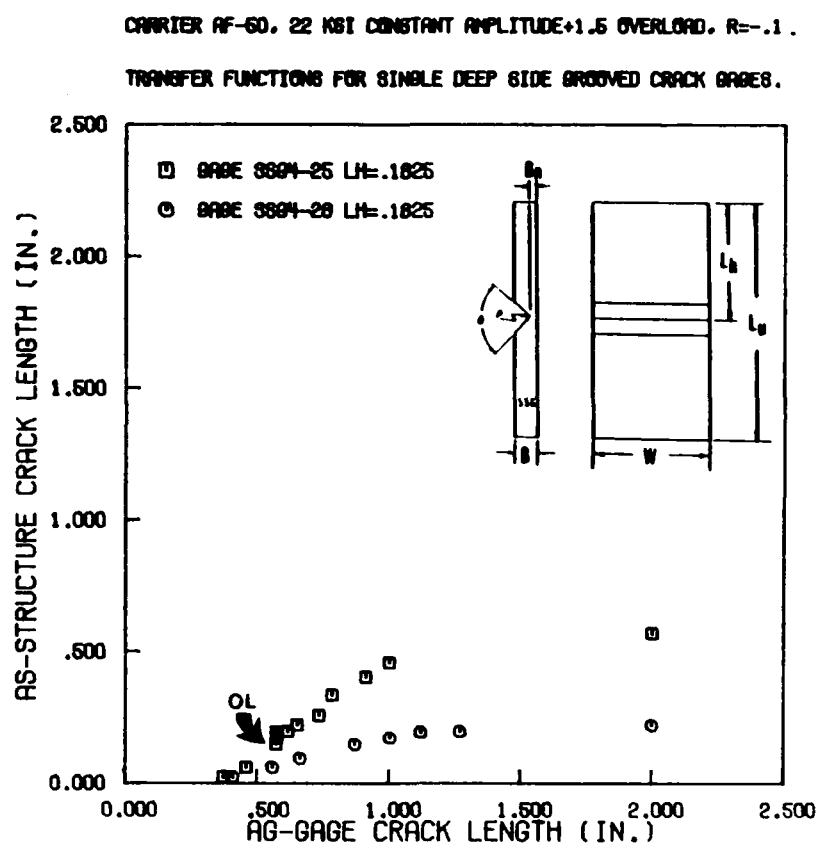

(d)

Figure A8, continued

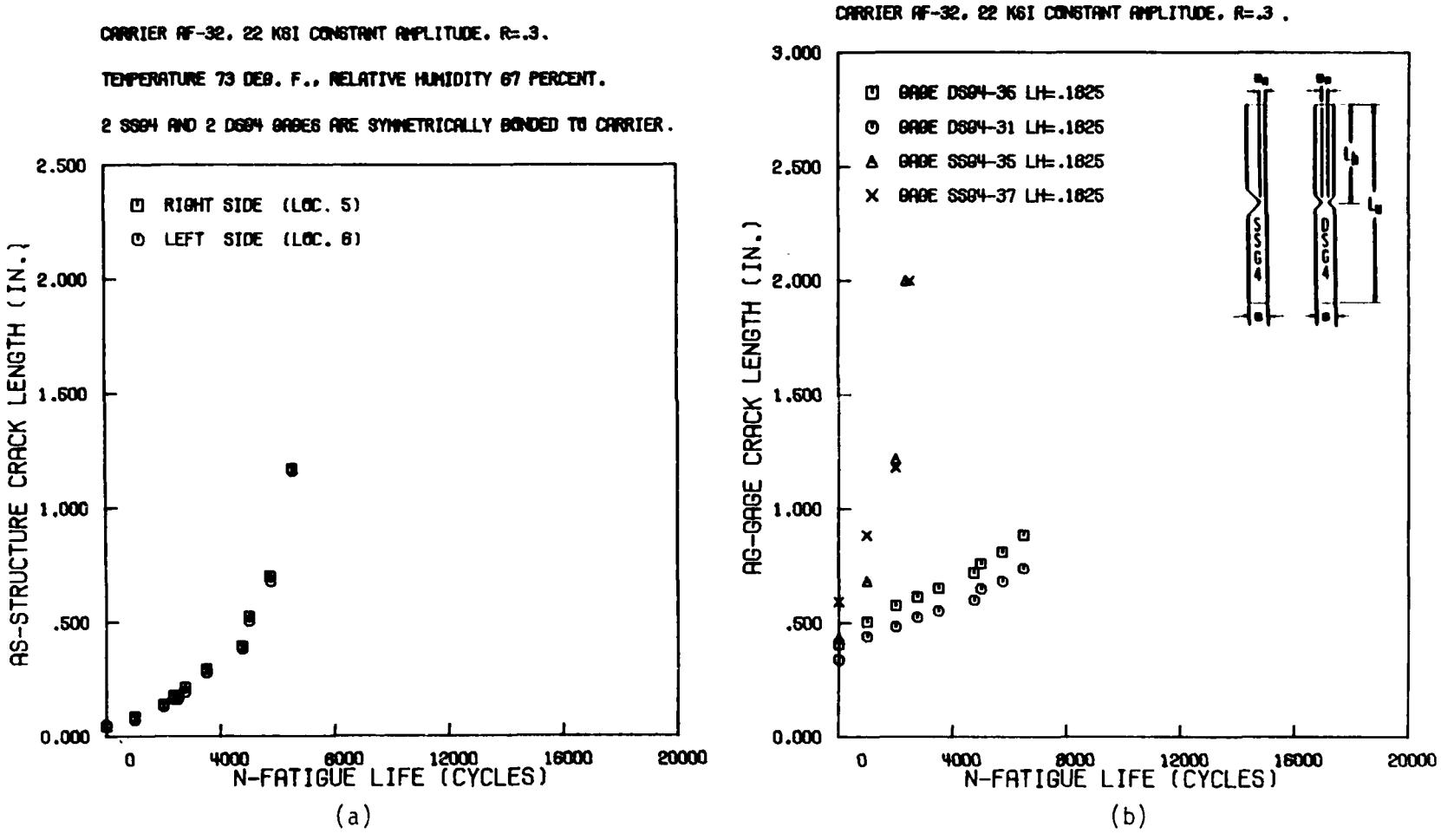

Figure A9 Crack growth data for carrier AF-32

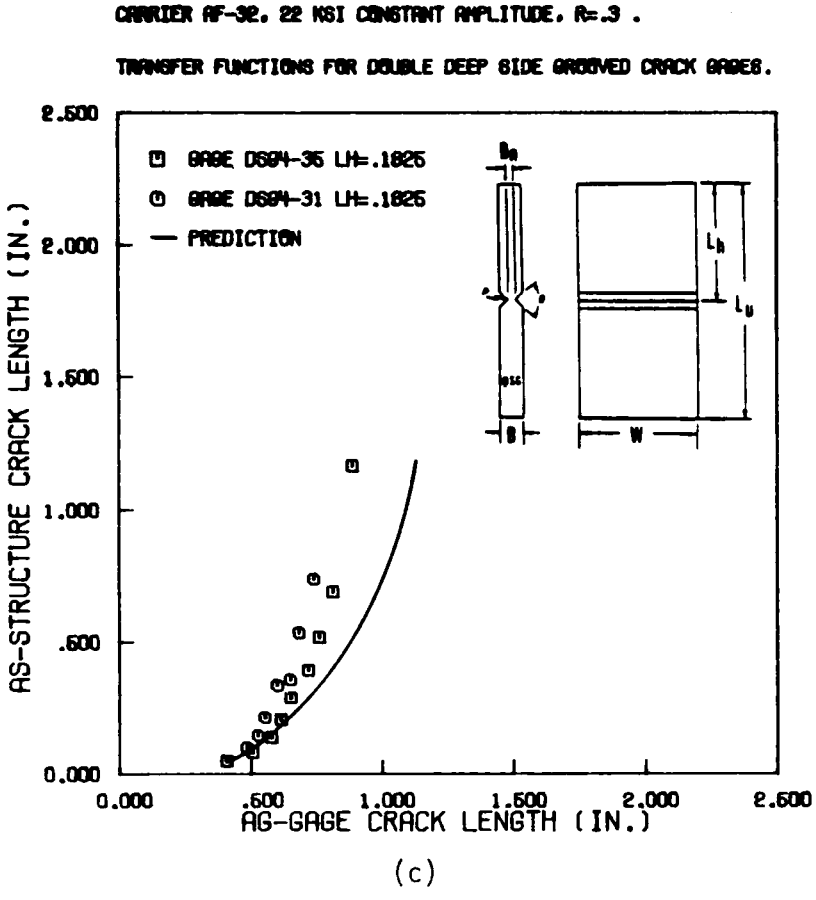

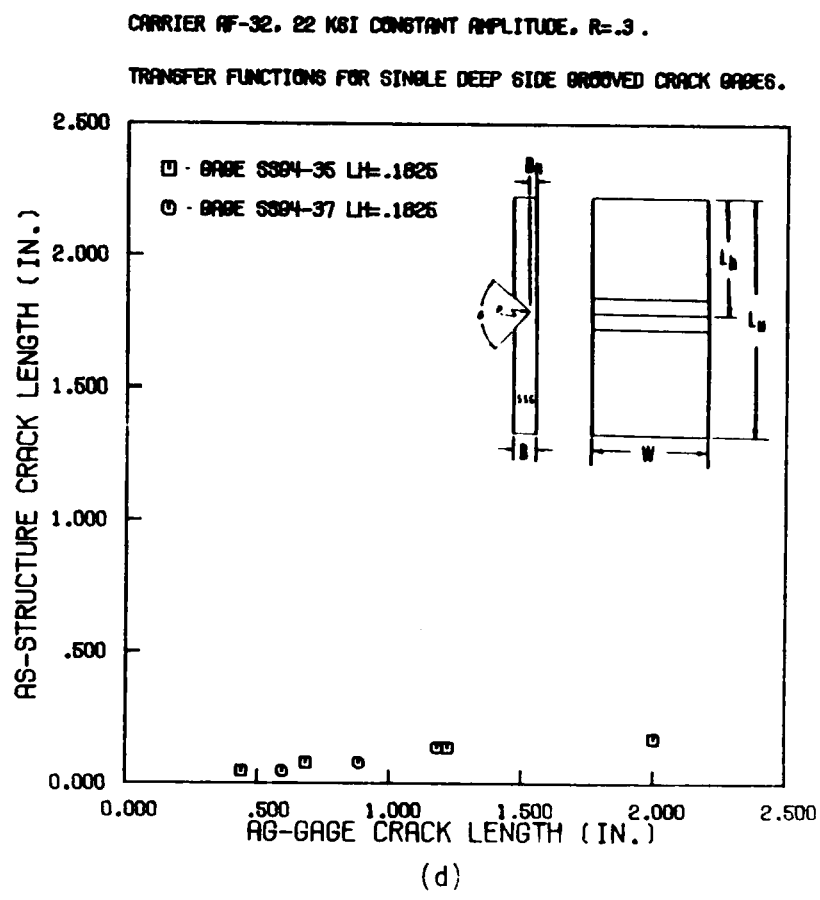

Figure A9. continued

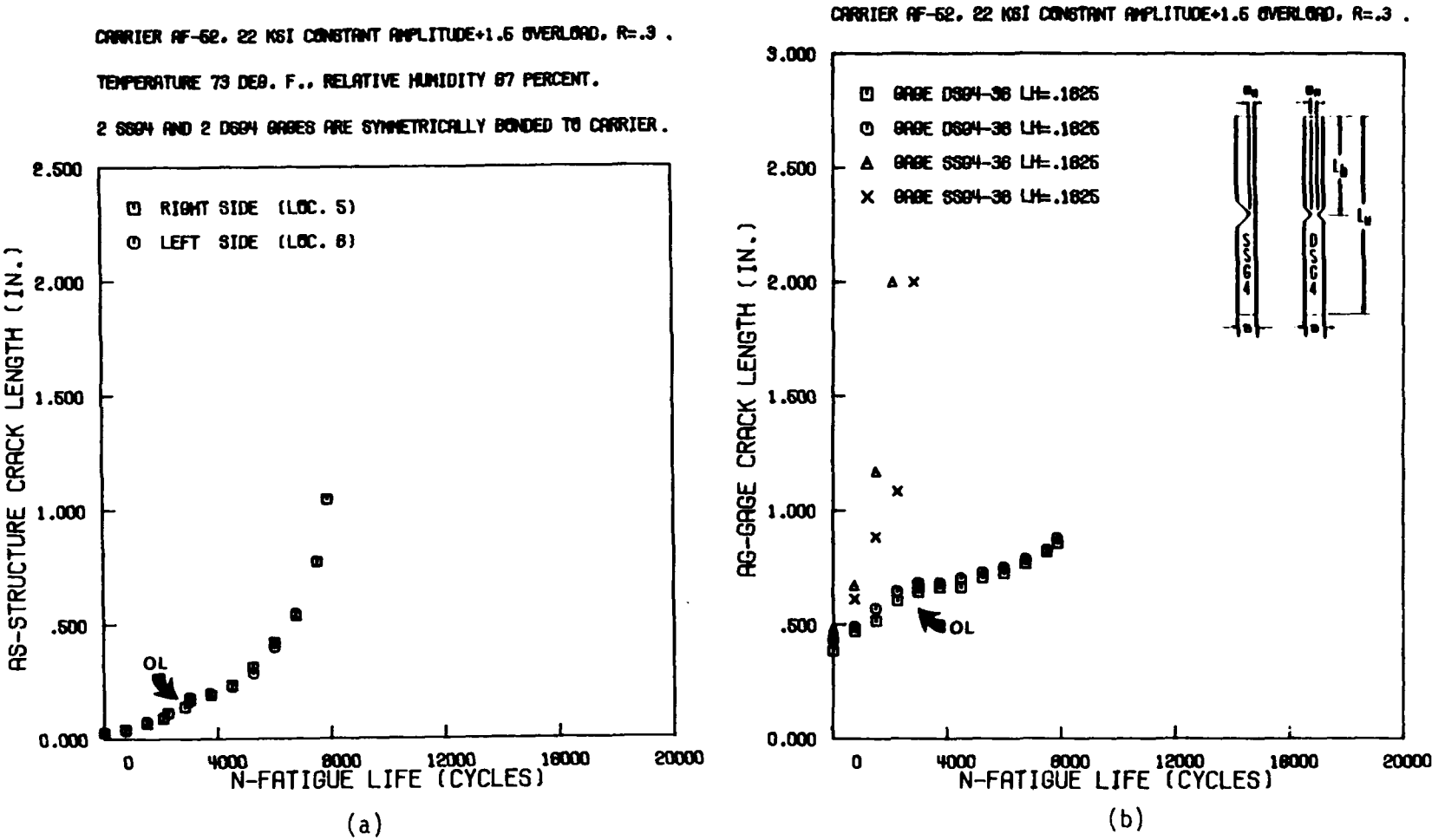

Figure A10 Crack growth data for carrier AF-52

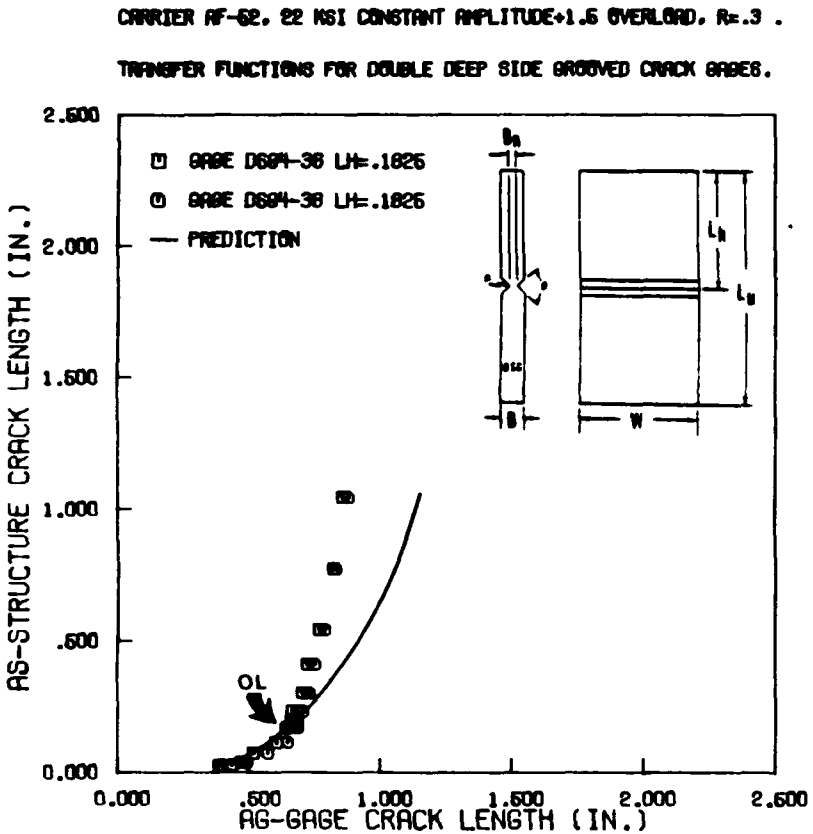

(c)

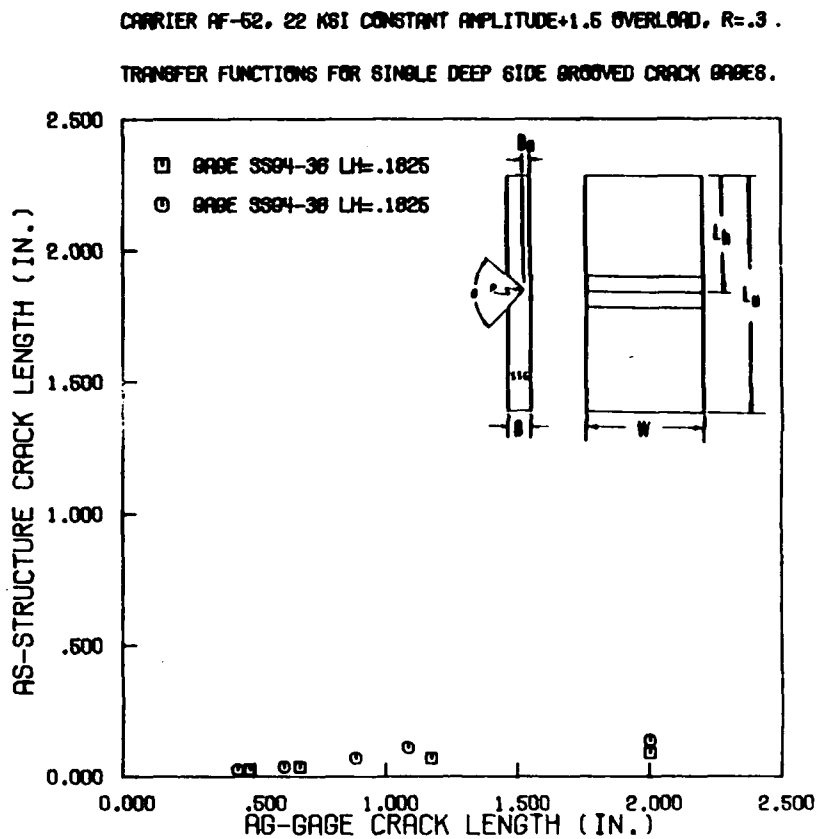

(d)

Figure A10, continued

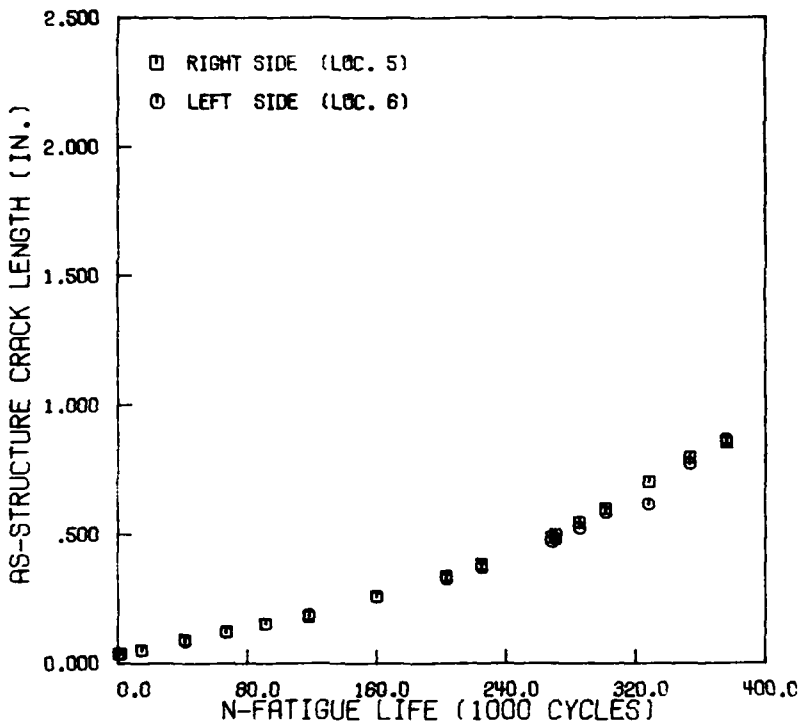

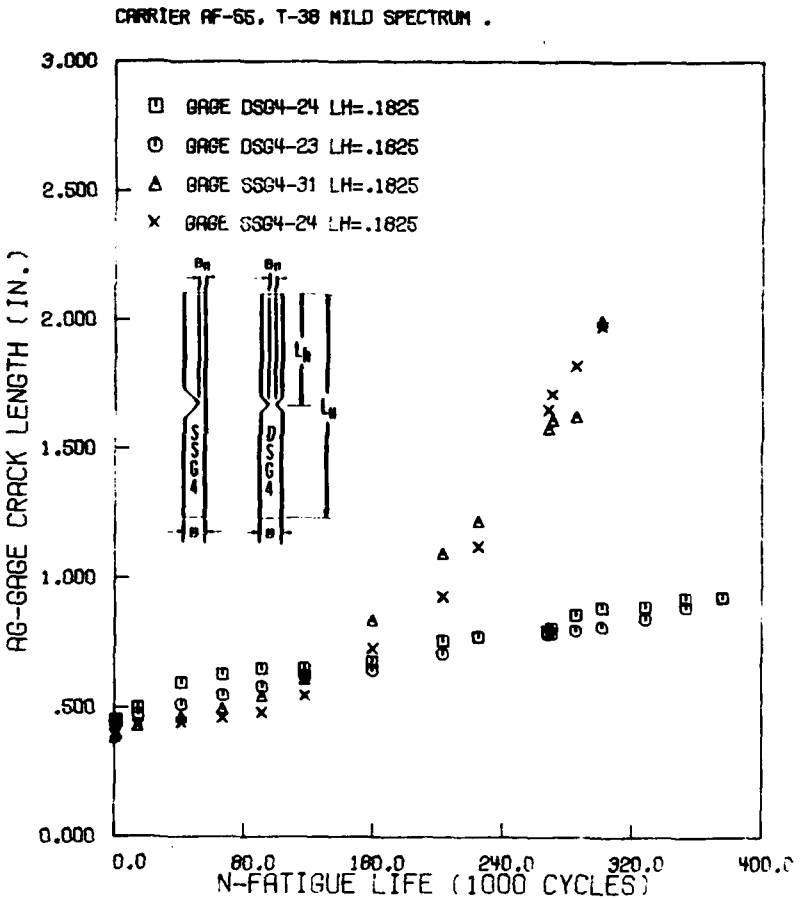

Figure A11 Fatigue crack growth data for Carrier 55, subjected to T-38 Mild Spectrum

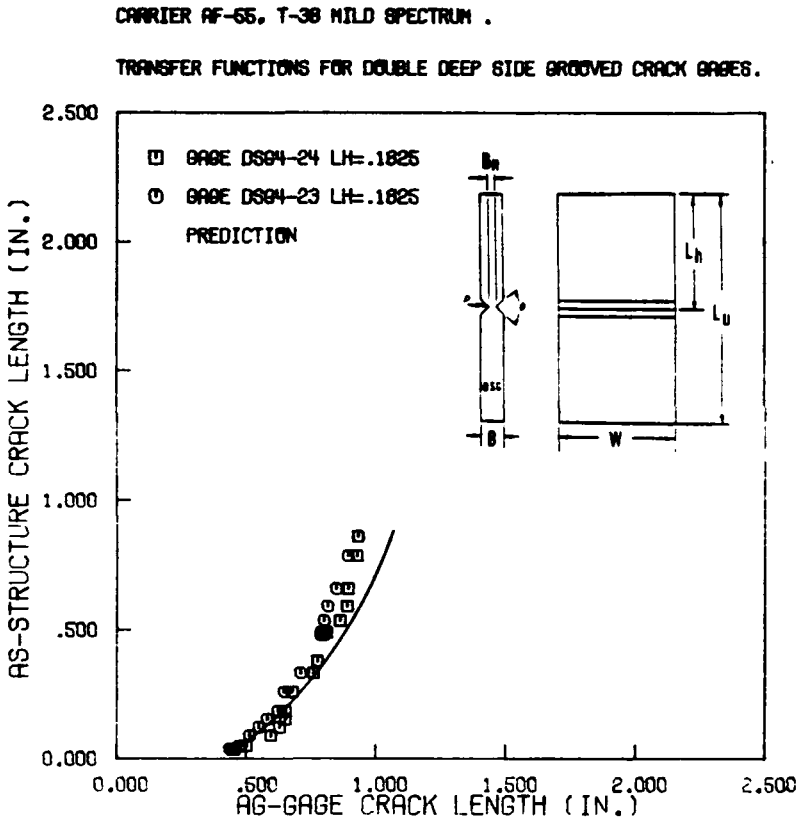

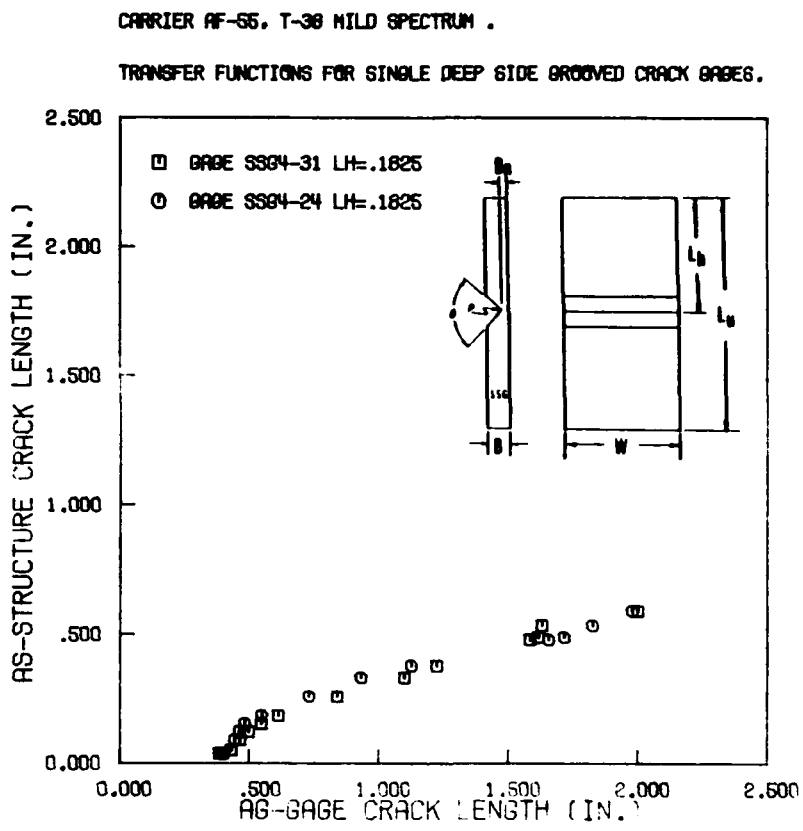

Figure A.1, continued

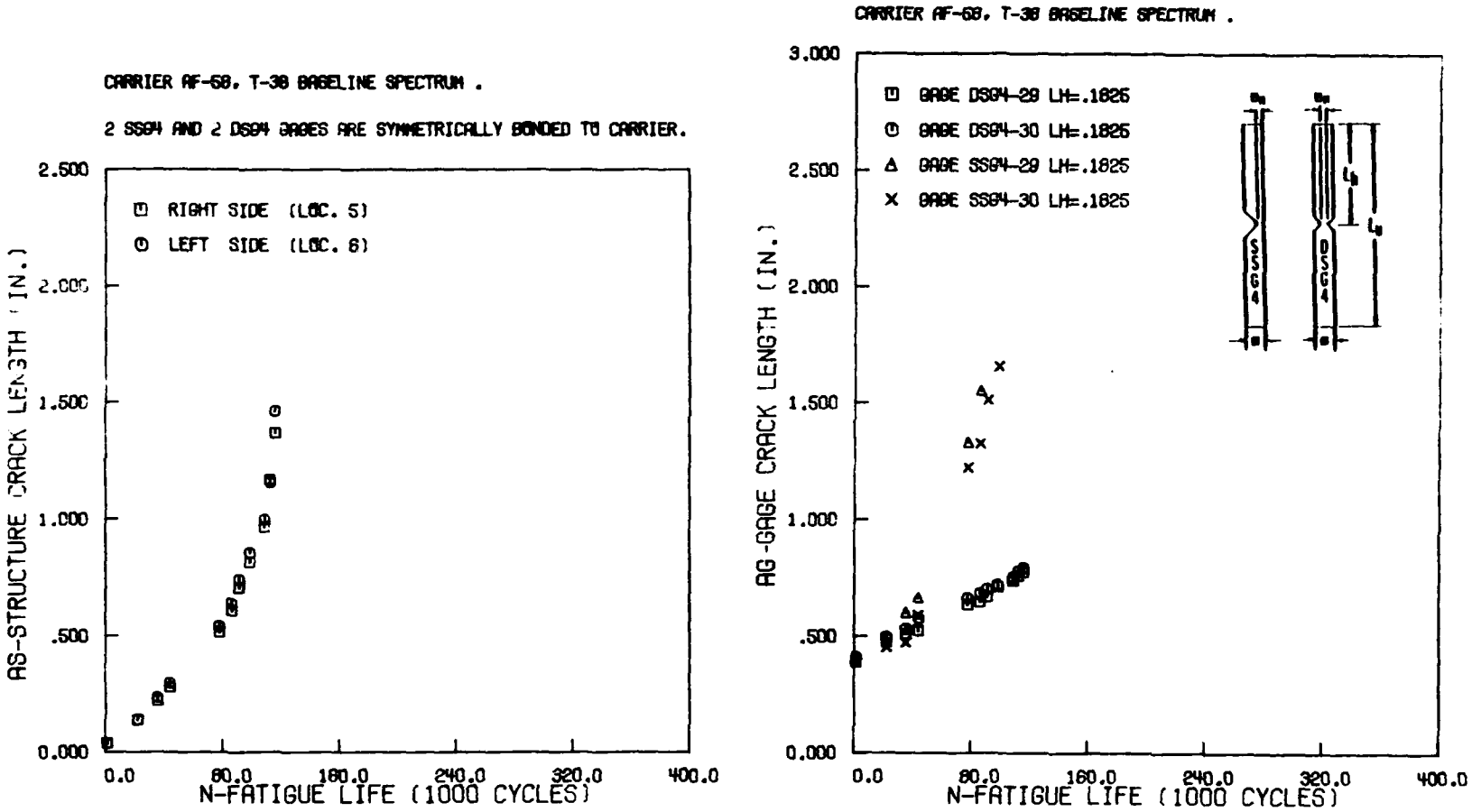

Figure A12 Fatigue crack growth data for carrier 58, subjected to T-38 Baseline Spectrum

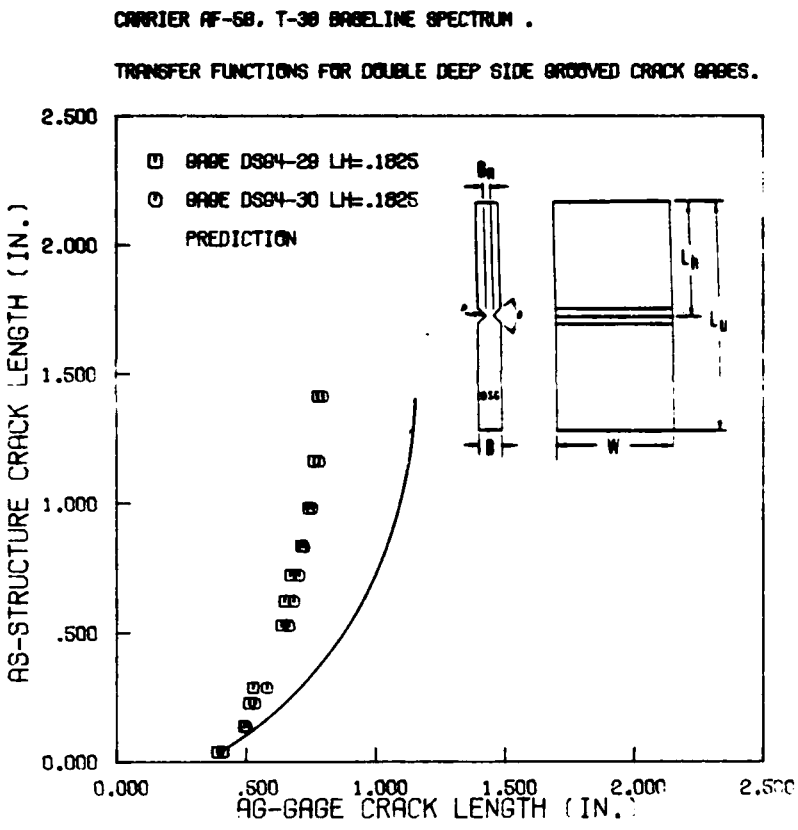

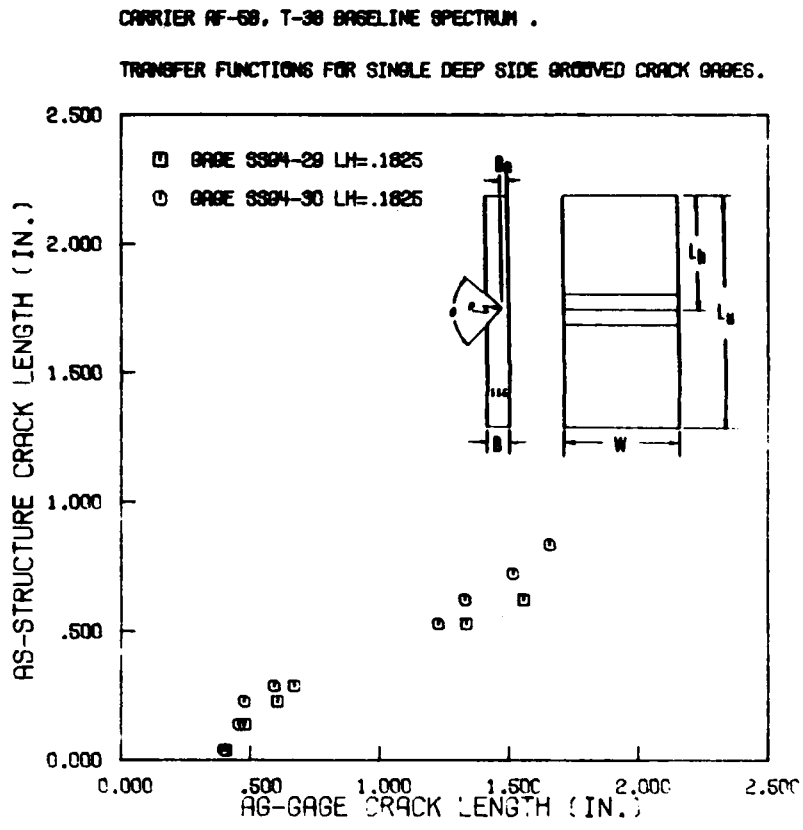

Figure A12. continued

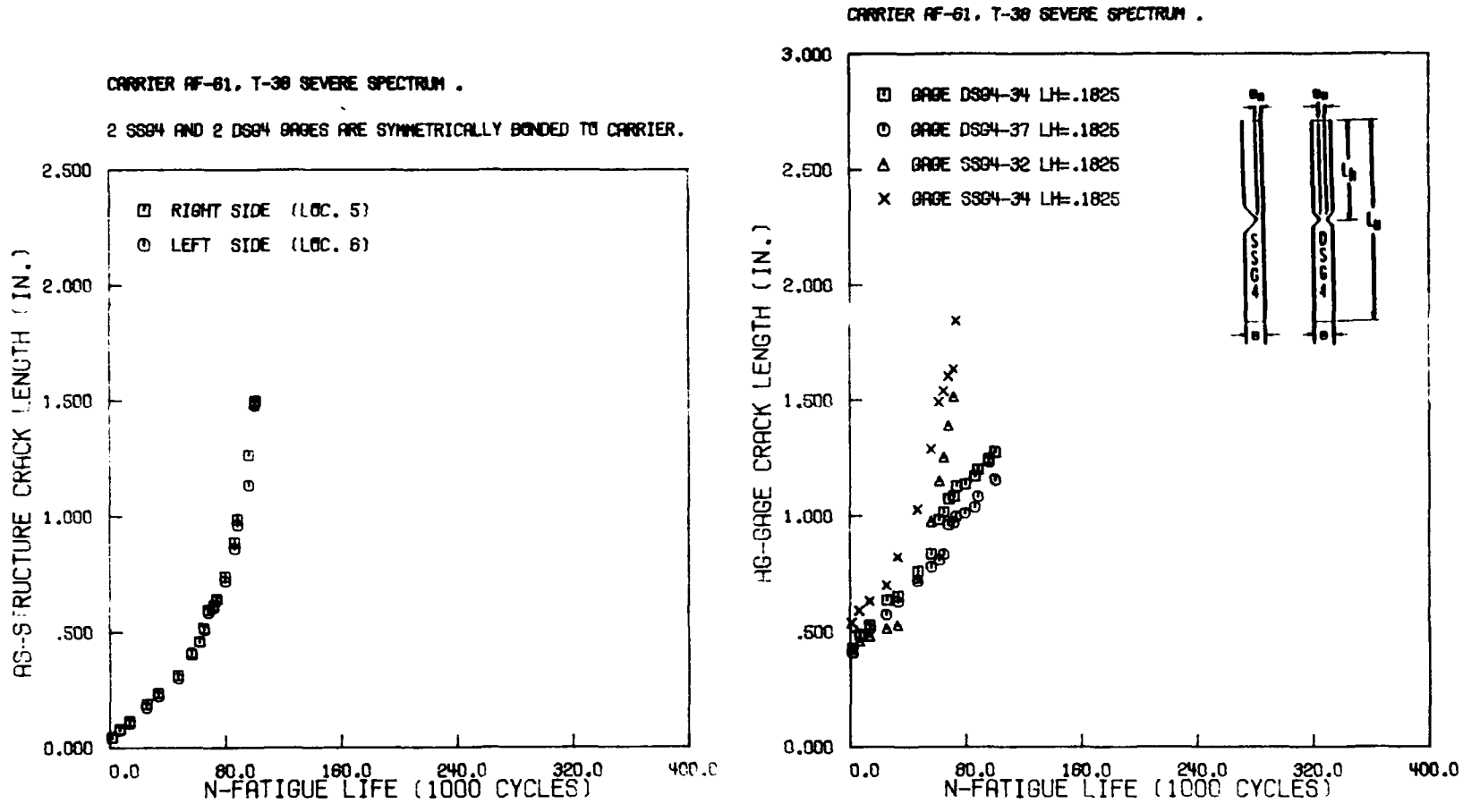

Figure A13 Fatigue crack growth data for carrier 61, subjected to T-38 Severe Spectrum

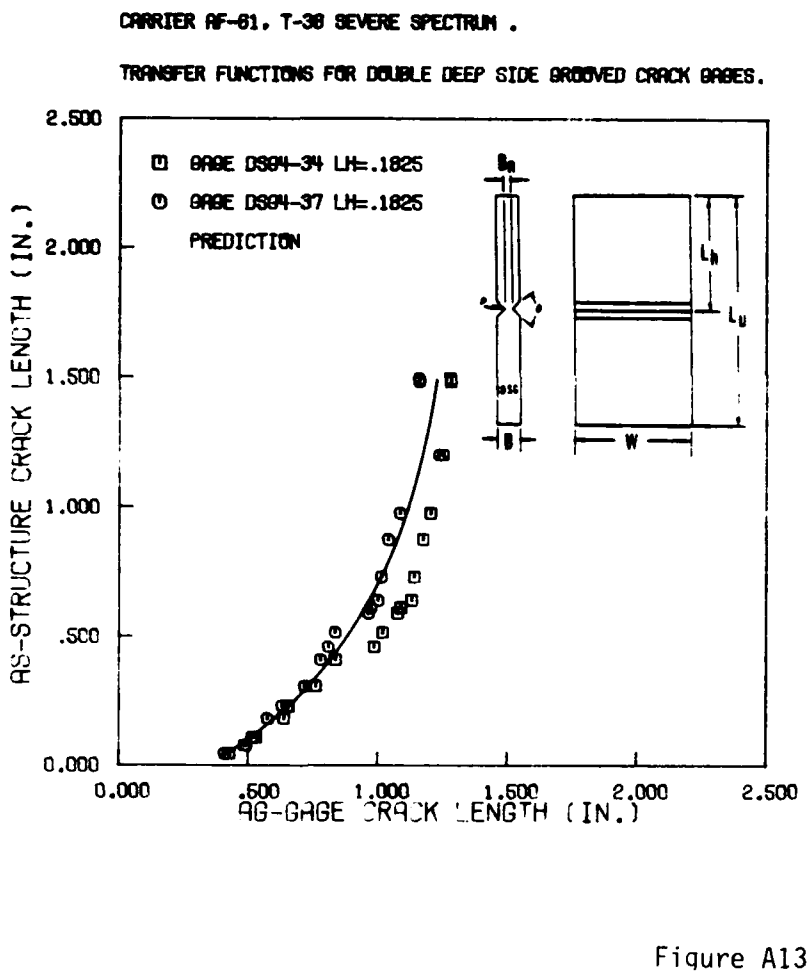

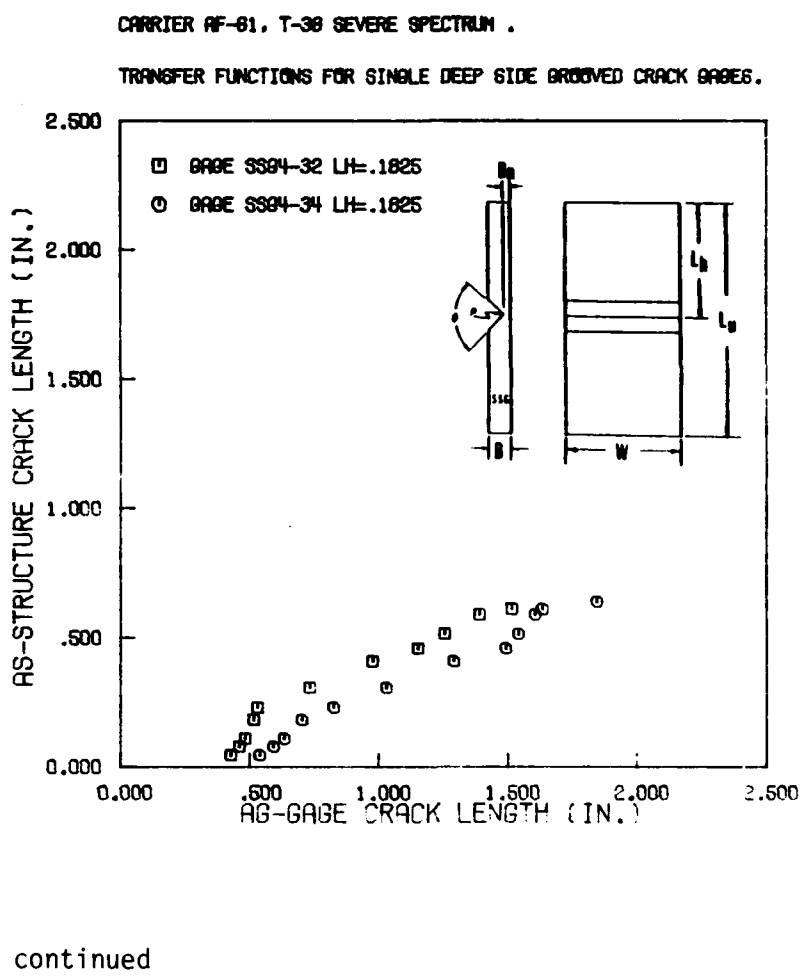

Figure A13, continued

APPENDIX B

BOEING TEST SPECIMEN NOMENCLATURE

The Boeing crack gage data reported in Reference 10 were used here to evaluate the double gage model calculations. Since approximately 20 different crack locations were of interest, the following nomenclature was used to identify the individual gage and structural flaws. Each crack was given the following nomenclature:

AFCG - X - Y - Z

Here X refers to the test number (1 to 6), Y identifies the side of the test specimen where the gages were mounted or the crack length measured (1 or 2), and Z identifies the particular location as shown in Figure 26. Note that locations 1 through 5 identify structural cracks, while locations 6 through 10 refer to crack gages.

LIST OF REFERENCES

1. "Aircraft Structural Integrity Program, Airplane Requirements," MIL-STD-1530A, Air Force Aeronautical Systems Division, December, 1975.

2. A.P. Berens, D.S. Morcock, K.E. Brown, J.C. Davis, R.L. Johnson, C.E. Larson, D.J. White, Handbook of Force Management Methods, AFWAL Flight Dynamics Laboratory, Wright-Patterson AFB, Ohio 45433, AFWAL-TR-81-3079, April 1981.

3. C.L. Guadagino, Evaluation of a Damage Accumulation Monitoring System as an Individual Aircraft Tracking Concept, AFWAL Flight Dynamic Laboratory, Wright-Patterson AFB, Ohio 45433, AFWAL-TR-82-3023, May 1982.

4. A.F. Grandt, Jr., R.L. Crane, and J.P. Gallagher, "A Crack Growth Gage for Assessing Flaw Growth Potential in Structural Components," Fracture, Proceedings of the Fourth International Conference on Fracture, Vol. 3, Waterloo, Canada, pp. 39-45, 19-24, June 77.

5. N.E. Ashbaugh, and A.F. Grandt, Jr., "Single-Edge-Cracked Crack Growth Gage for Monitoring Possible Fatigue Crack Growth," Service Fatigue Loads Monitoring, Simulation and Analysis, ASTM STP 671, 1979, pp. 94-117.

6. J.A. Ori, and A.F. Grandt, Jr., "Single-Edge-Cracked Crack Growth Gage," Fracture Mechanics, ASTM STP 677, 1979, pp. 533-549.

7. A. Dumanis-Modan, Evaluation of the Crack Gage as an Advanced Individual Tracking Concept, Ph.D. Thesis, Purdue University, W. Lafayette, Indiana 47907, December 1982.

8. P. Paris, and F. Erdogen, "A Critical Analysis of Crack Propagation Laws," Transactions of the ASME, Journal of Basic Engineering, Vol. 85, No. 3, December 1963, pp. 528-534.

9. W.S. Johnson, and S.J. Paquette, "Service Life Monitoring Coupons - Accounting for Potential Crack Growth in Fleet Aircraft," presented at 18th SDM Conference AIAA/ASME, San Diego, CA, March 21-23, 1977.

10. G.G. Cassatt, Evaluation of the Crack Gage Concept for Monitoring Aircraft Flaw Growth Potential, Air Force Materials Laboratory, Wright-Patterson AFB, Ohio, 45433, AFML-TR-79-4932, June 1979.

11. C. Saff, F-4 Service-Life Tracking Program (Crack Growth Gages), Air Force Flight Dynamics Laboratory, Wright-Patterson AFB, Ohio, 45433, AFFDL-TR-79-3148, December 1979.

12. W.J. Mills, and R.W. Hertzberg, "The Effect of Sheet Thickness on Fatigue Crack Retardation in 2024-T3 Aluminum Alloy," Engineering Fracture Mechanics, 1975, Vol. 7, No. 4, pp. 705-711.

13. G.R. Chanani, Fundamental Investigation of Fatigue Crack Growth Retardation in Aluminum Alloys, Air Force Materials Laboratory, Wright-Patterson AFB, Ohio, 45433, AFML-TR-76-156, September 1976.

14. D.E. Macha, A.F. Grandt, Jr., and B.J. Wicks, "Effects of Gas Turbine Engine Load Spectrum Variables on Crack Propagation," Effect of Load Spectrum Variables on Fatigue Crack Initiation and Propagation, ASTM STP 714, American Society for Testing and Materials, 1980.

15. S. Matsuoka, and K. Tanaka, "The Influence of Sheet Thickness on Delayed Retardation Phenomena in Fatigue Crack Growth in HT80 Steel and A5083 Aluminum Alloy," Engineering Fracture Mechanics, Vol. 13, No. 2, 1980, pp. 293-306.

16. T.T. Shih, and R.P. Wei, "Effect of Specimen Thickness on Delay in Fatigue Crack Growth," Journal of Testing and Evaluation, STEVA, Vol. 3, No. 1, Jan. 1975, pp. 46-47.

17. C.N. Freed and J.M. Krafft, "Effect of Side Grooving on Measurements of Plane-Strain Fracture Toughness," Journal of Materials, Vol. 1, No. 4, December 1966, pp. 770-790.

18. G. Green and J.F. Knott, "Effects of Side Grooves on Initiation and Propagation of Ductile Fracture," Metals Technology, Vol. 2, Part 9, September 1975, pp. 422-427.

19. W.R. Andrews and C.F. Shih, "Thickness and Side-Groove Effects on J- and δ-Resistance Curves for A533-B Steel at 90°C," Elastic-Plastic Fracture, ASTM STP 668, American Society for Testing and Materials, 1979, pp. 426-450.

20. W.L. Server, Wullaert, R.A., and Ritchie, R.O., "On the Use of Side-Grooves in Estimating J_{IC} Fracture Toughness with Charpy-Size Specimens," Journal of Engineering Materials Science and Technology, Vol. 102, No. 2, April 1980, pp. 192-199.

21. T.C. Lindley and C.E. Richards, "The Relevance of Crack Closure to Fatigue Crack Propagation," Materials Science and Engineering, Vol. 14, No. 3, June 1974, pp. 281-293.

22. P.J. Bernard, T.C. Lindley, and C.E. Richards, "Mechanisms of Overload Retardation During Fatigue Crack Propagation," Fatigue Crack Growth Under Spectrum Loads, ASTM STP 595, American Society for Testing and Materials, 1976, pp. 78-97.

23. J.P. Hess, A.F. Grandt, Jr., and A. Dumanis, "Effect of Side-Grooves on Fatigue Crack Retardation," Fatigue of Engineering Materials and Structures (in press).

24. K.J. Bathe, E.L. Wilson, and F.E. Peterson, "SAP IV a Structural Analysis Program for Static and Dynamic Response of Linear Systems, Earthquake Engineering Research Center, EERC 73-11, University of California at Berkeley, June 1973.

25. R.E. Peterson, Stress and Strain Concentration Factors, John Wiley and Sons, Seventh Edition, 1974, pp. 20-48.

26. R.J. Roark and Y.C. Young, Formulas for Stress and Strain, McGraw-Hill, Fifth Edition, 1975, pp. 590-593.

27. F.J. Giessler and J.P. Gallagher, Evaluation of the Crack Growth Gage Concept as an Individual Aircraft Tracking Device, Volume I, AFWAL Flight Dynamics Laboratory, Wright Patterson AFB, Ohio 45433, AFWAL-TR-83-3082, September 1983.

28. J.C. Rice, "Stresses in an Infinite Strip Containing a Semi-Infinite Crack", Journal of Applied Mechanics, Vol. 34, pp. 248-249, March 1967.

29. J. Congleton, "K Calibration for Deep-Side-Grooved Specimens", International Journal of Fracture, Vol. 14, 1978, pp. R65-R68.

30. O.L. Bowie, "Analysis of an Infinite Plate Containing Radial Cracks Originating from the Boundary of an Internal Circular Hole", Journal of Mathematics and Physics, Vol. 35, 1956.

31. D.A. Virkler, B.M. Hillberry, and P.K. Goel, The Statistical Nature of Fatigue Crack Propagation , Air Force Flight Dynamics Laboratory, Wright-Patterson AFB, Ohio 45433, AFFDL-TR-78-43, April 1978.

32. S.D. Conte and C. deBoor, Elementary Numerical Analysis, McGraw-Hill Kogakuska, 2nd edition, 1972, pp. 307-318.

*USGPO: 1984-759-062-614